

UCSF

UC San Francisco Electronic Theses and Dissertations

Title

Insights into Illicit Transport and Transcription Regulation from a Chemical-Genomic Screen in Escherichia coli

Permalink

<https://escholarship.org/uc/item/0c11c54b>

Author

Shiver, Anthony Lyndon

Publication Date

2015

Peer reviewed|Thesis/dissertation

Insights into Illicit Transport and Transcription Regulation from a
Chemical-Genomic Screen in *Escherichia coli*

by

Anthony Lyndon Shiver

DISSERTATION

Submitted in partial satisfaction of the requirements for the degree of

DOCTOR OF PHILOSOPHY

in

Biophysics

in the

GRADUATE DIVISION

of the

UNIVERSITY OF CALIFORNIA, SAN FRANCISCO

Dedication and acknowledgements

This dissertation is dedicated to my family, which has supported and enabled me in all of my accomplishments. Thank you to my Mother and Father, for sacrificing for me and supporting me in following my dreams. Thank you to Rahel, for supporting me and giving me an example of who I should be striving to be.

I would also like to thank my advisor, Carol Gross, for giving me support and advice throughout my PhD. Thanks to my thesis committee, Carol Gross, Nevan Krogan, and Jeff Cox, for helping me through an ambitious PhD project and being great mentors. Thanks to my lab members for making my PhD a fun process; Brian Sharon, Andrew Gray, Natalie Baggett, John Hawkins, Jason Peters, Byoung Mo Koo, Melanie Silvis, Candy Lu, Hendrik Osadnik, Yan Zhang, Marco Jost. Thanks to Bentley Lim, Monica Guo, and David Burkhardt for rolling fierce. Thanks as well to the program administrators, Rebecca Brown and Julia Molla, for working behind the scenes to help me graduate.

I would like to acknowledge everyone who has helped me in this work: Hendrik Osadnik, Kemardo Henry, John Hawkins, Bo Li, Bentley Lim, Jason Peters, Monica Guo, Danica Ganica-Fujimori, Kevin McCusker, Vanja Stojkovic, Hannes Braberg, Dina Schenidman-Duhovny, Andrey Parshin, Jookyung Lee, Maria Ozerova, Sergei Borukhov, Peter Cimermancic, Michael Fishbach, George Kritikos, Athanasios Typas and many others.

Portions of the text in this dissertation are a reprint of the material as it appears in the Proceedings of the National Academy of Sciences. The coauthor Carol Gross, listed in this publication, directed and supervised the research that formed the basis for the dissertation.

Statement from Carol Gross

This dissertation includes reprints of material published with coauthors other than Anthony Shiver. In Chapters 1 and 2, Anthony conceived of all experiments, performed all experiments except Chapter 2-Figure 2-Panel D, performed all analysis, and wrote the manuscript with me. In Chapter 3, Anthony conceived of and performed the experiments in Chapter 3-Figure 1, Chapter 3-Figure 4-Panels- C-D, and Chapter3-Supplementary Figure S8. He also wrote the manuscript with Sergei Borukhov and myself. His work warranted co-first-authorship for the manuscript from Chapter 3, and first authorship for the manuscript to be published from chapters 1 and 2. This dissertation contains a complete body of work driven by Anthony, significantly expands the knowledge of the field, and as such is comparable to a standard dissertation.

Insights into Illicit Transport and Transcription Regulation from a Chemical-Genomic Screen in *Escherichia coli*.

Anthony Shiver

Abstract

Living organisms are comprised of crowded and highly interconnected networks of biological molecules and metabolites. The scale and complexity of these networks makes them difficult to completely characterize, even for relatively streamlined organisms like the bacterium *Escherichia coli* K-12. After decades of work, many aspects of the growth and physiology of *E. coli* remain poorly understood. Its regulatory pathways remain only partially mapped. Functional-genomic approaches hold the promise of speeding discovery and characterization of the molecular networks underpinning life.

In this work, a chemical-genomic screen was conducted for two purposes. First, we were interested in the genetic-networks that make up an *E. coli* cell. Could we build on previous work to expand our knowledge of gene function in this model bacterium? Second, we were interested in pushing the resolution of functional genomics, not to characterize the relationship between genes in an organism but to characterize the relationships of amino acids and structural features of a single enzyme; RNA polymerase (RNAP).

To accomplish these tasks, we first used oligo-mediated recombineering to build a library of over 150 mutants in RNAP. We then screened this library of mutant strains, along with the KEIO deletion library of *E. coli*, for growth across more than 100 unique chemical stresses using colony array technology. This generated a map that expanded the chemical-sensitivity landscape of *E. coli*.

From features within this landscape, we identified a unique mechanism of illicit transport wherein the translation inhibitors kasugamycin and blasticidin S gain access to the cytoplasm of *E. coli* by hijacking the peptide ABC-importers Dpp and Opp. We used genetic analysis, *in vivo* translation assays, and *in vitro* binding assays to show that the peptide ABC-importers directly import the two drugs.

Next, we identified a new binding interface within RNAP that allows for the binding and function of the critical transcription regulator DksA. We used genetic analysis, *in vitro* site-specific crosslinking, molecular modeling, and functional assays of transcription both *in vivo* and *in vitro*. We found that the lineage specific insertion SI1 directly binds DksA and is critical for the effects of DksA on transcription.

Table of Contents

Introduction.....	1 - 11
Introduction.....	2 - 3
A Parts-List of <i>Escherichia coli</i> Using Chemical Genomics	3 - 5
Illicit Transport in <i>Escherichia coli</i> and Beyond.....	5 - 6
A Molecular Handle for Transcription	6 - 9
References	9 - 11
Chapter 1: A Parts-List of <i>Escherichia coli</i> Using Chemical Genomics	12 - 33
Introduction.....	13
Results	15- 18
Methods.....	20 - 22
References.....	22 - 24
Supplementary Information	25 - 30
Supplementary References.....	31 - 32
Chapter 2: Illicit Transport in <i>Escherichia coli</i> and Beyond	33 - 51
Introduction.....	34
Results	34 - 43
Discussion.....	43 - 45
Methods.....	45- 47
References.....	47 - 50
Supplementary Information	51
Chapter 3: A Molecular Handle for Transcription	52 - 107
Introduction.....	52 - 53

Results	54 - 71
Discussion.....	71 - 73
Methods.....	73 - 80
References.....	80 - 84
Supplementary Information	85 - 107

List of Tables

Introduction**Chapter 1: A Parts-List of *Escherichia coli* Using Chemical Genomics**

Supplementary Table 1: Conditions included in the current library 27 - 28

Supplementary Table 2: Cold-shock phenotypes at 10°C 29 - 30

Chapter 2: Illicit Transport in *Escherichia coli* and Beyond**Chapter 3: A Molecular Handle for Transcription**

Supplementary Table S1: RNA polymerase mutant DksA function 99

Supplementary Table S2: *dksA* mutant growth effects 100

Supplementary Table S3: Evolutionary conservation of SI1 101

Supplementary Table S4: Conservation of DksA interface 102

Supplementary Table S5: Conservation within DksA coiled-coil 103

Supplementary Table S6: Bacterial strains and plasmids 104 - 107

List of Figures

Introduction**Chapter 1: A Parts-List of *Escherichia coli* Using Chemical Genomics**

Figure 1: A new screen expands the phenotypic landscape of <i>E. coli</i>	14
Figure 2: New conditional phenotypes in the integrated dataset.....	19
Supplementary Figure 1: Between-screen correlation is associated with the number of conditional-phenotypes.....	25
Supplementary Figure 2: The smaller dataset suffers from a wider distribution of pairwise correlations.....	26

Chapter 2: Illicit Transport in *Escherichia coli* and Beyond

Figure 1: Peptide permeases determine kasugamycin and blasticidin S susceptibility in <i>E. coli</i> K-12	35
Figure 2: Opp and Dpp directly import kasugamycin and blasticidin S.....	38
Figure 3: OppA and DppA work with their cognate pores.....	41
Figure 4: Opp indirectly affects aminoglycoside resistance.....	44
Supplementary Figure 1: Opp Overexpression increases the rate of kasugamycin uptake ...	51

Chapter 3: A Molecular Handle for Transcription

Figure 1: β -SI1 is critical for growth during amino acid limitation.....	55
Figure 2: Probing of DksA-RNAP spatial organization by Bpa-crosslinking.....	56 - 57
Figure 3: Detailed views of the structural model of the DksA-RNAP complex	61
Figure 4: Comparison of the phenotypes of RNAP $\Delta\beta$ -SI1 and $\Delta\beta$ -SI1-1.2.....	64
Figure 5: Phenotypes of selected single point DksA mutants with significant functional impairment.....	67

Figure 6: Susceptibility of the RNAP β active-site region mutants β -R678A and β -R1106A to DksA inhibition	69
Supplementary Figure S1: Site-specific DksA-Bpa crosslinking to RNAP β and β' subunits	85
Supplementary Figure S2: Mapping of the crosslink sites on β and β' for DksA-Bpa variants	86 - 87
Supplementary Figure S3: Visualization of the DksA-Bpa crosslink sites in the 3D model of DksA-RNAP complex	88 - 89
Supplementary Figure S4: RNAP-binding assay of mutant DksAs	90 - 91
Supplementary Figure S5: Inhibitory activity of mutant DksAs	92 - 93
Supplementary Figure S6: In vivo inhibitory activity of DksA C-terminal truncation mutants	94
Supplementary Figure S7: Growth phenotypes of $\Delta dksA$ cells expressing mutant DksAs during amino acid limitation.....	95
Supplementary Figure S8: Mutations in β -SI1 display a synthetic genetic interaction with $\Delta dksA$	96
Supplementary Figure S9: Effect of mutation in RNAP β and β' on the inhibitory activity and binding affinity of DksA	97

Introduction

"It is interesting to contemplate a tangled bank, clothed with many plants of many kinds, with birds singing on the bushes, with various insects flitting about, and with worms crawling through the damp earth, and to reflect that these elaborately constructed forms, so different from each other, and dependent upon each other in so complex a manner, have all been produced by laws acting around us."

-Charles Darwin, *On the Origin of Species*, 6th ed

Citations:

Parshin A*, **Shiver AL***, Lee J, Ozerova M, Schneidman-Duhovny D, Gross CA, Borukhov S. DksA regulates RNA polymerase in Escherichia coli through a network of interactions in the secondary channel that includes Sequence Insertion 1. *Proc Natl Acad Sci U S A*. 2015 Dec 15;112(50):E6862-71.

*These authors contributed equally to this work.

Shiver AL, Osadnik H, Kritikos G, Li B, Krogan NJ, Typas A, Gross CA Illicit transport of antibacterial compounds revealed by an expanded chemical-genomic dataset of *E. coli* (in preparation)

The metaphor of a tangled bank encapsulates the wonder that most feel when thinking of the complex networks that connect and govern organisms. The driving forces of life are all found on a small bank, inhabited by a myriad of individuals, all competing for space and resources, all striving to reproduce. There was another world on this bank that Darwin never saw. A world lurking just behind, right below, and within the world he described. Moving down to the microscopic scale, it becomes immediately apparent that other forms of life, completely foreign to us, are dominant on this planet. Indeed, a single gram of the damp earth trodden by Darwin's creatures contains tens of thousands of unique microbial species and more than one million individual organisms (1). Earth is the domain of microbial life.

The miniature bank that these microorganisms inhabit hosts the same evolutionary forces: feast, famine, competition, cooperation, and extinction. It has also produced the same complexity, the same diversity, and the same interdependencies. There are bacteria that have specialized in fixing nitrogen and those that denitrify, bacteria that produce methane and those that use it for energy. While the force of natural selection has shaped these microbial communities, the microscopic world is too wild to be limited to Darwin's hypotheses on inheritance and evolution. Horizontal gene transfer via self-replicating systems like bacteriophage and plasmids breaks the law of vertical inheritance, complicating our concept of a species, and the bacterial systems that fight these self-replicating systems often operate through a decidedly Lamarckian mechanism of inheritance.

Microbial life has much to teach us, and we have only begun to learn its secrets. Despite many differences, there are a few key traits shared by all forms of life. One of the fundamental similarities between all forms of life is the DNA code, another the mechanism by which this DNA code is read. A recent push in microbiology has been to interpret the information contained

within the genome of an organism and predict what it means for the capabilities and lifestyle of an organism. This is critical to begin to unravel the complex interdependencies and behaviors of a microbial ecosystem, especially for those species that have yet to be cultured. However, our ability to interpret the information in these genomes is limited. Many of the genes that we find have an unknown function, getting us no closer to better characterizing a microbial species. Is there a way to quickly characterize gene function? If so what extra can we learn about the lifestyle and behaviors of a microbe?

In answering these questions for a single bacterial organism, *Escherichia coli* K-12, we made new connections that brought us back to the tangled bank and the diversity of bacterial life. We found a new molecular detail in the ancient chemical warfare that has been waged between microbial species. A critical antibiotic for agriculture, kasugamycin, uses a Trojan-horse mechanism to enter bacterial cells and kill them. We also identified a new molecular handle used to control transcription, the mechanism by which the DNA code is first read. This handle is a molecular marker that can be used to identify transcription regulatory mechanisms in a diverse set of bacteria.

A Parts-List of *Escherichia coli* Using Chemical Genomics

With the burgeoning field of genomics an ever-increasing number of bacterial species have had their genome sequenced and assembled. These sequenced genomes contain all of the information necessary for the growth and reproduction of an organism under a wide variety of environmental conditions. However, our ability to understand this information is still lacking. By analogy, a sequenced genome contains a “parts-list” of an organism. While we can find and list the genes found within a genome, we often have little information on the function of these individual genes. That is, we have a parts-list of an organism, but no notes on the purpose of many of the

parts. The list of genes of unknown function in bacteria is considerable. Even well studied organisms like *Escherichia coli* have no known function for ~20% of the ~4500 genes present.

The field of functional genomics has arisen in the attempt to use genome-wide approaches to characterize gene function on a global scale. One methodology, chemical genomics, has made important strides towards characterizing gene function in bacteria. Chemical-genomic approaches use large mutant libraries and large set of growth conditions to search for a connection between genotype and phenotype that can lead to unraveling the function of a gene. The discovery of a phenotype for a particular mutant in a specific condition, termed a conditional phenotype, is a powerful tool to associate gene function with the biological processes that are associated with growth in a particular condition. Growth without nutrients can identify auxotrophs, growth after exposure to UV irradiation can identify genes involved in the SOS response and DNA repair, etc. Testing a comprehensive mutant library of an organism against a comprehensive set of growth conditions thus has the potential to identify the function of every gene in an organism, completely annotating its parts-list.

Nichols *et al.* used a large-scale deletion library of *E. coli* and screened for growth across more than 100 unique chemical stresses and growth conditions (2). Despite the discovery a large number of conditional phenotypes, roughly half of the library was “unresponsive” to the test set of growth conditions. This indicated that many conditional-phenotypes remained to be discovered. Motivated both by a desire to characterize new conditions and discover novel gene functions, we sought to expand the chemical-genomic dataset of *E. coli* K-12. We screened the same large-scale mutant library against more than 50 conditions, split equally between those that overlapped the large-scale chemical-genomics dataset of Nichols *et al.* and entirely new perturbations designed to broaden the scope of chemical stresses used against *E. coli* K-12. We

successfully integrated the current screen with the Nichols *et al.* dataset, creating a resource that contained new conditional phenotypes while taking full advantage of previous experimental efforts. The integrated dataset provides an expanded global snapshot of drug action and stress response in *E. coli* K-12. We highlight expanded views of the genetic determinants of stress responses, conditional-sensitivities that differentiate antibiotic families according to mechanism, and new correlative leads for gene function.

Illicit Transport in *Escherichia coli* and Beyond

Many bacterial genes are devoted to the acquisition and use of different nutrients. ABC-importers recognize beneficial compounds and import them into the cytoplasm. The inner membrane is impermeable to hydrophilic compounds, preventing their entry. To circumvent this issue, bacteria express inner membrane transport complexes that recognize solutes and transport them into the cytoplasm. Often individual compounds have devoted ABC-importers, as is the case for many amino acids. In addition to beneficial compounds, the inner membrane is a barrier to hydrophilic antibiotics. Antibiotics with cytoplasmic targets must overcome this barrier to exert their effects. To accomplish this, many antibiotics mimic beneficial compounds to be recognized and imported by the devoted import complexes. The process of a harmful antibiotic being transported through an import complex devoted to another beneficial compound is known as illicit transport. The antibiotics that use this mechanism for import are also referred to as Trojan-horse compounds.

The peptide permeases, a diverse class of bacterial ABC-importers, recognize and import peptides for metabolism and signaling. Many of the peptide ABC-importers investigated so far can recognize a wide range of peptide primary sequences. This sequence non-specificity is important for being able to recognize the N^{20} possible peptides of length N. The peptide ABC-

importers illicitly transport multiple antibiotics. These include compounds that are peptides (3), antibiotics with peptide moieties (4), and others (5). Because of these relaxed recognition requirements, the peptide ABC-importers were recognized early on as a tempting target for the import of designer molecules, and successfully used to import impermeable amino acid analogues (6).

In the middle of the 20th century there was a concerted effort to find antifungal compounds that were effective against *Magnaporthe oryzae*, the causative agent of rice blast. In the 1950s, blasticidin S was discovered and developed as a treatment for rice blast. In the 1960s, kasugamycin was discovered and found to be superior to blasticidin S in many aspects. While both compounds are translation inhibitors with a significant overlap in sensitive organisms, including *Escherichia coli*, they are chemically dissimilar and were thought to be unrelated.

By investigating a new feature in the integrated dataset, we discovered and characterized an illicit transport mechanism for kasugamycin and blasticidin S. The compounds are illicitly transported through two prominent peptide ABC-importers in *Escherichia coli*. Blasticidin S is imported through oligopeptide permease (Opp) and Kasugamycin is imported through both Opp and dipeptide permease (Dpp). Kasugamycin has recently been used for treatment of *Erwinia amylovora*, a bacterial phytopathogen that causes fire blight, in the U.S. Loss of peptide ABC-importer function may be the first resistance mechanism to treatment and the identification of this mechanism may allow for rapid assessment of drug resistance and better antibiotic stewardship.

A Molecular Handle for Controlling Transcription

In bacteria, all transcription is performed by a single, essential, enzyme-complex: RNA polymerase (RNAP). In addition to being the target of a number of antibiotics, RNAP is a model

system for studying regulation, protein-DNA interactions, and structure-function relationships. Structure-function studies have focused on critical features of the active site region whereas peripheral regions the enzyme complex have received little or no effort. Furthermore, biochemical approaches have by necessity been limited to a small subset of promoters and DNA sequences, leaving the larger context of transcription in the cell unexplored. Braberg et al (7) demonstrated that functional genomic approaches like genetic-interaction analysis could be leveraged as an *in vivo* approach for structure-function analysis. In this way the cellular context of transcription is preserved. Also, due to the high-throughput nature of functional genomics, a wider set of features of RNAP can be queried at once. This opens the possibility of discovering function for a much wider set of the features of RNAP. Motivated by these goals, we sought to leverage the power of chemical-genomics to study the structure-function relationships of *E. coli* RNAP.

We generated a library of over 100 hypomorphic mutations of RNAP at the endogenous loci in an isogenic background of *Escherichia coli*. We mutated residues in multiple features of *E. coli* RNAP, including deletions of two lineage-specific insertions (LSI). Lineage-specific insertions are folded domains inserted into the large subunits of RNAP that have been inherited in specific lineages of bacteria (8, 9). In *Escherichia coli* and other proteobacteria, RNAP carries four lineage-specific insertions (10, 11). One insertion, Sequence Insertion 1 (SI1), is in the β -lobe. Another, Sequence Insertion 2 (SI2), is in the β -flap. The third, β -insertion 11 (β i11) is in the β -protrusion. The fourth and final lineage-specific insertion is Sequence Insertion 3 (SI3) in the β ' trigger loop. SI3 is essential for viability in *Escherichia coli* and intimately connected to the transcription cycle as well as regulation by the transcription factor DksA (12, 13). Conversely, the function of SI1, SI2, and β i11 remain unknown. We were capable of deleting both SI1 and

SI2 on the chromosome for the first time and included these deletions in the chemical-genomic screen. After screening the LSI deletions for conditional-phenotypes across more than 100 unique conditions, we discovered a unique signature for SI1. This led us to the discovery that SI1, much like SI3, is critical for the regulation of transcription by the transcription factor DksA.

In *Escherichia coli*, the global regulatory response to amino acid starvation is orchestrated by the second messenger guanosine-3',5'-bisdiphosphate (ppGpp), which is a widely conserved master regulator (14). Accumulation of ppGpp during amino acid scarcity triggers the stringent response, which down-regulates expression of rRNA and tRNA while increasing expression of amino acid biosynthetic enzymes. In *E. coli*, ppGpp works synergistically with the transcription factor DksA to initiate the stringent response (15, 16). Both ppGpp and DksA are critical for virulence and growth under duress in many pathogenic proteobacteria (17).

DksA is a relatively small protein with a prominent N-terminal coiled-coil domain and a globular C-terminal domain consisting of a Zn²⁺-binding region and a C-terminal α -helix (16). It belongs to a class of regulators that bind directly to RNA polymerase (RNAP) without contacting DNA (18). DksA modulates RNAP activity by preventing formation of or destabilizing the intermediate complex (RP_i) on the pathway to the open complex (RP_o), which is competent for initiation. For promoters with intrinsically unstable open complexes, such as rRNA promoters, DksA binding leads to decreased transcription (15).

Using both chemical-genomic and high-resolution mapping of site-specific cross-links, we identify β subunit Sequence Insertion 1 (β -SI1) as a binding site for DksA and describe evidence for a bipartite binding site comprised of β -SI1 and the conserved β' rim helices. We also show that the tip of DksA interacts with the highly conserved substrate-binding region of the β subunit active site. This work advances our mechanistic understanding of DksA activity in *E. coli* and

expands our knowledge of the evolutionary conservation of transcription regulation by DksA and ppGpp, connecting direct regulation of RNAP by ppGpp and DksA to the presence, in RNAP, of both SI1 and SI3.

References

1. Roesch LF, et al. (2007) Pyrosequencing enumerates and contrasts soil microbial diversity. *ISME J* 1(4):283–290.
2. Nichols RJ, et al. (2011) Phenotypic Landscape of a Bacterial Cell. *Cell* 144(1):143–156.
3. Nisbet TM, Payne JW (1979) Specificity of peptide uptake in *Saccharomyces cerevisiae*, and isolation of a bacilysin-resistant, peptide-transport-deficient mutant. *FEMS Microbiol Lett* 6:193–196.
4. Novikova M, et al. (2007) The *Escherichia coli* Yej Transporter Is Required for the Uptake of Translation Inhibitor Microcin C. *J Bacteriol* 189(22):8361–8365.
5. McKinney DC, et al. (2015) Illicit Transport via Dipeptide Transporter Dpp is Irrelevant to the Efficacy of Negamycin in Mouse Thigh Models of *Escherichia coli* Infection. *ACS Infect Dis* 1(5):222–230.
6. Ames BN, Ames GF-L, Young JD, Tsuchiya D, Lecocq J (1973) Illicit Transport: The Oligopeptide Permease. *Proc Natl Acad Sci* 70(2):456–458.
7. Braberg H, Moehle EA, Shales M, Guthrie C, Krogan NJ (2014) Genetic interaction analysis of point mutations enables interrogation of gene function at a residue-level resolution. *BioEssays* 36(7):706–713.

8. Jokerst RS, Weeks JR, Zehring WA, Greenleaf AL (1989) Analysis of the gene encoding the largest subunit of RNA polymerase II in *Drosophila*. *Mol Gen Genet MGG* 215(2):266–275.
9. Sweetser D, Nonet M, Young RA (1987) Prokaryotic and eukaryotic RNA polymerases have homologous core subunits. *Proc Natl Acad Sci U S A* 84(5):1192–1196.
10. Lane WJ, Darst SA (2010) Molecular Evolution of Multisubunit RNA Polymerases: Sequence Analysis. *J Mol Biol* 395(4):671–685.
11. Lane WJ, Darst SA (2010) Molecular evolution of multisubunit RNA polymerases: structural analysis. *J Mol Biol* 395(4):686–704.
12. Artsimovitch I, Svetlov V, Murakami KS, Landick R (2003) Co-overexpression of *Escherichia coli* RNA Polymerase Subunits Allows Isolation and Analysis of Mutant Enzymes Lacking Lineage-specific Sequence Insertions. *J Biol Chem* 278(14):12344–12355.
13. Furman R, Tsodikov OV, Wolf YI, Artsimovitch I (2013) An Insertion in the Catalytic Trigger Loop Gates the Secondary Channel of RNA Polymerase. *J Mol Biol* 425(1):82–93.
14. Braeken K, Moris M, Daniels R, Vanderleyden J, Michiels J (2006) New horizons for (p)ppGpp in bacterial and plant physiology. *Trends Microbiol* 14(1):45–54.
15. Paul BJ, et al. (2004) DksA: A Critical Component of the Transcription Initiation Machinery that Potentiates the Regulation of rRNA Promoters by ppGpp and the Initiating NTP. *Cell* 118(3):311–322.

16. Perederina A, et al. (2004) Regulation through the Secondary Channel—Structural Framework for ppGpp-DksA Synergism during Transcription. *Cell* 118(3):297–309.
17. Dalebroux ZD, Svensson SL, Gaynor EC, Swanson MS (2010) ppGpp Conjures Bacterial Virulence. *Microbiol Mol Biol Rev* 74(2):171–199.
18. Haugen SP, Ross W, Gourse RL (2008) Advances in bacterial promoter recognition and its control by factors that do not bind DNA. *Nat Rev Microbiol* 6(7):507–519.

Chapter 1

A Parts-List of *Escherichia coli* Using Chemical Genomics

Contributing Authors:

Hendrik Osadnik, George Kritikos, Bo Li, Nevan Krogan, Athanasios Typas, Carol Gross

Citations:

Shiver AL, Osadnik H, Kritikos G, Li B, Krogan NJ, Typas A, Gross CA Illicit transport of antibacterial compounds revealed by an expanded chemical-genomic dataset of *E. coli* (in preparation).

Large-scale chemical-genomic screens of the model organism *E. coli* K-12 (1–6) have provided a critical resource for the bacterial research community. Investigation of the conditional-phenotypes of a particular mutant or condition from these screens has contributed to insights that catalyzed the mechanistic characterization of multiple molecular systems (7–9). As these screens continue to be used to generate new biological insights, updated methodologies and data mining techniques hold the promise of opening new avenues of investigation into these large-scale datasets (10). It is critical to update and maintain chemical-genomic resources to take advantage of new techniques, interrogate the biology of new antibacterial compounds, and discover new functional connections between genes.

Motivated both by a desire to characterize new conditions and discover novel gene functions, we sought to expand the chemical-genomic dataset of *E. coli* K-12. We screened the same large-scale mutant library of deletions and hypo-morphs used previously (4, 5) against more than 50 conditions, split equally between those that overlapped the large-scale chemical-genomics dataset of Nichols *et al.* (2011 dataset) and entirely new perturbations designed to broaden the scope of chemical stresses used against *E. coli* K-12. We successfully integrated the current screen with the 2011 dataset, creating a resource that contained new conditional phenotypes correlative connections while taking full advantage of previous experimental efforts.

The integrated dataset provides an expanded global snapshot of drug action and stress response in *E. coli* K-12. We highlight expanded views of the genetic determinants of stress responses, conditional-sensitivities that differentiate antibiotic families according to mechanism, and new correlative leads for gene function.

Figure 1

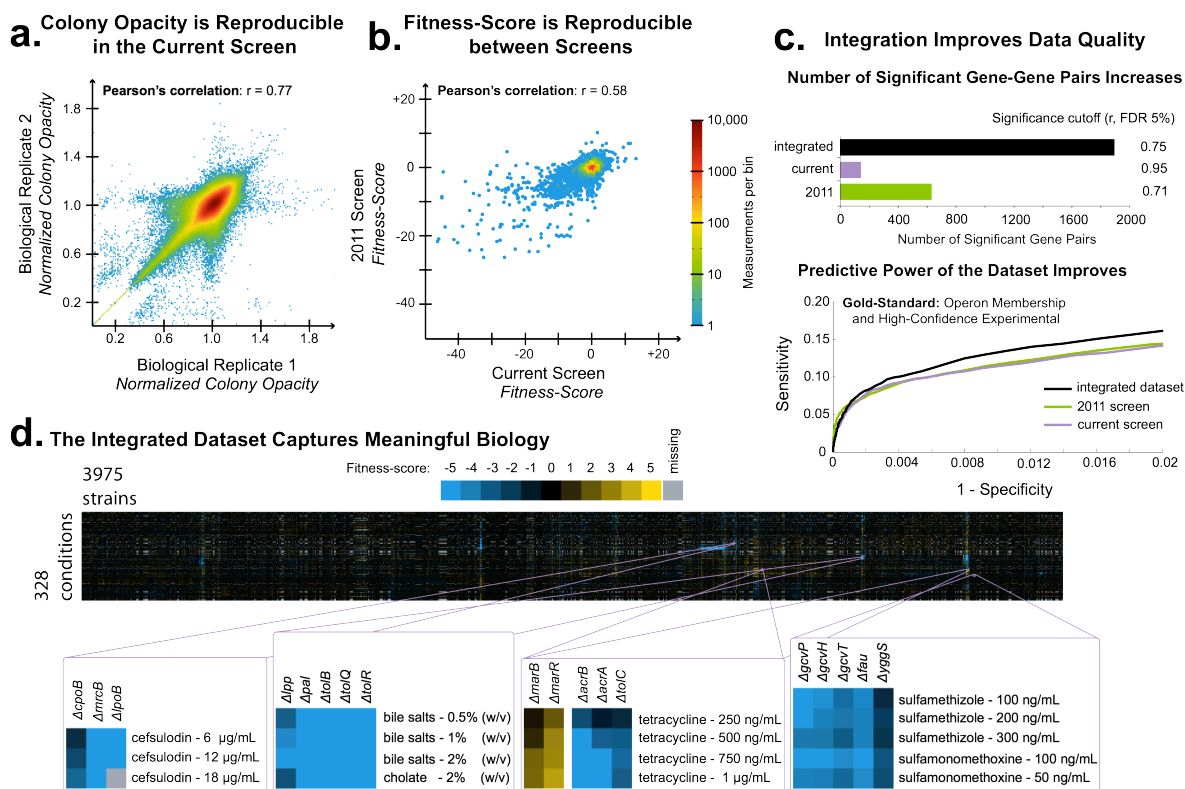


Figure 1: A new screen expands the phenotypic landscape of *E. coli*. (a) Colony opacity is reproducible in the current screen. Normalized colony opacity, relative to the plate median, is plotted for biological replicates from individual images. (b) Fitness-score is reproducible between screens. The statistical fitness-score for individual chemical-genetic interactions was compared for equivalent conditions between the current screen and reanalyzed images from the 2011 dataset. The scatter plots in (a-b) are colored according to local density using same log-10 scale color mapping. (c) Integration improves data quality. (top panel) The number of pairwise correlations whose value exceeds the statistically significant cutoff are plotted for the current, reanalyzed 2011, and integrated datasets (bottom panel) ROC curve analysis was used to compare the predictive power of pairwise correlations from the datasets using operon co-membership and high-confidence experimental associations as a gold standard. The low-fallout portion of the ROC curve is shown. (d) The integrated dataset captures meaningful biology. Fitness scores from the integrated dataset are shown as a heat-map after two-dimensional hierarchical clustering. Gene clusters and relevant conditional phenotypes from the 2011 dataset are shown as blow-ups. Tree diagrams for the blown-up clusters are omitted for clarity.

A new screen expands the set of conditional-phenotypes in *E. coli* K-12.

We tested the sensitivities of 3994 mutants of *E. coli* K-12 to more than 50 unique stresses. The new stresses tested included many toxic chemicals not used as antibiotics, with the intention of detecting a wider set of conditional-phenotypes (**Supplementary Table 1**). Arrayed strains were pinned onto an agar plate containing a compound of interest and grown to a defined average colony size. Plates were imaged, colony opacity was quantified using Iris (Kritikos *et al.* in preparation) opacity measurements were filtered and normalized, and a modified t-statistic was assigned to each of the >200,00 gene-condition interactions (4, 11). Normalized colony opacity measurements in the current screen were reproducible between biological replicates (**Figure 1A**) ($r=0.76$) indicating that the screen captured reproducible conditional-phenotypes.

To integrate data from the current screen into the larger 2011 dataset, we reanalyzed the original images in the 2011 screen with the current analysis pipeline. Fitness-scores for conditions in both screens were well correlated ($r=0.58$, Pearson's correlation) (**Figure 1B**). The extent of agreement between the common conditions was also clearly associated with the number of phenotypes detected ($s=0.83$, Spearman's rank correlation) (**Supplemental Figure 1**). We found that the current screen could be integrated with an existing resource, that higher signal for a particular condition improved its reproducibility between these experiments, and that careful treatment to eliminate differences in analysis improved the extent of integration.

Integration with a larger dataset was critical for interpreting relative associations from the current, smaller-scale, screen (**Figure 1C**). When only the 50 conditions from the current screen were used to calculate gene-gene correlations, the distribution of pairwise correlations was widened (IQR=0.26) compared to the larger dataset (IQR=0.17) (**Supplementary Figure 2**). A statistically significant cutoff for gene-gene correlations also required a much higher cutoff

($r=0.95$, Pearson's correlation), passed by only 139 gene-pairs. Integration with the 2011 dataset reduced the width of the distribution of correlations (IQR=0.16), reduced the cutoff for significance ($r=0.75$, Pearson's correlation) and increased the number of significant gene pairs by an order of magnitude.

We also used a hybrid gold standard test-set to benchmark the power of gene-gene correlations from the integrated dataset to predict known biological associations. Our test-set combined high-confidence experimental associations (12) with operon membership (13). The integrated dataset performed similarly to both the current and 2011 screen (**Figure 1C**). Finally, clustering of the integrated dataset revealed that, despite using a unique analysis pipeline, we recapitulated each of the novel biological associations reported in the 2011 screen (**Figure 1D**). Dataset integration thus allowed us to collect new information from a limited set of conditions while benefiting from the more robust statistical features and broader scope of a much larger dataset.

New conditional-phenotypes in the integrated dataset

The integrated dataset also revealed new conditional-phenotypes and gene-gene correlations from data collected in the current screen, and we highlight here some of these features. Rescreening of the MreB inhibitor A22 identified a wide set of sensitivities from the Rcs pathway and its regulon, resulting in co-clustering of genes from the Rcs pathway and colanic acid biosynthesis (**Figure 2A**). A22 is an MreB inhibitor and a known activator of Rcs (14, 15) and a broadened signal from the new data lends further support to a model in which Rcs-dependent activation of colanic acid biosynthesis is an adaptive response to this drug. The current screen also identified new genes not previously associated with survival of A22, like *ftsP*, a stress-specific cell division gene associated with survival of low-osmolarity conditions (16).

Cold shock at 10°C also resulted in a particularly rich profile, with 3-fold more conditional-

sensitivities than the next lowest temperature (16°C) (**Supplementary Table 2**). Ribosome assembly is especially defective at 10°C and below and many cold-sensitive mutants have ribosome assembly defects (17). Indeed, 20% of the conditional-sensitivities in the current screen come from genes with translation-related GO annotations ($p=10^{-9}$, Fisher's exact test)(**Supplementary Table 2**). Many of these genes have been previously associated with either ribosome assembly or cold-shock and hits from the screen also identify new functionally important cold-shock genes. These include the ribosome binding protein YjgA (18) and the cold-shock induced protein YmcE (19). Despite a high level of redundancy between the RNA-binding cold-shock proteins, $\Delta cspB$ was defective for growth at 10°C. CspB is preferentially induced at lower temperatures (20) and this may reflect a specialization of CspB for 10°C, either in expression or function.

Multiple families of antibiotics target the ribosome and inhibit translation but differ in binding site and molecular mechanism, reviewed in (21). In the screen, deletions in different translation stress pathways had differential sensitivities that distinguished these drug families (**Figure 2B**). The trans-translation complex ($\Delta ssrA/\Delta smpB$) was sensitized to aminoglycosides (gentamicin) and macrolides (clarythromycin) while the alternative rescue factor ($\Delta arfA$) was specifically sensitized to the tetracycline family (tetracycline). The ribosome-bound ppGpp synthase ($\Delta relA$) was uniquely sensitized to tRNA synthetase inhibitors from the current screen (serine hydroxamate, pseudomonic acid A). Treatment with the aminonucleoside blasticidin S revealed strong sensitivities from the cytoplasmic protease HslUV as well as adaptors to the inner membrane protease FtsH ($\Delta hflC,K$), a set of sensitivities shared with the aminoglycosides. These differential effects may represent adaptive responses that are specific for the effects of individual drugs, e.g. recognition of uncharged tRNAs in the A-site by RelA (22).

The current screen also added new informative gene-gene correlations. To visualize this, we built a network model that used correlation across all conditions to associate genes. We filtered the network to exclude lower correlations ($r < 0.5$) and highlighted new connections identified from data in the current screen using red edges. Though the information added from the current screen only accounts for 16% of the overall conditions, the integrated dataset revealed a number of new high-value correlations representing meaningful biology. New information from A22 (Figure 2C), cold shock (Figure 2D), and blasticidin S (Figure 2E) all resulted in new connections in the gene network. New conditional-phenotypes also drove clustering of peptide permease complex members and their regulators (Figure 2F). We explore this feature further in the next chapter.

Figure 2

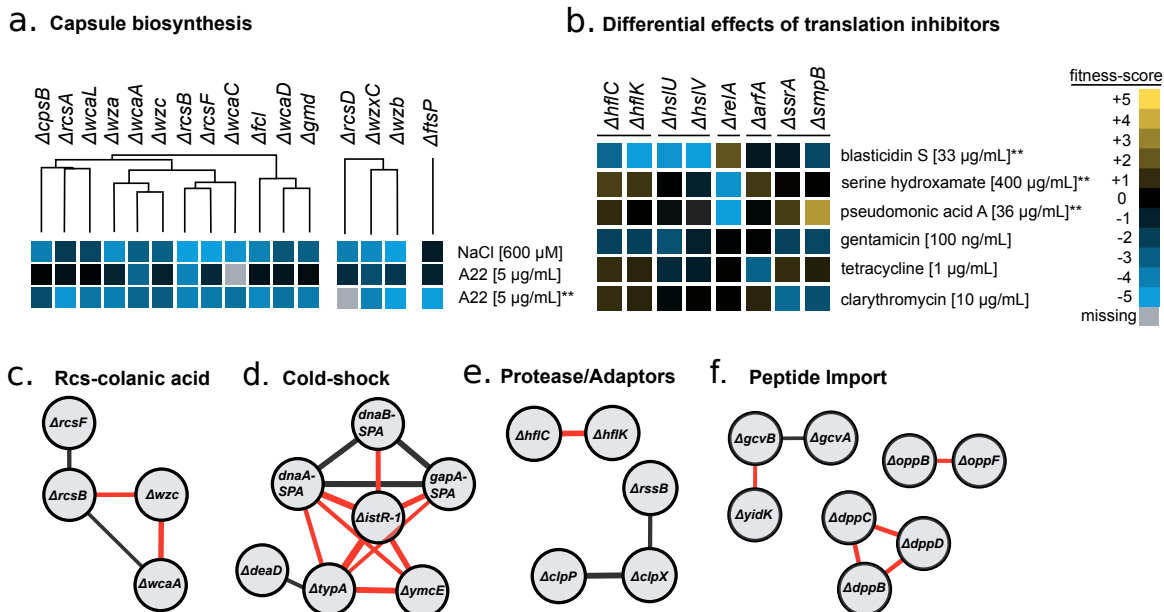


Figure 2: New conditional phenotypes in the integrated dataset

(a) Heat-map of fitness-scores for the colanic acid hierarchical cluster in the integrated dataset. A22 treatment from the current screen expands the set of sensitized colanic acid biosynthesis genes within the screen. The current screen also identifies *ftsP* as a deletion sensitized to A22. (b) Heat-map of fitness-scores highlighting differential sensitivities to translation inhibitors. Double asterisk (**) indicates conditions introduced by the current screen. (c-f) Networks built using pairwise correlations from the integrated dataset. Correlations above $r=0.5$ are plotted as connections between genes, line thickness is proportional to the strength of correlation. Correlations that increased more than 50% in the integrated dataset due to information from the current screen and resulted in new hierarchical clusters are highlighted in red.

Methods

Media, growth conditions, strains, plasmids, and oligos

Chemical sensitivity screens used LB Lennox agar plates (1% (w/v) tryptone, 0.5% (w/v) yeast extract, 90 mM sodium chloride, 2% (w/v) bacto agar) unless otherwise specified. M9 minimal plates used in the screen contained M9 salts, 0.2% (w/v) glucose, and 2% (w/v) bacto agar. Ordered libraries grown during the chemical-genomics screens were incubated at 37°C until colonies reached a defined size (8 hours - 1.5 week) then a photograph was taken of the plate. The KEIO deletion library is derived from BW25113.

Data collection and processing

The chemical genomics screen was conducted using the same methodology as reported previously (4) with few modifications. Ordered libraries were arrayed on rectangular agar plates, grown in the presence of antibiotic or other stress until the colonies reached a defined average size, and then imaged. One condition, 4°C survival, entailed growth of colonies on LB plates at 37°C for 6 hours, followed by incubation of the colony array at 4°C for 5 weeks. Colonies were pinned to a fresh plate, surviving cells were allowed to grow for 6 hours at 37°C, and a photograph was taken.

Plate photographs were taken with a Canon Powershot G10, using an in-house assembly to control plate illumination. Images were analyzed using in-house software (Iris) (Kritikos et al. in preparation) that segments images and measures the total intensity of pixels within the colony to calculate an opacity metric. Data filtering, normalization, and calculation of the fitness-score (11) are similar to the steps performed by Nichols et al. The original photographic images from Nichols et al. were reanalyzed using Iris and subjected to the

same filtering and normalization steps before integration with data from the current screen.

Clustering, significant phenotypes and correlations, and network analysis

Unreliable measurements were removed from the dataset at multiple points in the analysis and each condition had a different number of measurements (fitness-scores) that passed analysis. Before data integration, clustering, and network analysis were performed, conditions and strains with less than 75% reliable measurements were removed from analysis. Hierarchical clustering was performed using the Cluster 3.0 command line interface, using uncentered correlation and pairwise complete-linkage. Data was visualized using Java Treeview.

To predict reliable phenotypes, we used the method described by Nichols et al. to determine the false-discovery rate and set a cut-off for the fitness-score that reflected an FDR of 5%. Using this method, 95% of the cutoff values for negative (sensitization) fitness-scores fell in the range (-2.7, -1.5) while 95% of the cutoff values for positive (resistance) fitness-scores fell in the range (1.6, 2.8).

To predict reliable pairwise correlations, a non-parametric estimate was used as described in Nichols et al. We randomized the elements of mutant fitness-score profiles individually, creating a dataset where each mutant retained its distribution of fitness-scores but randomly shuffled across all conditions. We then calculated all pairwise correlations from this randomized dataset and saved the highest correlation. This process was repeated for 1000 randomized datasets, and the 95th percentile was calculated for the distribution of maximum correlations. This value, the cutoff at which 95% of randomized matrices do not produce a higher correlation, was used as the high confidence cutoff for reliable correlations. Missing values were imputed with 0 before running the randomized correlations to reduce computational cost.

For the network analysis, pairwise correlations above 0.5 were exported into Cytoscape and clustered. Subnetworks were chosen that correspond to genes mentioned in the text. Connections were highlighted in red for correlations that i) improved by more than 50% in the integrated dataset, ii) included signal from conditional-phenotypes introduced by the current screen, and iii) corresponded to genes that co-clustered in the hierarchical clustering of the integrated dataset but not the 2011 dataset alone.

References

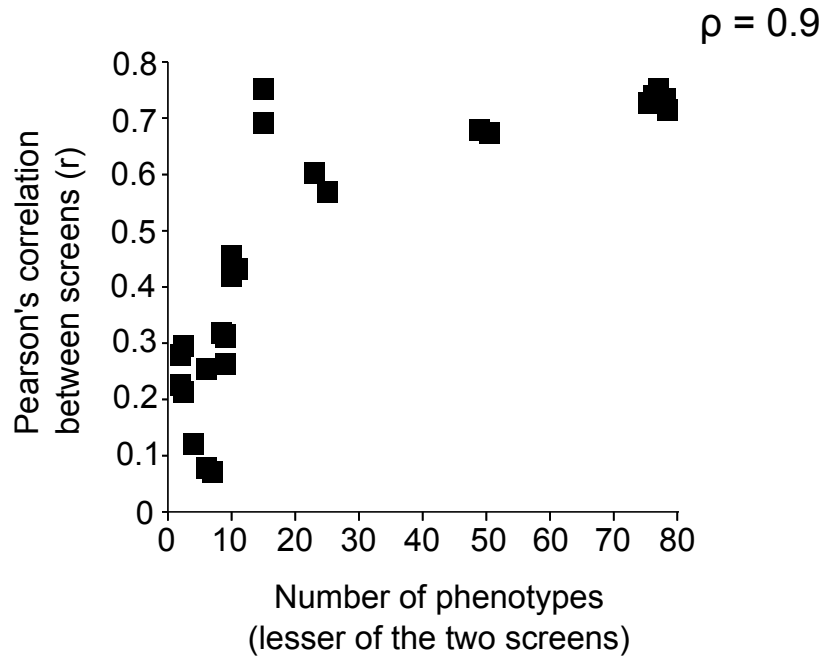
1. Hu P, et al. (2009) Global Functional Atlas of Escherichia coli Encompassing Previously Uncharacterized Proteins. *PLoS Biol* 7(4). doi:10.1371/journal.pbio.1000096.
2. Joyce AR, et al. (2006) Experimental and Computational Assessment of Conditionally Essential Genes in Escherichia coli. *J Bacteriol* 188(23):8259–8271.
3. Nakayashiki T, Mori H (2013) Genome-wide screening with hydroxyurea reveals a link between nonessential ribosomal proteins and reactive oxygen species production. *J Bacteriol* 195(6):1226–1235.
4. Nichols RJ, et al. (2011) Phenotypic Landscape of a Bacterial Cell. *Cell* 144(1):143–156.
5. Paradis-Bleau C, Kritikos G, Orlova K, Typas A, Bernhardt TG (2014) A Genome-Wide Screen for Bacterial Envelope Biogenesis Mutants Identifies a Novel Factor Involved in Cell Wall Precursor Metabolism. *PLoS Genet* 10(1). doi:10.1371/journal.pgen.1004056.
6. Tran L, Baarsel JA van, Washburn RS, Gottesman ME, Miller JH (2011) Single-Gene Deletion Mutants of Escherichia coli with Altered Sensitivity to Bicyclomycin, an Inhibitor of Transcription Termination Factor Rho. *J Bacteriol* 193(9):2229–2235.

7. Guo MS, et al. (2014) MicL, a new σ E-dependent sRNA, combats envelope stress by repressing synthesis of Lpp, the major outer membrane lipoprotein. *Genes Dev* 28(14):1620–1634.
8. Pandey SP, et al. (2014) Central role for RNase YbeY in Hfq-dependent and Hfq-independent small-RNA regulation in bacteria. *BMC Genomics* 15:121.
9. Peters JM, et al. (2012) Rho and NusG suppress pervasive antisense transcription in *Escherichia coli*. *Genes Dev* 26(23):2621–2633.
10. Snijder B, Liberali P, Frechin M, Stoeger T, Pelkmans L (2013) Predicting functional gene interactions with the hierarchical interaction score. *Nat Methods* 10(11):1089–1092.
11. Collins SR, Schuldiner M, Krogan NJ, Weissman JS (2006) A strategy for extracting and analyzing large-scale quantitative epistatic interaction data. *Genome Biol* 7(7):R63.
12. Szklarczyk D, et al. (2015) STRING v10: protein–protein interaction networks, integrated over the tree of life. *Nucleic Acids Res* 43(Database issue):D447–D452.
13. Salgado H, et al. (2013) RegulonDB v8.0: omics data sets, evolutionary conservation, regulatory phrases, cross-validated gold standards and more. *Nucleic Acids Res* 41(Database issue):D203–D213.
14. Cho S-H, et al. (2014) Detecting Envelope Stress by Monitoring β -Barrel Assembly. *Cell* 159(7):1652–1664.
15. Iwai N, Nagai K, Wachi M (2002) Novel S -Benzyliothiourea Compound That Induces Spherical Cells in *Escherichia coli* Probably by Acting on a Rod-shape-determining

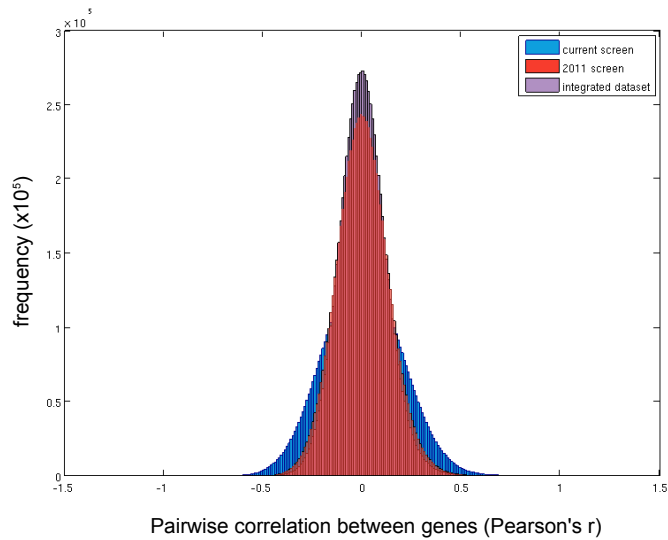
- Protein(s) Other Than Penicillin-binding Protein 2. *Biosci Biotechnol Biochem* 66(12):2658–2662.
16. Samaluru H, SaiSree L, Reddy M (2007) Role of SufI (FtsP) in Cell Division of *Escherichia coli*: Evidence for Its Involvement in Stabilizing the Assembly of the Divisome. *J Bacteriol* 189(22):8044–8052.
 17. Guthrie C, Nashimoto H, Nomura M (1969) STRUCTURE AND FUNCTION OF *E. coli* RIBOSOMES, VIII. COLD-SENSITIVE MUTANTS DEFECTIVE IN RIBOSOME ASSEMBLY*. *Proc Natl Acad Sci U S A* 63(2):384–391.
 18. Jiang M, et al. (2006) The *Escherichia coli* GTPase CgtAE Is Involved in Late Steps of Large Ribosome Assembly. *J Bacteriol* 188(19):6757–6770.
 19. Polissi A, et al. (2003) Changes in *Escherichia coli* transcriptome during acclimatization at low temperature. *Res Microbiol* 154(8):573–580.
 20. Etchegaray J-P, Jones PG, Inouye M (1996) Differential thermoregulation of two highly homologous cold-shock genes, *cspA* and *cspB*, of *Escherichia coli*. *Genes Cells* 1(2):171–178.
 21. Wilson DN (2009) The A–Z of bacterial translation inhibitors. *Crit Rev Biochem Mol Biol* 44(6):393–433.
 22. Haseltine WA, Block R (1973) Synthesis of Guanosine Tetra- and Pentaphosphate Requires the Presence of a Codon-Specific, Uncharged Transfer Ribonucleic Acid in the Acceptor Site of Ribosomes. *Proc Natl Acad Sci* 70(5):1564–1568

Supplementary Information

Supplementary Figure 1

**Supplementary Figure 1 Between-screen correlation is associated with the number of conditional-phenotypes.**

Number of phenotypes for a repeated condition (lesser between the current and 2011 dataset) is plotted against the correlation between the two screens.

Supplementary Figure 2

Supplementary Figure 2: The smaller dataset suffers from a wider distribution of pairwise correlations.

Histograms of the distributions of pairwise correlations for the current, 2011, and integrated datasets. Bin size is 0.01.

Supplementary Table 1: Conditions included in the current library

New conditions tested against the E. coli K-12 KEIO library		
Condition [Concentration]	Measurements (3994)	Phenotype Rate (FDR 1%)
Toxic analogues		
M9 minimal glucose 5-fluorouridine [250 ng/mL]	3950	5.8%
M9 minimal glucose 5-methylanthranilic acid [20 µg/mL]	3877	6.4%
M9 minimal glucose 5-methyltryptophan [20 µg/mL]	3961	5.5%
M9 minimal glucose 7-azatryptophan [5 µg/mL]	3152	5.6%
M9 minimal glucose 7-azatryptophan [14 µg/mL]	1893	6.3%
tRNA Synthetase Inhibitors		
D,L-serine hydroxamate [600 µg/mL]	3991	3.4%
pseudomonic acid A [36 µg/mL]	3868	1.8%
Organic Solvents and Chaotropes		
DMSO [9.5% (v/v)]	3927	1.6%
guanidine hydrochloride [30 mM]	3883	1.4%
urea [320 mM]	3783	1.0%
urea [750 mM]	3230	1.6%
Bisguanates		
chlorhexidine [5 µg/mL]	3781	1.4%
Dicarboxylic acids		
azelaic acid [1 mg/mL]	2561	2.9%
Thiopyrrolones		
gliotoxin [10 µg/mL]	3928	2.9%
gliotoxin [10 µg/mL]	3953	3.2%
holomycin [2.5 µg/mL]	3887	2.9%
thiolutin [7 µg/mL]	3970	2.3%
Commercial Disinfectants		
iodine [0.75% (v/v)]	3716	3.8%
bleach [1% (v/v)]	3868	2.1%
Alcohols		
isopropanol [5% (v/v)]	1877	2.9%
n-butanol [1% (v/v)]	2529	3.0%
t-butanol [5% (v/v)]	3809	1.7%
isopentanol [0.5% (v/v)]	3198	1.5%
phenol [0.1% (v/v)]	3813	3.0%
Translation Inhibitors		
kasugamycin [20 µg/mL]	3982	2.3%
blasticidin S [33 µg/mL]	3992	1.6%
clindamycin [64 µg/mL]	3804	2.7%
Toxic Ions		
silver(II) [1 µM]	3910	1.7%
sodium fluoride [100 mM]	3735	1.6%
Cold Shock		
cold [10° C]	3339	2.3%
cold [25° C]	3881	2.2%
4° C survival [5 wk]	2629	3.9%
heat [39° C]	687	0.7%
Nutrient Source		
M9 minimal glucose + casamino acids [0.2% (w/v)+0.4% (w/v)]	3936	5.1%

Gyrase Inhibitor		
cinoxacin [3 µg/mL]	2019	2.6%
cinoxacin [6 µg/mL]	1912	2.6%
Combination Treatment		
cold+UV [10° C+12 sec]	3145	2.5%
M9 minimal glucose+UV [0.2% (w/v)+12 sec]	3901	5.6%
Conditions That Overlap with the 2011 Screen		
Condition [Concentration]	Measurements (3994)	Phenotype Rate (FDR 1%)
MreB inhibitor		
A22 [5 µg/mL]	3951	3.4%
β-lactam		
amoxicillin [1.5 µg/mL]	3954	2.7%
ampicillin [4 µg/mL]	3297	3.5%
ampicillin [4 µg/mL]	3813	2.1%
Envelope Stress		
SDS [1% (w/v)]	3979	2.8%
SDS [1% (w/v)]	3847	1.9%
bile salts [2% (w/v)]	3937	3.4%
deoxycholate [1% (w/v)]	3786	2.7%
EDTA [1 mM]	3903	3.0%
EDTA [1 mM]	3863	3.2%
SDS+EDTA [0.5% (w/v)+500 µM]	3962	3.6%
Nutrient Source		
M9min glucose [0.2% (w/v)]	3991	5.6%
M9min glucose [0.2% (w/v)]	3954	5.5%
M9min glucose [0.2% (w/v)]	3922	4.6%
M9min acetate [0.6% (w/v)]	1997	5.2%
Transcription Inhibitor		
rifampicin [4 µg/mL]	3986	4.8%
bicyclomycin [20 µg/mL]	3308	4.0%
DNA Damage		
pyocyanin [10 µg/mL]	3280	4.1%
acriflavine [10 µg/mL]	705	3.1%
UV [12 sec]	3904	1.2%
Gyrase Inhibitor		
ciprofloxacin [1 ng/mL]	3912	1.6%
Translation Inhibitors		
spectinomycin [4 µg/mL]	3744	1.3%
streptomycin [50 ng/mL]	3874	0.6%
tetracycline [500 ng/mL]	3928	3.0%
theophylline [500 µg/mL]	3819	1.8%
Toxic Ions		
copper(II) [2 mM]	3746	1.7%

Measurements: Number of deletion-strain colony sizes measured in a particular condition (out of 3994 possible). Conditions that had more than 75% of strains measured are bolded.

Phenotype Rate: The percentage of measured colony sizes that were determined to have a phenotype, at an FDR rate of 1%.

Supplementary Table 2: Cold-shock phenotypes at 10°C

gene	accession	GO term (translation-related)	cold-shock/ribosome reference	phenotype at 10	10C fitness score	10C opacity-fraction	phenotype at 16	16C fitness score	16C opacity-fraction
istR-1	ECK5002	GO:0006417	-	YES	12.9	33%	NO	NaN	NaN
ymcE	ECK0981		(1)	YES	-9.0	43%	NO	-1.0	87%
pheT-SPA	ECK1711	GO:0006412	-	YES	-7.5	50%	NO	NaN	NaN
crr	ECK2412		-	YES	-7.2	50%	NO	-0.9	83%
smpB	ECK2616	GO:0006414	-	YES	-6.9	45%	NO	-1.8	80%
rbfA	ECK3156		(2)	YES	-6.8	25%	NO	NaN	NaN
dnaB-SPA	ECK4044		-	YES	-6.7	60%	NO	NaN	NaN
dcrB	ECK3456		-	YES	-6.4	63%	NO	-1.0	92%
dnaA-SPA	ECK3694		(3)	YES	-6.1	69%	NO	NaN	NaN
ihfB	ECK0903	GO:0006417	-	YES	-6.0	53%	NO	0.2	100%
fusA-SPA	ECK3327	GO:0006412, GO:0006414	-	YES	-5.5	60%	NO	NaN	NaN
ihfA	ECK1710	GO:0006417	-	YES	-5.5	53%	NO	-0.7	88%
dnaJ	ECK0015		-	YES	-5.1	63%	NO	-1.8	85%
spr	ECK2169		-	YES	-5.1	65%	NO	-0.4	99%
cbrC	ECK3710			YES	-4.9	67%	NO	0.4	110%
sdhA	ECK0712		-	YES	-4.9	52%	NO	0.1	99%
nfuA	ECK3401		-	YES	-4.7	62%	NO	-1.4	83%
lipB	ECK0623		-	YES	-4.3	63%	NO	NaN	NaN
ahpC	ECK0599		-	YES	-4.0	67%	NO	-1.6	86%
rpsF	ECK4196	GO:0006412	(4)	YES	-4.0	41%	NO	-0.5	79%
aroK	ECK3377		-	YES	-3.9	62%	NO	NaN	NaN
racC	ECK1348		-	YES	-3.9	73%	NO	-0.6	93%
rnhA	ECK0214		(5)	YES	-3.8	69%	NO	-1.1	84%
yjgZ	ECK4267		-	YES	-3.5	78%	NO	1.6	116%
rluD	ECK2592		(6)	YES	-3.5	70%	NO	-1.5	74%
fliQ	ECK1947		-	YES	-3.5	75%	NO	-0.3	97%
fliF	ECK1936		-	YES	-3.4	77%	NO	0.1	102%
yhbJ	ECK3194		-	YES	-3.4	75%	NO	-0.4	99%
bamA{dup(218-219)}	ECK0176		-	YES	-3.3	48%	NO	NaN	NaN
frr-SPA	ECK0171	GO:0006412	-	YES	-3.1	71%	NO	NaN	NaN
der-SPA	ECK2507		(7)	YES	-3.1	70%	NO	NaN	NaN
rpmG	ECK3626	GO:0006412	-	YES	-3.1	72%	NO	-1.3	84%
rpiR	ECK4082		-	YES	-3.1	78%	NO	-0.5	94%
malT	ECK3405		-	YES	-2.9	82%	NO	0.4	104%
fepE	ECK0580		-	YES	-2.9	80%	NO	0.1	103%
gapA-SPA	ECK1777		-	YES	-2.9	83%	NO	NaN	NaN
apaH	ECK0050		-	YES	-2.9	79%	NO	-0.3	98%
rffM	ECK3787		-	YES	-2.9	78%	NO	-1.1	89%
dam	ECK3374		-	YES	-2.9	82%	NO	NaN	NaN

mukE-SPA	ECK0914		-	YES	-2.9	32%	NO	NaN	NaN	
glmS-SPA	ECK3722		-	YES	-2.9	63%	NO	NaN	NaN	
yjgH	ECK4242		-	YES	-2.8	79%	NO	-0.6	97%	
cspB	ECK1551		(8)	YES	-2.8	79%	NO	-0.4	97%	
yqeB	ECK2871		-	YES	-2.8	79%	NO	0.0	99%	
glgB	ECK3418		-	YES	-2.8	73%	NO	-1.1	84%	
yhcO	ECK3228		-	YES	-2.8	82%	NO	-0.4	97%	
hipA	ECK1500		-	YES	-2.7	77%	NO	-0.4	99%	
cpxA	ECK3904		-	YES	-2.7	77%	NO	-0.7	95%	
pstS	ECK3721		-	YES	-2.7	75%	NO	0.7	105%	
surA	ECK0054		-	YES	-2.7	57%	NO	0.1	84%	
kgtP	ECK2585		-	YES	-2.7	84%	NO	NaN	NaN	
rfe	ECK3776		-	YES	-2.7	80%	NO	-1.1	90%	
yggX	ECK2957		-	YES	-2.7	79%	NO	-1.1	87%	
murD-SPA	ECK0089		-	YES	-2.6	85%	NO	NaN	NaN	
fabF	ECK1081		-	YES	-2.6	82%	NO	-1.4	83%	
prfC	ECK4366	GO:0006412, GO:0006415, GO:0006417	-	YES	-2.6	77%	NO	NaN	NaN	
sixA	ECK2334		-	YES	-2.5	80%	NO	-0.3	94%	
tam	ECK1512		-	YES	-2.5	82%	NO	-0.5	97%	
dadA	ECK1177		-	YES	-2.5	83%	NO	-0.6	95%	
typA	ECK3864	GO:0006412	(9)	YES	-	11.7	30%	YES	-4.8	62%
deaD	ECK3150	GO:0006417	(10)	YES	-6.4	51%	YES	-5.3	48%	
ptsN	ECK3193		-	YES	-6.0	58%	YES	-1.9	75%	
yjgA	ECK4229		(12)	YES	-5.9	52%	YES	-3.2	66%	
rsmA	ECK0052		(11)	YES	-4.1	72%	YES	-2.5	68%	
rpmE	ECK3928	GO:0006412	-	YES	-3.0	78%	YES	-2.4	70%	
gmm	ECK2045		-	NO	-2.1	85%	YES	-2.1	84%	
rnIB	ECK2627		-	NO	-0.9	91%	YES	-3.4	63%	
fpr	ECK3916		-	NO	-0.7	93%	YES	-2.0	79%	
yaiS	ECK0361		-	NO	-0.5	94%	YES	-2.1	71%	
yjfY	ECK4195		-	NO	-0.1	100%	YES	-2.3	77%	
cpsG	ECK2042		-	NO	0.0	94%	YES	-2.8	67%	
fis	ECK3248		-	NO	0.2	106%	YES	-2.3	70%	
yfdG	ECK2344		-	NO	NaN	NaN	YES	-2.6	76%	
yfcA	ECK2321		-	NO	NaN	NaN	YES	-3.1	34%	
ycbC	ECK0911		-	NO	NaN	NaN	YES	-1.8	77%	
dinJ	ECK0227		-	NO	NaN	NaN	YES	-2.1	71%	
dedD	ECK2308		-	NO	NaN	NaN	YES	-2.1	54%	
secB	ECK3599		-	NO	NaN	NaN	YES	-5.6	47%	

Supplementary References

1. Polissi A, et al. (2003) Changes in *Escherichia coli* transcriptome during acclimatization at low temperature. *Res Microbiol* 154(8):573–580.
2. Dammel CS, Noller HF (1995) Suppression of a cold-sensitive mutation in 16S rRNA by overexpression of a novel ribosome-binding factor, RbfA. *Genes Dev* 9(5):626–637.
3. Guo L, Katayama T, Seyama Y, Sekimizu K, Miki T (1999) Isolation and characterization of novel cold-sensitive *dnaA* mutants of *Escherichia coli*. *FEMS Microbiol Lett* 176(2):357–366.
4. Britton RA, Lupski JR (1997) Isolation and Characterization of Suppressors of Two *Escherichia coli* *DnaG* Mutations, *DnaG2903* and *ParB*. *Genetics* 145(4):867–875.
5. Massé E, Drolet M (1999) R-loop-dependent hypernegative supercoiling in *Escherichia coli* *topA* mutants preferentially occurs at low temperatures and correlates with growth inhibition. *J Mol Biol* 294(2):321–332.
6. Raychaudhuri S, Conrad J, Hall BG, Ofengand J (1998) A pseudouridine synthase required for the formation of two universally conserved pseudouridines in ribosomal RNA is essential for normal growth of *Escherichia coli*. *RNA* 4(11):1407–1417.
7. Hwang J, Inouye M (2006) The tandem GTPase, *Der*, is essential for the biogenesis of 50S ribosomal subunits in *Escherichia coli*. *Mol Microbiol* 61(6):1660–1672.

8. Etchegaray J-P, Jones PG, Inouye M (1996) Differential thermoregulation of two highly homologous cold-shock genes, *cspA* and *cspB*, of *Escherichia coli*. *Genes Cells* 1(2):171–178.
9. Choudhury P, Flower AM (2015) Efficient Assembly of Ribosomes Is Inhibited by Deletion of *bipA* in *Escherichia coli*. *J Bacteriol* 197(10):1819–1827.
10. Charollais J, Dreyfus M, Iost I (2004) *CsdA*, a cold-shock RNA helicase from *Escherichia coli*, is involved in the biogenesis of 50S ribosomal subunit. *Nucleic Acids Res* 32(9):2751–2759.
11. Connolly K, Rife JP, Culver G (2008) Mechanistic insight into the ribosome biogenesis functions of the ancient protein *KsgA*. *Mol Microbiol* 70(5):1062–1075.
12. Jiang M, et al. (2006) The *Escherichia coli* GTPase *CgtAE* Is Involved in Late Steps of Large Ribosome Assembly. *J Bacteriol* 188(19):6757–6770.

Chapter 2

Illicit transport in *Escherichia coli* and beyond

Contributing Authors:

Hendrik Osadnik, George Kritikos, Bo Li, Nevan Krogan, Athanasios Typas, Carol Gross

Citations:

Shiver AL, Osadnik H, Kritikos G, Li B, Krogan NJ, Typas A, Gross CA Illicit transport of antibacterial compounds revealed by an expanded chemical-genomic dataset of *E. coli* (in preparation)

By investigating new features in the integrated dataset, we discovered and characterized an illicit transport mechanism for kasugamycin and blasticidin S. The compounds are illicitly transported through two prominent peptide ABC-importers in *Escherichia coli*. Blasticidin S is imported through oligopeptide permease (Opp) and Kasugamycin is imported through both Opp and dipeptide permease (Dpp). Kasugamycin has recently been approved by the EPA for treatment of *Erwinia amylovora*, a bacterial phytopathogen that causes fire blight. Loss of peptide ABC-importer function may be the first resistance mechanism to treatment and the identification of this mechanism may allow for rapid assessment of drug resistance and better antibiotic stewardship.

Two peptide permeases determine the susceptibility of *E. coli* K-12 to kasugamycin and blasticidin S.

Kasugamycin (Ksg), an aminoglycoside, and blasticidin S (BcS), an aminonucleoside, are translation inhibitors. Ksg has an amidine group within the kasugamycin-tail and Bcs has a guanidine group in its blastidic acid moiety (**Figure 1A, features highlighted**). Oligopeptide permease (Opp) and Dipeptide permease (Dpp) are two of the major import machineries for peptides in *E. coli* and *S. typhimurium* (1–3). Dpp is specific for dipeptides (4) while Opp can import peptides less than 5 amino acids in length (5). Opp and Dpp share a similar protein complex and operon structure that is generally conserved among the peptide permeases of gram negative bacteria, reviewed in (6) (**Figure 1B**). A periplasmic binding protein (PBP) freely diffuses in the periplasm (*geneA*). The PBP binds peptides and delivers them to the transmembrane domains (TMD) of its cognate pore, encoded by *geneB* and *geneC*. The cytoplasmic nucleotide-binding domain (NBD) subunits then energize transport into the cytoplasm (*geneD*, *geneF*).

Figure 1

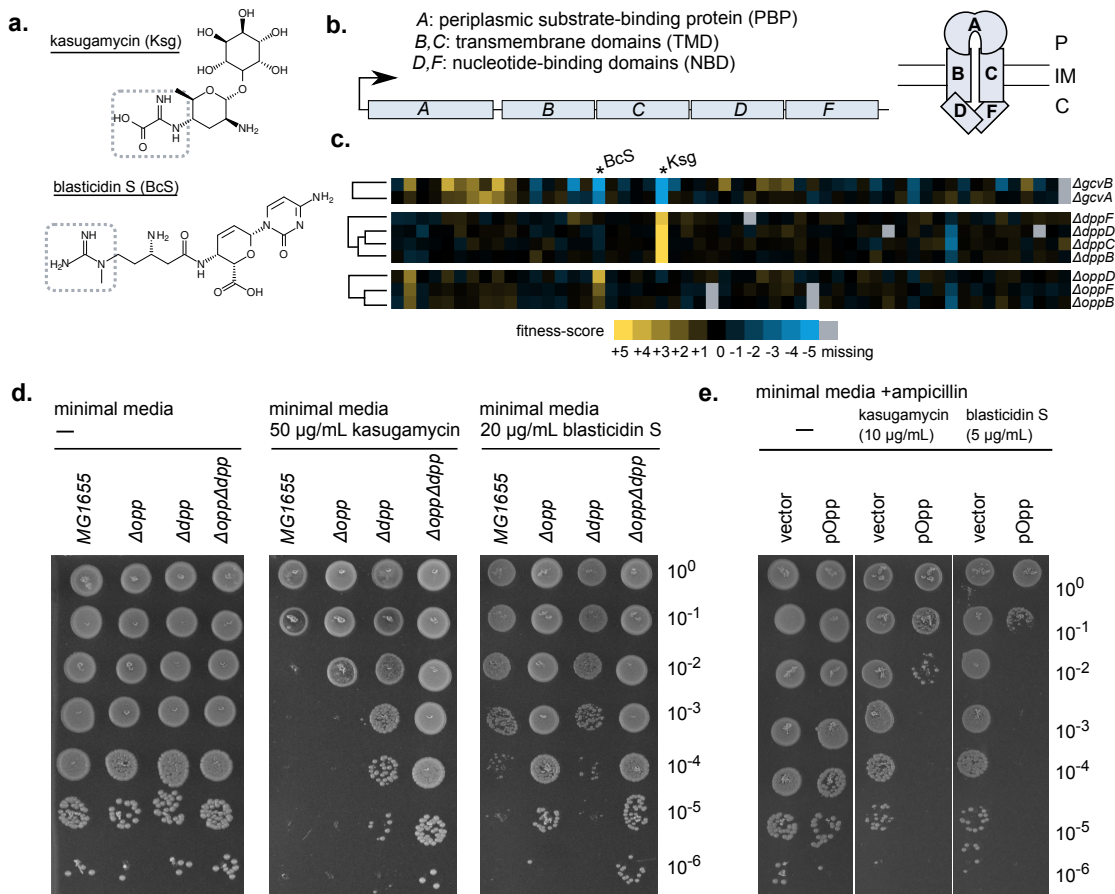


Figure 1: Peptide permeases determine kasugamycin and blasticidin S susceptibility in *E. coli* K-12.

(a) Structures of kasugamycin and blasticidin S. Imine containing groups are highlighted for each drug. **(b)** Generalized operon and complex structure of Opp and Dpp. Operon (left) and complex (right) structures of the peptide permeases. The letter reflects the gene/protein name for either operon (A: oppA/dppA OppA/DppA). P: periplasm, IM: inner membrane, C: cytoplasm. **(c)** Peptide permease deletions are resistant to kasugamycin and blasticidin S in the screen. Heat-map of fitness scores for hierarchical clusters of Dpp, Opp, and the negative regulators GcvA,B. Kasugamycin (Ksg) and blasticidin S (BcS) are highlighted. **(d)** Peptide permease deletions show an increase in MIC to Ksg and BcS. 10-fold spot dilutions are shown for operon deletions Δopp , Δdpp and the double mutant $\Delta opp\Delta dpp$. **(e)** Overexpression of Opp results in a decrease in the MIC of Ksg and BcS. 10-fold spot dilutions are shown for the opp operon cloned into pTrc99a (pOpp) and an empty vector control (vector). Basal expression of opp from pTrc99a (no induction) is sufficient to decrease the MIC to both Ksg and BcS.

Data from our current screen revealed a potential connection between Ksg, BcS, and the two peptide permeases Opp and Dpp (**Figure 1C**). Single gene deletions of the four Dpp genes encoding the pore and ABC-subunits ($\Delta dppB,C,D,F$) clustered due to shared resistance to Ksg. Likewise, deletions of three Opp subunits clustered ($\Delta oppB,D,F$) with a clear resistance to BcS. Negative regulators of Opp and Dpp expression ($\Delta gcvB$, Δhfq , and $\Delta gcvA$) shared sensitivities to Ksg and BcS. These results implied a proportional relationship between peptide permease expression and sensitivity to Ksg and BcS. This was particularly interesting because of a recurring and similar association between expression of OppA (the PBP of the Opp complex) and aminoglycoside sensitivity in *E. coli* K-12 (7–9).

We investigated these phenotypes further using clean deletion mutants of each operon (Δopp and Δdpp) constructed in an independent background. Given the original observations of drug efficacy for both kasugamycin and blasticidin S (10, 11), we moved from rich media, as used in the screen, to minimal media buffered at a neutral pH of 7.5. Spot dilutions revealed that the deletion strains grew equivalently to the WT strain in minimal media, but were resistant to Ksg and BcS (**Figure 1C**). Both Δopp and Δdpp were more resistant to Ksg than the WT strain. The effect of the two deletions were additive, as the $\Delta dpp \Delta opp$ double mutant was more resistant than either single mutant alone. For BcS, Δopp alone was sufficient to confer high-level resistance. Finally, we confirmed that overexpression of the entire Opp operon from a plasmid (pOpp), was sufficient to confer sensitivity to both drugs (**Figure 1D**).

We hypothesized that Opp directly imported BcS, while both Dpp and Opp together directly imported Ksg. This model explained the observed mutant susceptibilities as well as the increased potency of the drugs in defined media, due to increased expression of both Opp and Dpp (12, 13). In contrast to these encouraging observations, expression of oligopeptide permease has

repeatedly been associated with resistance to the larger aminoglycoside family in which Ksg resides (7–9, 14) but tests for a direct effect of the Opp system on aminoglycoside import have been negative (15). Furthermore, while these systems are known for non-selective uptake, neither Ksg nor BcS is structurally similar to verified substrates of these two permeases. We therefore experimentally tested whether Ksg and BcS were directly imported by the peptide permeases Opp and Dpp.

Opp and Dpp directly import kasugamycin and blasticidin S.

Both Ksg and BcS bind the ribosome and inhibit translation. Assuming that entry into the cytoplasm is the rate-limiting step for drug action, we reasoned that an *in vivo* assay quantifying the shutdown rate of translation after drug treatment would serve as an acceptable proxy for the kinetics of drug import. We quantified translation rate by measuring ³⁵S-methionine (³⁵S-Met) incorporation into a TCA insoluble fraction and followed the decreasing rate of incorporation after addition of the drugs. When treated with saturating concentrations of either Ksg (**Figure 2A**) or BcS (**Figure 2B**), WT *E. coli* K-12 exhibited a rapid decrease in ³⁵S-Met incorporation on the scale of minutes. The decay rate of ³⁵S-Met incorporation in the presence of Ksg was best fit with a double exponential (**Figure 2A**). Ksg specifically inhibits translation initiation (16) and the slow term may be a result of translation runoff. Importantly, the rate of translation shutdown for both drugs was 7 to 10-fold slower in the permease deletion strains as compared to WT (**Figure 2A, B**). Conversely, although less striking in magnitude, the rate of translation shutdown by kasugamycin was significantly faster when the *opp* operon was overexpressed (p=0.02 Student's t-test) (**Supplementary Figure 1**). These results connected the observed drug sensitivities with a clear uptake phenotype. Deleting the Dpp and Opp permeases decreases the rate of import of the drugs, whereas overexpressing the *opp* operon has the converse effect.

Figure 2

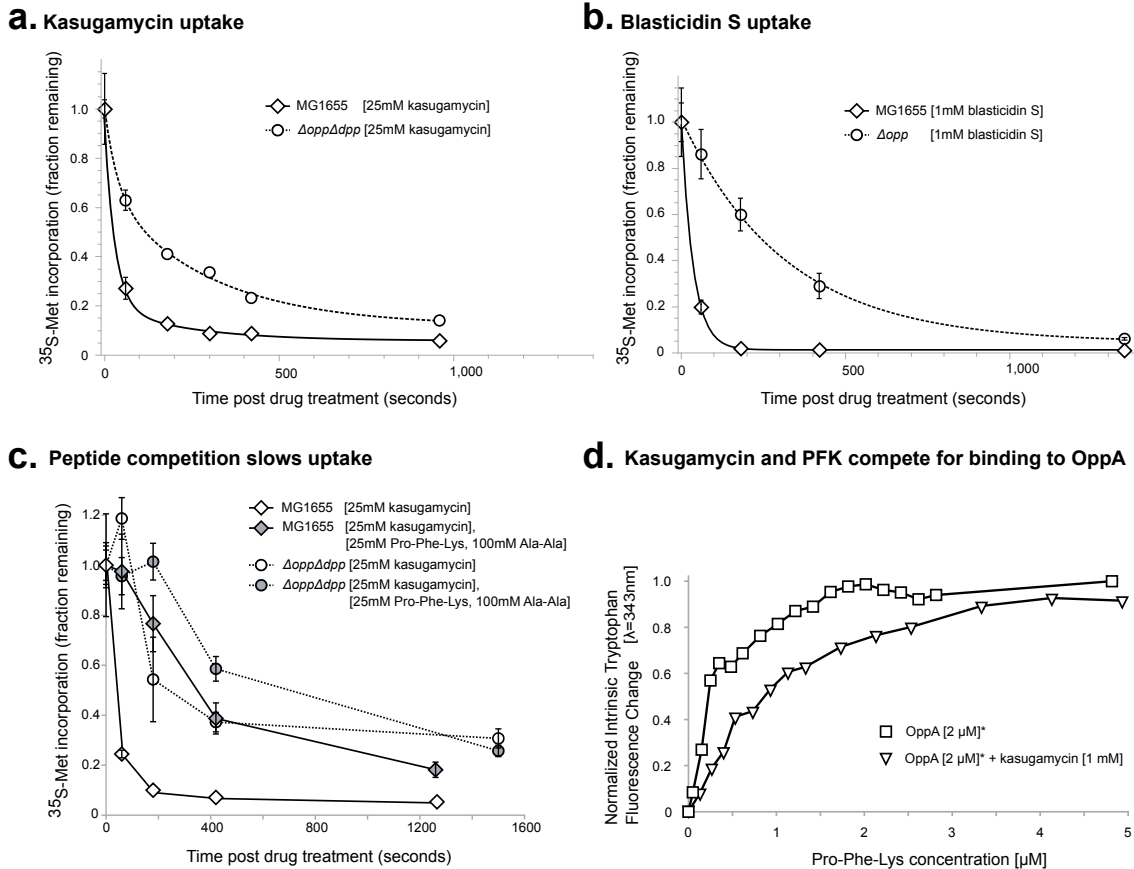


Figure 2: Opp and Dpp directly import kasugamycin and blasticidin S

(a-c) Prolonged shutdown kinetics of ^{35}S -methionine incorporation reflect reduced uptake rates. Error bars represent standard deviation of technical replicates ($n=3$). Each experiment was repeated with at least one biological replicate, with similar results. Data fit with double exponential (a) and single exponential (b) decay functions. (d) PFK binding to OppA induces an increase in intrinsic tryptophan fluorescence, as measured at 343nm. Kasugamycin [1mM] increases the effective concentration of PFK required to reach half-maximal fluorescence shift. (*) Reported concentrations do not take into account the active fraction.

We further tested if the peptide permeases were directly importing Ksg using two independent approaches. First, we used an *in vivo* substrate competition assay (**Figure 2C**) to test for the ability of Ksg to compete for uptake with high affinity substrates of Opp and Dpp. Indeed, when Ksg was co-administered with both Pro-Phe-Lys (PFK, a preferred Opp substrate) and Ala-Ala (AA, a preferred Dpp substrate), the rate of translation inhibition by Ksg was slowed dramatically, approximating that of the $\Delta dpp\Delta opp$ double mutant strain. In contrast, the uptake rate in a $\Delta dpp\Delta opp$ strain was insensitive to the addition of competitors. This is consistent with Ksg being directly imported by Opp and Dpp *in vivo*.

Second, we used an *in vitro* binding assay to show that Ksg bound competitively to purified OppA. We expressed and purified OppA-6XHis and tested for Ksg binding using intrinsic tryptophan fluorescence. The OppA binding site contains multiple tryptophan residues and changes in fluorescence signal have been used for binding measurements of many peptide substrates of OppA. Addition of 1 mM Ksg markedly increased the apparent K_D of OppA for its high-affinity substrate PFK (**Figure 2D**). This is consistent with competitive binding between Ksg and PFK. While Ksg did not directly alter the intrinsic tryptophan fluorescence of OppA, this is likely due to different binding modes for peptides as compared to the antibiotic. A different, less specific mode of binding is also in agreement with the lower affinity of Ksg compared to peptide substrates in our *in vivo* and *in vitro* assays. Taken together, these experiments provide strong support for a model in which Opp and Dpp directly import Ksg and BcS in *E. coli* K-12.

Opp and Dpp work independently to import Ksg

There are multiple demonstrations of distinct PBPs delivering substrates to the same pore for import (17). This includes MppA, a PBP that interacts with both the Opp and Dpp pores to

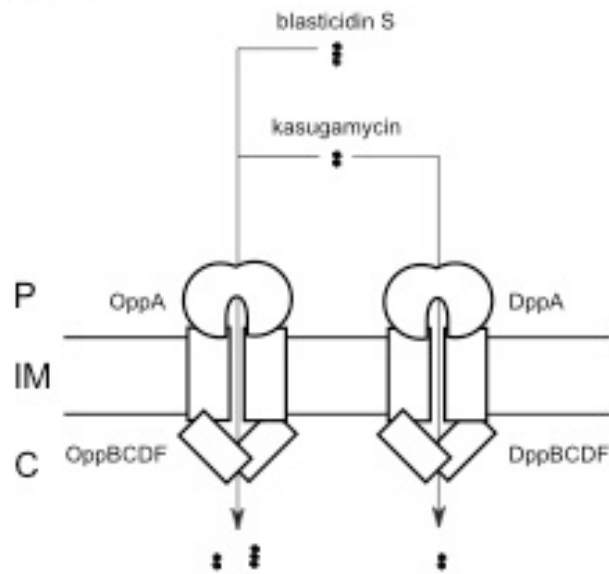
deliver different substrates (18, 19), a phenomenon we refer to as PBP-crosstalk. Given the apparent cooperation of the Opp and Dpp systems during Ksg import, we were interested in testing whether PBP-crosstalk played a role in this process. We used MIC changes to examine genetic interactions within and between the two ABC-importers. There were two possible results. If PBP-crosstalk did occur (more than 1 PBP delivers the antibiotic to the same pore) deleting the TMDs would have had a stronger effect than deleting the PBPs, as the PBP functions would have been redundant. If no PBP-crosstalk occurred, deleting the PBP, the pore, or both would have given an equivalent resistance change (an epistatic interaction). As an example, deletion of the Opp PBP ($\Delta oppA$), TMD ($\Delta oppB$), or entire complex (Δopp) conferred the same high level of resistance to BcS, an epistatic interaction between the PBP and pore of Opp (**Figure 3A**). This allows us to conclude that import through OppA/OppBCDF is the major entry point of BcS into *E. coli* K-12 in defined media (**Figure 3B**).

For Ksg, both Opp and Dpp must be inactivated for higher-level resistance. Double mutants of both PBPs ($\Delta oppA\Delta dppA$) and both TMDs ($\Delta oppB\Delta dppB$) resulted in an equivalent 4-fold increase in MIC to the entire operon double mutants ($\Delta opp\Delta dpp$), indicating that only OppA and DppA were involved in transport for these two complexes (**Figure 3A**). Similar to BcS import, an epistatic interaction between the PBP and TMD of Opp for Ksg sensitivity indicated that only OppA interacts with the Opp pore during Ksg import. The MIC changes of Dpp mutants were less than 2-fold in these broth-dilution assays. However, the epistatic interactions of Dpp mutants in an opp- background indicate that PBP-crosstalk does not occur at the Dpp complex, and we conclude that Dpp and Opp work without PBP-crosstalk to independently import Ksg in *E. coli* K-12 (**Figure 3B**).

Figure 3

a. Genetic interactions of permease subunits

	minimal media	
	kasugamycin	blasticidin S
<i>E. coli</i> K-12 MG1655	50 µg/mL	3-4 µg/mL
<i>Δopp</i>	100 µg/mL	60 µg/mL
<i>ΔoppA</i>	100 µg/mL	60 µg/mL
<i>ΔoppB</i>	100 µg/mL	60 µg/mL
<i>Δopp Δdpp</i>	200 µg/mL	60 µg/mL
<i>ΔoppA ΔdppA</i>	200 µg/mL	60 µg/mL
<i>ΔoppB ΔdppB</i>	200 µg/mL	60 µg/mL

b. Import model**Figure 3: OppA and DppA work with their cognate pores**

(a) Genetic interactions of permease complex subunits. MICs of kasugamycin and blasticidin S were determined with a 2-fold broth dilution method. Bold font indicates resistance to the drug treatment. **(b)** Import model. OppA delivers both kasugamycin and blasticidin S to the Opp pore for import, DppA delivers kasugamycin to the Dpp pore.

Opp is indirectly associated with aminoglycoside resistance in *E. coli* K-12

Despite the clear association of OppA levels with aminoglycoside resistance, direct tests of $\Delta oppA$ found no change in resistance (9), contradicting a model in which aminoglycosides are illicitly transported through oligopeptide permease. Given our clear results that MIC changes of Ksg and BcS were more pronounced in defined media than rich, and that the reported effects of $\Delta oppA$ were measured in rich media, we sought to revisit the direct connection between Opp and aminoglycoside import.

We first confirmed that, like Ksg, aminoglycosides were much more effective against *E. coli* K-12 in defined media. To our surprise, we also found a clear though small increase in the MIC of Δopp for multiple members of the aminoglycoside family (**Figure 4A**). However, we found that the double mutant $\Delta opp\Delta dpp$ lost the small resistance gained by Δopp alone (**Figure 4A**). Further deletion of any of the remaining peptide permeases Yej, Ddp, and Sap did not restore resistance (**Figure 4B**). Finally, neither $\Delta oppA$ nor $\Delta oppB$ recapitulated the resistance of the full operon deletion (**Figure 4C**). We note that in the construction of Δopp we also removed DNA upstream of *oppA*, including an uncharacterized sRNA RNA0-359 (20) that resided within the deletion boundaries. One early study that identified aminoglycoside resistance in a strain carrying a nonsense mutation in OppA also reported a transition mutation within GO-10697 in the same strain (8) and earlier attempts to replace OppA with a kan^R cassette used imprecise boundaries that could conceivably have also removed GO-10697 (7). This may explain the discrepant results from the precise deletions of *oppA* (9).

While we discuss one possible explanation for these results, they directly support the conclusion of Nakamatsu *et al.* While mutations in the *opp* operon can have an effect on susceptibility to a wide range of aminoglycosides, this phenomenon is indirect. Opp and Dpp illicitly transport BcS and Ksg, but do not import the wider family of aminoglycosides.

Discussion

The rational design of antibiotics that use illicit transport for drug entry was demonstrated soon after the discovery and characterization of oligopeptide permease (21), and has remained an interesting possibility for multiple import complexes (22, 23). The discovery of illicit transport of kasugamycin through the peptide permeases could facilitate further efforts to design trojan horse compounds that hijack Dpp and Opp for import. Together with heme (19) and blasticidin S, structure-function studies on these non-canonical substrates may identify a common motif

Figure 4

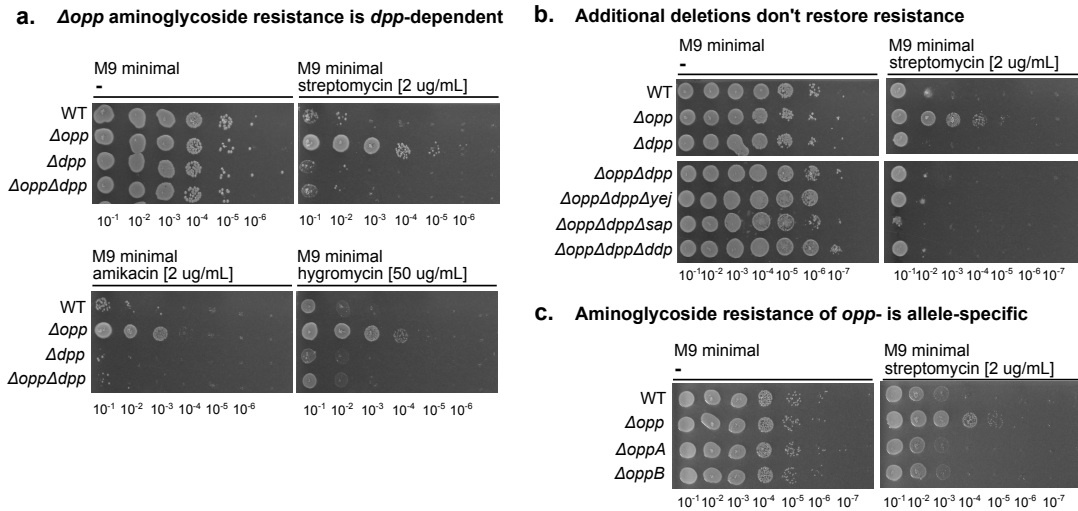


Figure 4: Opp indirectly affects aminoglycoside resistance.

(a-c) 10-fold spot dilutions on minimal media with drug after 24 hours of growth. At least one biological replicate was run for each interaction, with similar results. (a) Δopp is resistant to the family of aminoglycosides, but $\Delta opp\Delta dpp$ is not. (b) Additional deletions of peptide ABC-importers do not restore resistance to a $\Delta opp\Delta dpp$ mutant. (c) Aminoglycoside resistance is specific to the full operon deletion allele.

that can provide the affinity necessary for illicit transport through the peptide permeases. While kasugamycin and blasticidin S both show a wide variation in susceptibility between species, this specificity could prove useful for targeted therapies against susceptible pathogens, like *Pseudomonas aeruginosa*(24)

The characterization of illicit transport pathways for kasugamycin and blasticidin S also highlight how little is known about the diversity of substrates, systems-level connections, and evolutionary conservation of the ABC-import systems of bacteria. In *E. coli* K-12 the Opp system alone imports BcS, while in *P. aeruginosa* PA14 the Npp and Dpp systems appear to cooperate in importing BcS (25). Further understanding of both the sequence determinants of

substrate binding and the functional connections between import systems will clearly be critical for dissecting these illicit transport pathways and predicting possible mechanisms of resistance in different species. It is especially interesting that, while ABC-importers are not present in eukaryota, kasugamycin and blasticidin S share activity against the fungus *Magneporthe oryzae* (10, 11). The common import pathway we demonstrated for these two drugs in *E. coli* may have non-homologous equivalents, or may have been horizontally transferred, across the domains of life.

Methods

Media, growth conditions, strains, plasmids, and oligos

Media for kasugamycin and blasticidin S sensitivity was M9 minimal supplemented with metal cations and buffered at pH 7.5 (M9 salts, 0.4% (w/v) glucose, 100 μ M magnesium sulfate, 100 μ M calcium chloride, 5 μ M iron(III) chloride, 20 mM Tris-HCl, pH 7.5). To promote high translation rates, media used for 35 S-methionine incorporation was MOPS EZ rich (-Met), 0.4% (w/v) glucose (Teknova M2101,M2102,M2103,M2109,G0520). All experiments subsequent to the chemical-genomics screen were conducted using strains of MG1655.

MIC determination

A liquid broth-dilution method was used to determine MIC values for the antibiotics. Fresh colonies were picked, resuspended in minimal media, and diluted to a final O.D.₄₅₀ of .0005. Antibiotics were added in a 1:2 dilution series spanning a 64-fold dilution range. After 24 hours of growth, 150 μ L of culture was transferred to a 96-well spectrophotometer plate, and the O.D.₄₅₀ was measured using a Varioskan spectrophotometer (Thermo electron corporation). After blank subtraction, culture densities were normalized to a no drug control, and the first

concentration at which normalized density fell below 10% was defined as the MIC of the drug. This quantitative measure corresponded well with a qualitative metric based on spinning down the cells and visually inspecting the size of cell pellet.

³⁵S-Methionine incorporation

Overnight cultures of relevant strains were grown inoculated into MOPS rich defined methionine dropout media (MOPS RDM-Met) at a starting O.D.₄₅₀ of .005 and grown to an O.D.₄₅₀ of 0.2. To quantify translation rate, 900 μ L of culture was added to 30 μ L of labeling mix (10 μ Ci L-³⁵S-methionine, 50 μ M cold L-methionine, in MOPS RDM-Met) (Easytag L-³⁵S-Methionine, Perkin Elmer Corp.), incubated for 1 min in the water bath, then quenched with 100 μ L of 50%(w/v) trichloroacetate (TCA) and stored on ice. A 100 μ L aliquot of the quenched reaction mixture was deposited on a glass fiber filter (Merck Millipore Ltd. APFC02500) and washed with 10% (w/v) TCA followed by 95% (v/v) ethanol. ³⁵S-methionine incorporation into the TCA-insoluble fraction was quantified with Beckman Coulter LS6500 multipurpose scintillation counter. To follow translation shutdown, saturating concentrations of translation inhibitors were added to growing cultures. Translation rate was quantified following addition of drug and normalized to a timepoint taken 2 minutes prior to drug treatment.

OppA purification and binding assays

The oppA gene from E. coli MG1655 was amplified and cloned into pBAD22 using NcoI and HindIII restriction enzymes. E. coli BW25113 was then transformed with the resulting plasmid, and over-production was induced in an exponentially growing culture at OD(260nm) of 0.6 by addition of 0.05% (w/v) arabinose. The purification, including partial unfolding of the protein to remove bound substrates, as well as the binding assays followed the protocol in (26). The changes made were clearing of the lysate for 1h at 140.000 g (Beckman L8-M ultracentrifuge),

using urea instead of guanidinium hydrochloride for partial unfolding of OppA, as well as adjusting the MES buffer pH to 6.7 instead of 6.0 during purification, as we found the protein to be more stable at this pH. OppA was highly concentrated and free of visible protein contaminations after Ni-IMAC as judged by SDS-PAGE and staining with Coomassie Blue, and was thus used in binding assays after extensive buffer exchange to remove the imidazole (Milipore Amicon Ultra centrifugation filters, 10,000 MWCO). The spectral characteristics of our purified OppA were identical to those reported previously. All Fluorescence assays (Fluoromax-3, Jobin Yvon Horiba) were performed in 20mM 4-morpholineethanesulfonic acid (pH 6.0) and 150mM NaCl, as described (26).

References

1. A J Sussman, Gilvarg C (1971) Peptide Transport and Metabolism in Bacteria. *Annu Rev Biochem* 40(1):397–408.
2. Abouhamad WN, Manson M, Gibson MM, Higgins CF (1991) Peptide transport and chemotaxis in *Escherichia coli* and *Salmonella typhimurium*: characterization of the dipeptide permease (Dpp) and the dipeptide-binding protein. *Mol Microbiol* 5(5):1035–1047.
3. Higgins CF, Hardie MM (1983) Periplasmic protein associated with the oligopeptide permeases of *Salmonella typhimurium* and *Escherichia coli*. *J Bacteriol* 155(3):1434–1438.
4. Manson MD, Blank V, Brade G, Higgins CF (1986) Peptide chemotaxis in *E. coli* involves the Tap signal transducer and the dipeptide permease. *Nature* 321(6067):253–256.
5. Payne JW, Gilvarg C (1968) Size Restriction on Peptide Utilization in *Escherichia coli*. *J Biol Chem* 243(23):6291–6299.

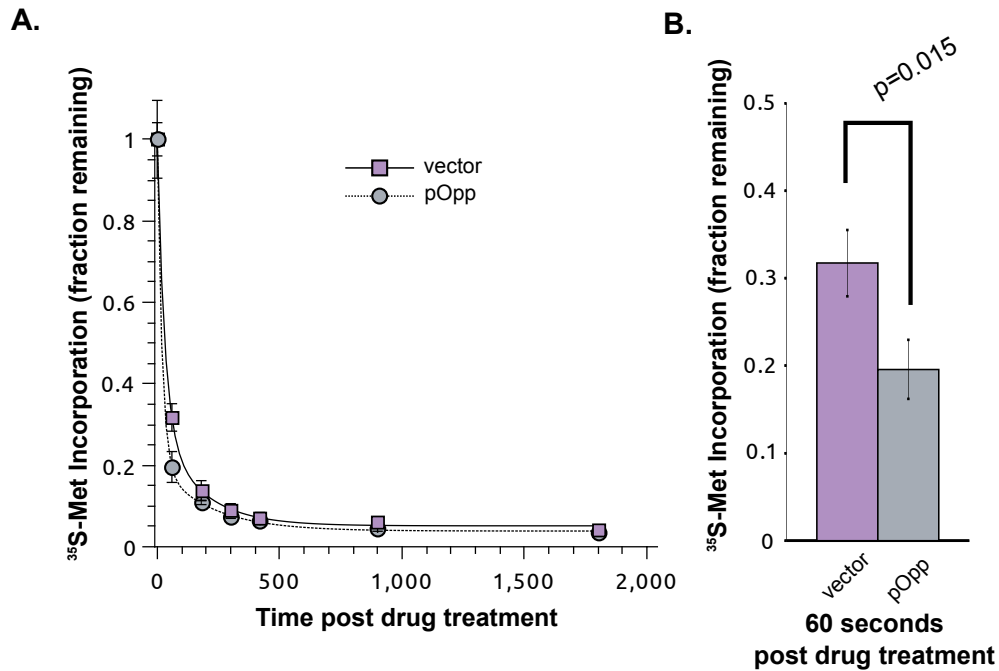
6. Berntsson RP-A, Smits SHJ, Schmitt L, Slotboom D-J, Poolman B (2010) A structural classification of substrate-binding proteins. *FEBS Lett* 584(12):2606–2617.
7. Kashiwagi K, et al. (1992) Increase of sensitivity to aminoglycoside antibiotics by polyamine-induced protein (oligopeptide-binding protein) in *Escherichia coli*. *J Bacteriol* 174(13):4331–4337.
8. Kashiwagi K, et al. (1998) Relationship between Spontaneous Aminoglycoside Resistance in *Escherichia coli* and a Decrease in Oligopeptide Binding Protein. *J Bacteriol* 180(20):5484–5488.
9. Acosta MBR, Ferreira RCC, Padilla G, Ferreira LCS, Costa SOP (2000) Altered expression of oligopeptide-binding protein (OppA) and aminoglycoside resistance in laboratory and clinical *Escherichia coli* strains. *J Med Microbiol* 49(5):409–413.
10. Takeuchi S, Hirayama K, Ueda K, Sakai H, Yonehara H (1958) Blasticidin S, a new antibiotic. *J Antibiot Tokyo* 11(1):1–5.
11. Umezawa H, et al. (1965) A new antibiotic, kasugamycin. *J Antibiot Tokyo* 18(2):101–103.
12. Andrews JC, Short SA (1986) opp-lac Operon fusions and transcriptional regulation of the *Escherichia coli* trp-linked oligopeptide permease. *J Bacteriol* 165(2):434–442.
13. Urbanowski ML, Stauffer LT, Stauffer GV (2000) The *gcvB* gene encodes a small untranslated RNA involved in expression of the dipeptide and oligopeptide transport systems in *Escherichia coli*. *Mol Microbiol* 37(4):856–868.

14. Suzuki S, Horinouchi T, Furusawa C (2015) Phenotypic changes associated with the fitness cost in antibiotic resistant *Escherichia coli* strains. *Mol Biosyst.* doi:10.1039/C5MB00590F.
15. Nakamatsu EH, et al. (2007) Oligopeptide uptake and aminoglycoside resistance in *Escherichia coli* K12. *FEMS Microbiol Lett* 269(2):229–233.
16. Poldermans B, Goosen N, Knippenberg PHV (1979) Studies on the function of two adjacent N₆,N₆-dimethyladenosines near the 3' end of 16 S ribosomal RNA of *Escherichia coli*. I. The effect of kasugamycin on initiation of protein synthesis. *J Biol Chem* 254(18):9085–9089.
17. Higgins CF, Ames GF (1981) Two periplasmic transport proteins which interact with a common membrane receptor show extensive homology: complete nucleotide sequences. *Proc Natl Acad Sci U S A* 78(10):6038–6042.
18. Park JT, Raychaudhuri D, Li H, Normark S, Mengin-Lecreulx D (1998) MppA, a Periplasmic Binding Protein Essential for Import of the Bacterial Cell Wall Peptidyl-Alanyl- γ -d-Glutamyl-meso-Diaminopimelate. *J Bacteriol* 180(5):1215–1223.
19. L toff  S, Delepelaire P, Wandersman C (2006) The housekeeping dipeptide permease is the *Escherichia coli* heme transporter and functions with two optional peptide binding proteins. *Proc Natl Acad Sci* 103(34):12891–12896.
20. Raghavan R, Groisman EA, Ochman H (2011) Genome-wide detection of novel regulatory RNAs in *E. coli*. *Genome Res* 21(9):1487–1497.

21. Ames BN, Ames GF-L, Young JD, Tsuchiya D, Lecocq J (1973) Illicit Transport: The Oligopeptide Permease. *Proc Natl Acad Sci* 70(2):456–458.
22. Curtis NA, et al. (1988) Iron-regulated outer membrane proteins of *Escherichia coli* K-12 and mechanism of action of catechol-substituted cephalosporins. *Antimicrob Agents Chemother* 32(12):1879–1886.
23. Bantysh O, et al. (2015) Enzymatic Synthesis and Functional Characterization of Bioactive Microcin C-Like Compounds with Altered Peptide Sequence and Length. *J Bacteriol* 197(19):3133–3141.
24. Takeuchi T, et al. (1965) Pharmacology of kasugamycin and the effect on *Pseudomonas* infection. *J Antibiot Tokyo* 18(2):107–110.
25. Pletzer D, et al. (2015) The *Pseudomonas aeruginosa* PA14 ABC Transporter NppA1A2BCD Is Required for Uptake of Peptidyl Nucleoside Antibiotics. *J Bacteriol* 197(13):2217–2228.
26. Klepsch MM, et al. (2011) *Escherichia coli* Peptide Binding Protein OppA Has a Preference for Positively Charged Peptides. *J Mol Biol* 414(1):75–85.

Supplementary Information

Supplementary Figure 1

**Supplementary Figure 1: Opp overexpression increases the rate of kasugamycin uptake**

(a) Time course of ³⁵S-methionine incorporation after drug treatment. Error bars represent standard deviation from biological replicates (n=2). **(b)** Comparison of ³⁵S-met incorporation rate at 60 seconds post treatment with kasugamycin. The reported p-value was calculated using a paired-value two-tailed student's t-test.

Chapter 3

A molecular handle for controlling transcription.

Contributing Authors:

Andrey Parshin, Jookyung Lee, Maria Ozerova, Dina Schneidman-Duhovny, Carol Gross, Sergei Borukhov

Citations:

Parshin A*, **Shiver AL***, Lee J, Ozerova M, Schneidman-Duhovny D, Gross CA, Borukhov S. DksA regulates RNA polymerase in Escherichia coli through a network of interactions in the secondary channel that includes Sequence Insertion 1. Proc Natl Acad Sci U S A. 2015 Dec 15;112(50):E6862-71.

*These authors contributed equally to this work.

Sensing and responding to nutritional status is one of the major challenges of microbial life. In *Escherichia coli*, the global regulatory response to amino acid starvation is orchestrated by the second messenger guanosine-3',5'-bisdiphosphate (ppGpp), which is a widely conserved master regulator [1]. Accumulation of ppGpp during amino acid scarcity triggers the stringent response, which down-regulates expression of rRNA and tRNA while increasing expression of amino acid biosynthetic enzymes. In *E. coli*, ppGpp works synergistically with transcription factor DksA to initiate the stringent response [2, 3]. Both ppGpp and DksA are critical for survival of stress and virulence in many pathogenic proteobacteria [4].

DksA is a relatively small protein with a prominent N-terminal coiled-coil domain and a globular C-terminal domain consisting of a Zn²⁺-binding region and a C-terminal α -helix [3]. It belongs to a class of regulators that bind directly to RNA polymerase (RNAP) without contacting DNA [5]. DksA modulates RNAP activity by preventing formation of or destabilizing the intermediate complex (RP_i) on the pathway to the open complex (RP_o), which is competent for initiation. For promoters with intrinsically unstable open complexes, such as rRNA promoters, DksA binding leads to decreased transcription [2]. DksA is a critical determinant of the stringent response and a model system for an important class of transcription regulators, making it essential to understand how DksA interacts with RNAP at the molecular level.

High-resolution structural information of the DksA/RNAP interaction is currently unavailable. Current models agree that the coiled-coil domain of DksA inserts into the secondary channel of RNAP, the channel used by NTPs to access the active site; that the secondary channel rim helices of β' subunit are critical for DksA binding; and that residues at the tip of the coiled-coil of DksA are important for its activity. However, the precise placement of DksA is unknown. With the number of critical features that can be accessed through the secondary channel, even

small changes in the model can significantly change the details of the interaction and mechanistic interpretation, making it imperative to determine the DksA position more precisely.

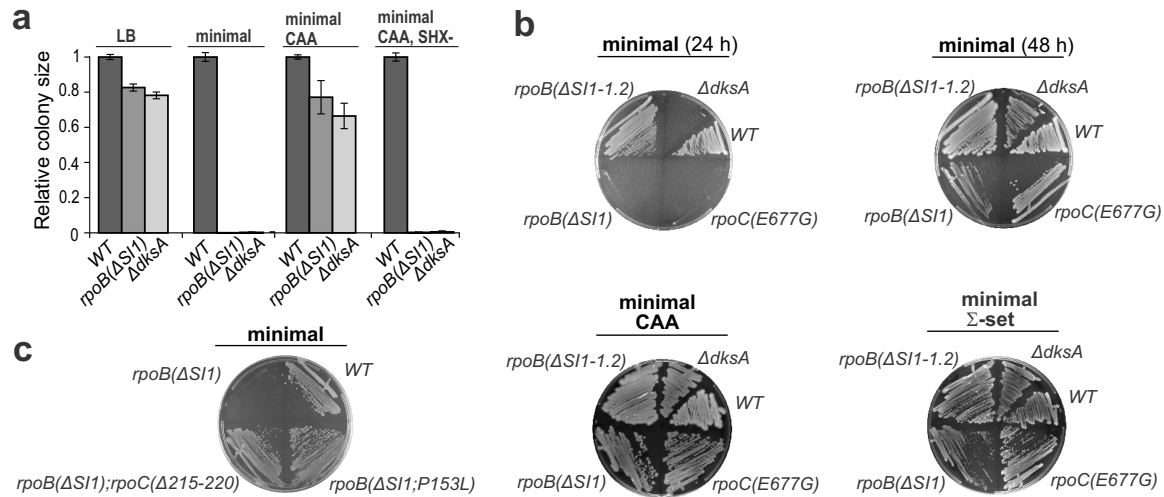
Using both chemical-genomic and high-resolution mapping of site-specific cross-links, we have discovered new features of RNAP that are essential for DksA binding and activity. Motivated by these novel findings, we have integrated information from cross-link mapping and extensive mutagenesis coupled to functional assays to revisit the model of DksA bound to RNAP, resulting in the highest resolution model of DksA binding to

date. We identify β subunit Sequence Insertion 1 (β -SI1) as a binding site for DksA and describe evidence for a bipartite binding site comprised of β -SI1 and the conserved β' rim helices. We also show that the tip of DksA interacts with the highly conserved substrate-binding region of the β subunit active site. This work advances our mechanistic understanding of DksA activity in *E. coli* and expands our knowledge of the evolutionary conservation of transcription regulation by DksA and ppGpp.

A chemical-genomic screen illuminates a connection between β Sequence Insertion 1 (β -SI1) and DksA.

A chemical-genomic screen of a large library of chromosomal RNAP mutants against many chemical conditions found that an RNAP mutant lacking the β -SI1 insertion, *rpoB*(Δ SI1), had a clear growth defect during amino acid starvation. This defect was manifested both when amino acids were omitted from the media and when starvation was mimicked with serine hydroxamate (SHX-), which prevents amino-acylation of seryl-tRNA (**Fig. 1A**). This phenotype is similar to

Figure 1

Figure 1. β -SI1 is critical for growth during amino acid limitation.

(A) Quantification of colony sizes of the wild type (WT) and mutant *E. coli* strains (*rpoB*($\Delta SI1$) and $\Delta dksA$) grown under indicated conditions. Colony sizes are normalized to the wild type strain (WT) for each condition. Error bars represent standard deviations ($n > 3$). CAA: casamino acids **(B)** Growth phenotypes of *rpoB*($\Delta SI1$) during amino acid limitation. The Σ -set of amino acids is comprised of D, Q, I, L, V, F, H, S, and T. **(C)** Spontaneous suppressors of *rpoB*($\Delta SI1$), *rpoC*($\Delta 215-220$) and *rpoB*(P153L), restore growth during amino acid limitation.

Figure 2

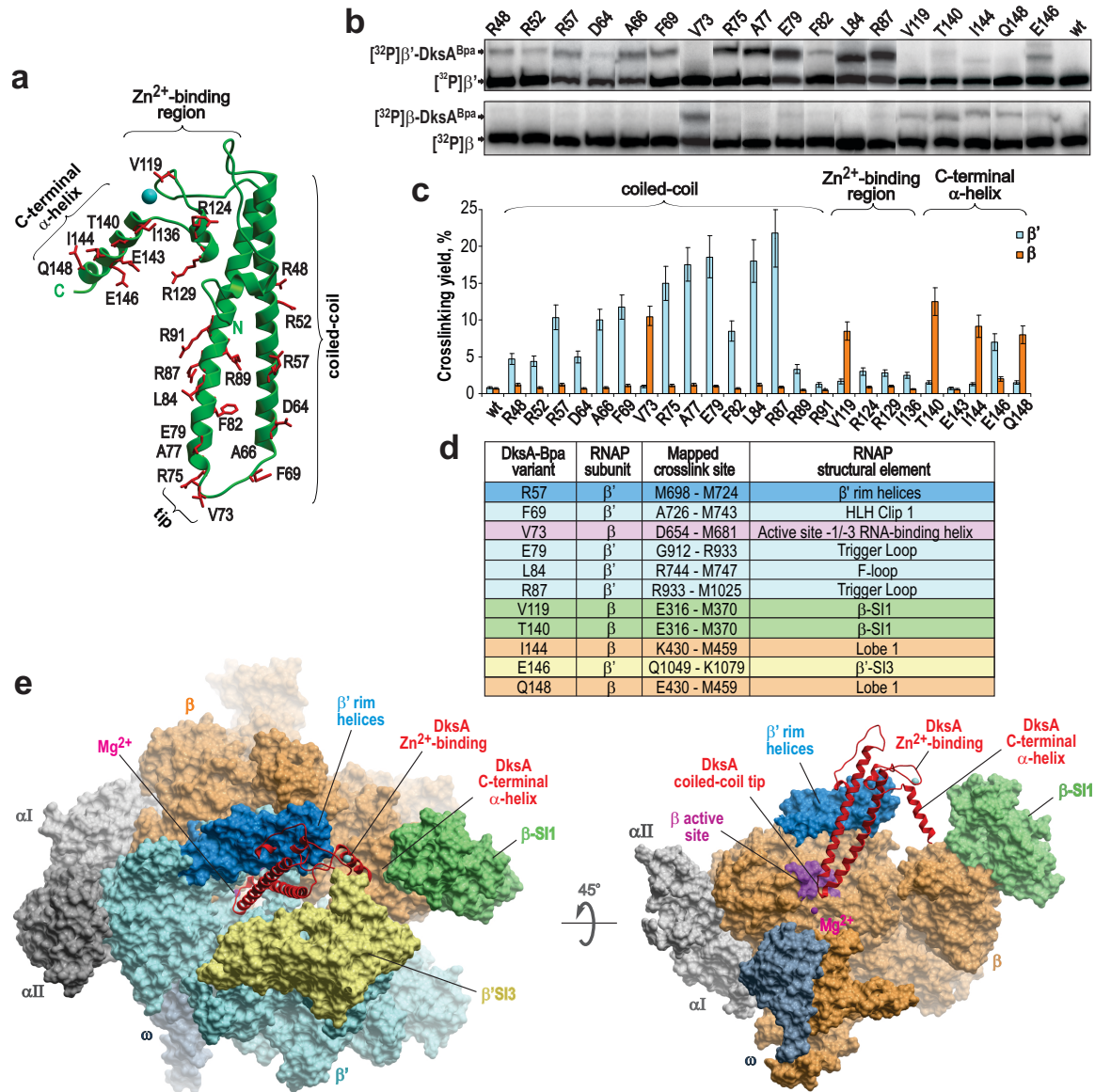


Figure 2. Probing of DksA-RNAP spatial organization by Bpa crosslinking.

(A) Ribbon structure of *E. coli* DksA (PDB: 1TJL) indicating its structural features, and the positions of the 24 residues substituted with Bpa (red sticks). (B) Autoradiograms of photo-crosslinked DksA-Bpa variants to RNAP core having either radiolabeled β' (top panel) or β (bottom panel). Position of crosslinked variants and free subunits is indicated by arrows. (C) Crosslinking yield of each DksA-Bpa variant to β' (cyan bars) and β (orange bars) with standard deviation ($n=3$) indicated. (D) Summary of the mapped crosslinked sites, color-coded to match the RNAP regions shown in (E). Structural elements listed are described in [65] (E) Structural model of the DksA-RNAP complex. Left panel, secondary channel surface view of *E. coli* RNAP holoenzyme (PDB: 4LK1) (α I, light grey; α II, grey; β , orange; β' , cyan; ω , slate grey; σ is omitted

for clarity) in complex with *E. coli* DksA (PDB: 1TJL), which is shown as a red ribbon with structural features indicated by arrows. The view emphasizes position of DksA relative to three secondary channel domains: β -SI1 (light green), β' -SI3 (light yellow) and β' rim helices (blue). Right panel, rotation by $\sim 45^\circ$ with β' surface removed to reveal the position of DksA coiled-coil tip relative to β subunit active site region. The -1/-3 RNA-binding helix (β D675-M681) and the NTP-binding loop (β S1105-N1108) are colored magenta; the catalytic Mg^{2+} -ion is a dark purple ball.

that of $\Delta dksA$, which led us to further compare their phenotypes.

The amino acid requirements of $\Delta dksA$ and $rpoB(\Delta S11)$ are equivalent. Both strains grew slowly when deprived of amino acids, but were not true auxotrophs as colonies became visible after two days of growth (**Fig. 1B**). Moreover, the same set of amino acids (the Σ -set: DQILVFHST) [6] is sufficient to complement the amino acid requirements of both $\Delta dksA$ and $rpoB(\Delta S11)$ (**Fig. 1B**). Finally, sequencing of suppressors that restored prototrophy to $rpoB(\Delta S11)$ identified two mutations in RNAP already known to suppress the amino acid requirements of $\Delta dksA$ and $ppGpp^0$: $rpoB(P153L)$ and $rpoC(\Delta 215-220)$ (**Fig. 1C**) [7–9]. The similarity of $rpoB(\Delta S11)$ and $\Delta dksA$ across a battery of tests suggested the two mutations may have similar effects on transcription. This led us to speculate that β -S11, located near DksA in models of the RNAP/DksA complex, is a previously unappreciated DksA binding site.

Bpa crosslinking probes reveal the proximity of DksA to β in the complex.

To map RNAP sites in close proximity to DksA, we incorporated p-benzoyl-p-phenylalanine (Bpa) into 24 surface-exposed residues of DksA, covering all of its structural features (**Fig. 2A**). UV-light activates Bpa to crosslink nearby alkyl carbons with a preference for aliphatic residues [10]. Bpa substitutions provide highly specific crosslinking information that can resolve unique binding partners in nearby features [11]. We tested each purified, radiolabeled variant for crosslinking to RNAP holoenzyme *in vitro*, identifying 18 variants that crosslinked to one of the two large subunits in RNAP (**Fig. S1A,S1B**). We distinguished crosslinking to β or β' by crosslinking unlabeled DksA-Bpa variants to RNAP radiolabeled in either the β or β' subunit (**Fig. 2B**). Thirteen DksA-Bpa variants preferentially crosslinked to β' , as expected from earlier results that identified β' as a crosslinking partner of DksA [12], and five preferentially crosslinked to β (**Fig. 2B, 2C**). To our knowledge this was the first evidence that β contributes to

DksA binding.

We mapped the crosslink sites in β and β' to greater resolution, using limited cyanogen bromide (BrCN) cleavage, which cleaves after methionine residues. The BrCN cleavage patterns of RNAP subunits are well-established [13,14], allowing for clear assignment of crosslink adducts to fragments of the large subunits (**Fig. S2A**). In some cases, we further refined the crosslinking region by enzymatically cleaving the crosslinked products with trypsin under single-hit conditions. In total, we located crosslink sites on β and β' for 11 DksA-Bpa variants to a precision of 10-50 residues (**Fig. S2B-K**). The results, summarized in Figure 2D and Supplementary Figure S3A-D, identified eight new crosslinking sites and increased the precision of three previously identified sites (DksA F69, E79, and E146) by an order of magnitude [12]. DksA-Bpa crosslinks mapped to two new regions in β that weren't predicted by current models; a region overlapping β -SI1 and one that included a substrate-binding region from β . This motivated us to revisit the structural model of DksA bound to RNAP.

A new evidence-based model for the DksA-RNAP complex.

We first sought to understand the general constraints on possible models of DksA and RNAP imposed by our new crosslinking data. For this purpose, we used computational docking with PatchDock [15] to generate nearly 130,000 different models of DksA bound to RNAP using two constraints: we required that the interface between the two structures satisfied shape complementarity rules and that at least one of the mapped crosslink regions contacted DksA directly (distance in structure $<20\text{\AA}$). This set was then filtered using distance constraints from the crosslinks. Simultaneous satisfaction of 7 crosslink constraints filtered the set to just three similar docking solutions (RMSD: $<11\text{\AA}$) sharing two prominent features. First, the tip of DksA inserted deep into the secondary channel and approached the substrate-binding site in β subunit.

Second, the C-terminal α -helix of DksA extended out towards β -SI1 in the secondary channel. Of the three docking positions, two positions placed the globular domain of DksA closer to the β' jaw domain (β' 1147-1245) while only one positioned the globular domain of DksA closer to the tip of the β' rim helices, a known binding determinant of DksA [12,16]. We used this solution for further refinement of the structural model. Notably, the best docking solution was still limited by a steric clash between the rim helices and the N-terminus of DksA, a structural feature that has been demonstrated to be dispensable for DksA function [16].

To create a refined model of DksA bound to RNAP that reflected residue-level information on the interaction, we used additional experimental information based on the functional characterization of ≥ 30 point mutants and several partial deletions. (**Fig. 2C, S4B, S4C, Methods**). We positioned DksA within the secondary channel so that functionally relevant residues made reasonable contacts in the interface. Importantly, only minor changes in the orientation and position of DksA in the automated model (RMSD: 7Å) were necessary (**Fig. S3E**). The final model (**Fig. 2E, model 3 in Fig. S3E**) suggests four likely interaction sites between DksA and RNAP: the DksA C-terminal α -helix and β -SI1 (**Fig. 3A**); the DksA Zn^{2+} binding domain and adjacent C-terminal α -helix with the tip of the β' rim helices (**Fig. 3B**); DksA residue D74 with residues in the β substrate binding region (**Fig. 3C**); and the middle of the DksA coiled-coil domain with the β' N-terminal rim helix (**Fig. 3D**).

Figure 3

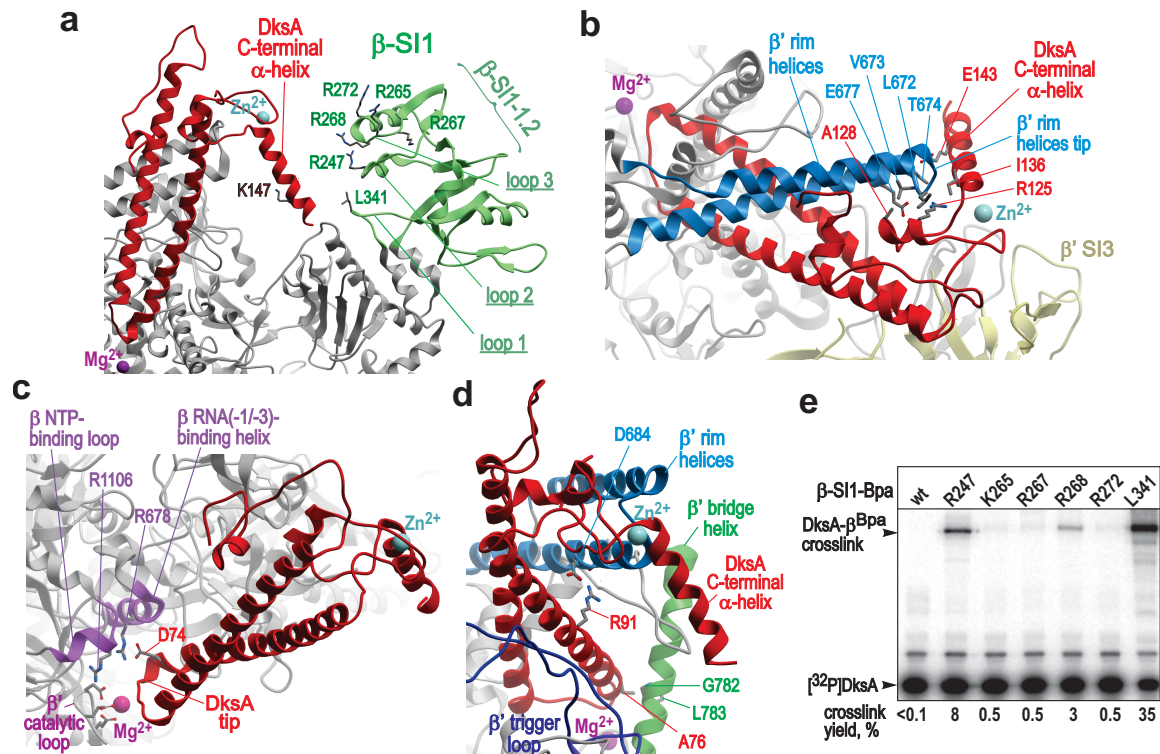


Figure 3. Detailed views of the structural model of the DksA-RNAP complex. (A) Structural view of possible interactions between the DksA C-terminal α -helix and β -SI1. Residues with Bpa substitutions in β -SI1 loop 1, 2 and 3 are depicted as sticks. **(B)** DksA Zn^{2+} -binding region and β' rim helices tip; in this and the following panels, critical contacts are depicted as sticks. **(C)** DksA coiled-coil tip residue D74 and β active-site region NTP-binding loop/RNA (-1/-3)-binding helix; and **(D)** DksA coiled-coil residue R91 and β' rim helix residues encompassing D684; DksA-A76 and β' bridge helix residues G782/L783. Color-coded as in Figure 2E, except β' bridge helix (green) and β' trigger loop (dark blue; open conformation as in PDB: 3LU0) **(E)** Autoradiogram of photo-crosslinking between wt DksA and RNAPs carrying six different Bpa substitutions in β -SI1.

β -SI1 interacts with DksA.

Consistent with the functional connection between β -SI1 and DksA discovered in our chemical-genomic screen, two DksA-Bpa adducts, DksA-V119Bpa and DksA-T140Bpa, mapped to a region of β overlapping with SI1 (**Fig. 2D**). We independently confirmed the physical proximity of DksA and β -SI1 in the bound complex using a "reciprocal" crosslinking experiment, showing that two β -SI1-Bpa derivatives, β -L341Bpa and β -K247Bpa, crosslinked to DksA with high efficiency (**Fig. 3E**). These reciprocal crosslinks are strong evidence of the proximity of β -SI1 and DksA in the complex.

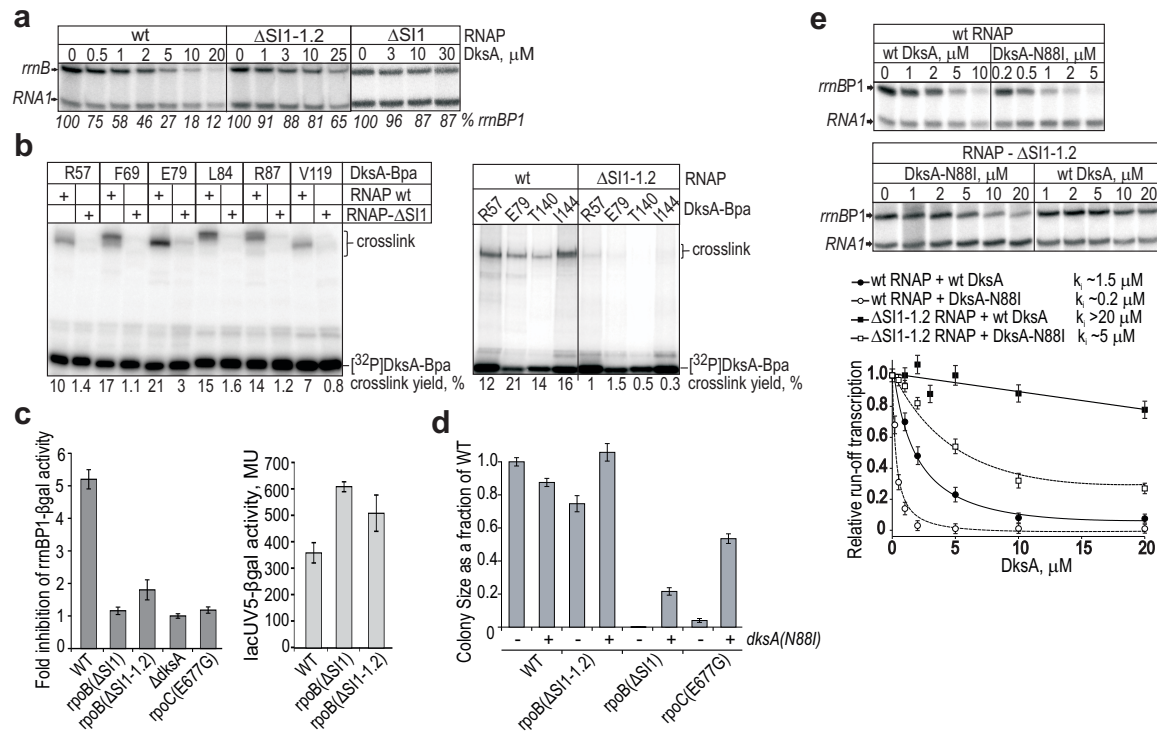
The β -SI1-1.2 (β -240-284) sub-domain of β -SI1 faces the secondary channel and is oriented towards DksA in the model; with loops 2 (β -E244-S252) and 3 (β -G266-R272) positioned as possible interfaces with DksA (**Fig. 3A**). Consistent with this prediction, both RNAP Δ SI1 and RNAP Δ SI1-1.2 mutant polymerases had dramatically decreased DksA-dependent inhibition of transcription from *rrnBP1* (**Fig. 4A**) and DksA binding *in vitro* (**Fig. 4B**). Moreover, multiple-alanine substitutions in both loop 2 and loop 3 of β -SI1-1.2 significantly decreased DksA binding and inhibitory activity *in vitro* (**Table S1, Fig. S9A, Fig. S9B**). Additionally, both *rpoB*(Δ SI1) and *rpoB*(Δ S II-1.1) exhibited a phenotype *in vivo*, failing to repress transcription from a reporter construct driven from an *rrnBP1* promoter during stationary phase growth. Loss of repression was similar in magnitude to that of Δ *dksA* and *rpoC*(E677C), a mutant in the β' rim helices that mimics the *in vivo* phenotypes of Δ *dksA* (**Fig. 4C**) [17]. Importantly, this effect was not due to a general transcriptional defect of *rpoB*(Δ SI1) or *rpoB*(Δ SI1-1.2): both deletion strains showed less than a two-fold increase in expression of *lacUV5-lacZ*, comparable to that described for Δ *dksA* [7] (**Fig. 4C**).

The defect of RNAP Δ SI1-1.2 in repressing transcription either *in vivo* or *in vitro* was only

slightly less than that of *rpoB*(Δ SII). However, *rpoB*(Δ SII-1.2) was less defective than *rpoB*(Δ SII) during growth without amino acids, as the strain suffered no lag and showed only a small (~30%) reduction in colony size relative to WT (**Fig. 4D, Fig. S8**). The discrepancy in the severity of phenotypes detected by these assays could be explained by their relative sensitivities or by differences in conditions. The binding defect of *rpoB*(Δ SII-1.2) may not be sufficient to disrupt growth without amino acids, or the elevated ppGpp levels during amino acid starvation could complement any partial defects through synergy with DksA [2].

The model predicted that the C-terminal α -helix of DksA spanned the junction from the β' rim helices to β -SII, with residues that could be reasonably expected to interact with either feature, motivating us to identify any DksA residues that could contribute to these interfaces. As previously reported [16], DksA was completely inactive when its C-terminal α -helix (140-152) was removed. DksA(1-139) lacked both RNAP binding and functional activity *in vitro* (**Fig. 5A,B, Fig. S4A, Fig. S5A**) and activity *in vivo* (**Fig. 5C, Fig. S6, Fig. S7**). Serial C-terminal truncations displayed a progressive loss of function *in vitro* and *in vivo* (**Fig. S4A, Fig. S5A, Fig. S6, Fig. S7**), which suggested multiple contacts between RNAP and this α -helix. We found two point mutants in the C-terminal α -helix that exhibited functional defects. DksA-E143A significantly reduced the binding and activity of DksA *in vitro* and DksA-K147A had smaller, but similar, effects (**Fig. 5B, Fig. S4B, and Fig. S5B**). Of these two point mutants, only DksA-E143A was defective in inhibiting transcription from *rrnBP1* *in vivo* (**Fig. 5C**) and both strains grew on minimal medium (**Fig. S7 and Table S2**). The smaller effects seen with single substitutions are consistent with multiple sites across the C-terminal α -helix additively contributing to binding. In our model, DksA-E143 is positioned to interact with the tip of the β' rim helices (**Fig. 3B**), whereas DksA-K147 is distal to the β' rim helices.

Figure 4

Figure 4. Comparison of the phenotypes of RNAP $\Delta\beta$ -SI1 and $\Delta\beta$ -SI1-1.2.

(A) Multiround transcription assays [2] comparing the concentration dependence of DksA inhibition of *rmnBP1* transcription initiated by wt RNAP (left), β - Δ SI1 RNAP (center) or β - Δ SI1-1.2 RNAP (right). The percentage of terminated *rmnBP1* transcripts made with DksA relative to that without DksA is indicated below each lane of the gel autoradiogram. (B) Autoradiograms of 6%-12% SDS PAGE of different DksA-Bpa photo-crosslinked to wt or mutant RNAP β - Δ SI1 (left panel) and to β - Δ SI1-1.2 (right panel). Crosslinking yield indicated below each lane. (C) Stationary phase inhibitory activity of DksA in strains with β - Δ SI1 and β - Δ SI1-1.2 mutations (derivatives of RLG5920, RLG4764, and RLG5022, see Table S6). Left Panel: fold inhibition of *rmnBP1*- β gal activity relative to that in a strain lacking DksA, assayed using an *rmnBP1*- β gal fusion reporter strain and measured 24 hrs after inoculation. Right panel: activity of wt and β -SI1 variants on a *lacUV5*- β gal fusion reporter measured 24 hrs after inoculation. (D) The fitness defect of *rpoB*(Δ SI1) on minimal media is partially suppressed by *dksA*(N88I) (derivatives of BW25113, see Table S6). Colonies were pinned onto minimal media and colony size was quantified and normalized to wt. Error bars reflect standard deviation ($n > 3$). (E) Left panel: same as in (A) except that reactions used the hyperactive DksA mutant, DksA-N88I; Right panel: quantification of the concentration dependence of DksA inhibitory activity in various strains from which k_i is calculated.

We also used genetic tests to characterize the interaction between β -SI1 and DksA. We first used a hyperactive DksA mutant (DksA-N88I) that has both higher affinity for and activity on RNAP, allowing it to suppress the auxotrophy of a $ppGpp^0$ strain [18]. We reasoned that DksA-N88I would also be sufficient to restore binding and activity to mutants in the proposed DksA/ β -SI1 interface. As predicted, DksA-N88I partially suppressed the *in vivo* growth defects of *rpoB*(Δ SI1), *rpoB*(Δ SI1-1.2) (**Fig. 4D**), and *dksA*(1-139) (**Fig. S7**). DksA-N88I also suppressed the *in vitro* defect in activity for RNAP Δ SI1-1.2 (**Fig. 4E, Table S1**). We next used epistasis analysis to test whether DksA binding was the sole function of β -SI1. If so, an *rpoB*(Δ SI1) Δ *dksA* double mutant phenotype should have been equivalent to either single mutant alone. This epistatic relationship held for a positive control, *rpoC*(E677G), known to interfere with DksA binding [17] (**Fig. S8**). In contrast, both *rpoB*(Δ SI1) Δ *dksA* and *rpoB*(Δ SI1-1.2) Δ *dksA* were synthetic sick in combination, showing an extended lag before any growth in minimal medium (**Fig. S8**). These results further support the conclusion that mutations in the DksA/ β -SI1 interface reduce binding and activity of DksA and, unexpectedly, show that β -SI1 contributes to growth on minimal media even in the absence of DksA.

In summary, multiple lines of evidence indicate that DksA and β -SI1 interact and that this interaction is critical for recruiting DksA to the initiation complex. This includes reciprocal crosslinking between DksA and β -SI1, the position of the C-terminal α -helix of DksA near β -SI1 in our model, and genetic validation of both sides of this interface.

The tip of the β' rim helices binds the Zn^{2+} -binding domain and adjacent C-terminal α -helix.

The model predicted that the Zn^{2+} -binding domain of DksA (G112-K139) contacted the tip of the β' rim helices (β' 670-674) (**Fig. 3B**), a feature of RNAP that is known to be critical for DksA

binding [19]. Multiple mutations in both sides of the proposed interface identify key residues that contribute DksA binding affinity.

DksA-R125A (**Fig. 5A**) was the most defective point mutant in DksA. The mutant lacked both binding and activity *in vitro* (**Fig. 5B,D,E**), was unable to inhibit *rrnB*P1 transcription *in vivo*, and did not support growth on minimal media (**Fig. 5C,F**). Even the more conservative substitution, DksA-R125K, resulted in a nearly complete loss of RNAP binding (>20-fold decrease; **Fig. 5E**). Loss of activity was suppressed in a DksA-R125A/N88I double mutant strain, consistent with the phenotype being due to a lack of binding (**Fig. 5F**).

Two other residues in the Zn^{2+} -binding domain (A128 and I136) were also important for DksA function. DksA-A128N and DksA-I136S were defective for both binding and activity *in vitro* (**Fig. 5B, Fig. S4B, Fig. S5B**) and inhibited expression from *rrnB* P1 very poorly *in vivo* (**Fig. 5C**). However, like the partially defective mutants of the β -S11/DksA interface, they were able to support growth without added amino acids (**Fig. S7**). A combination of DksA-E143A with these partially defective mutants (DksA-I136S/E143A and DksA-A128N/I136S/E143A) could not support growth without amino acids (**Fig. S7**), suggesting that combining these weaker mutations can have a synergistic effect on DksA binding.

In the model, DksA-R125 is positioned to interact with β' -E677 (**Fig. 3B**), DksA-A128 and DksA-I136 are positioned to interact with the two aliphatic side chains in the tip of the rim helices (**Fig. 3B**), and DksA-E143 is positioned to interact with tip residue β' T674. While the atomic-level resolution of this interaction remains to be determined, we note that structural modeling and mutagenesis together implicate a direct interaction between the Zn^{2+} -binding region of DksA and the tip of the β' rim helices. Functional analysis indicates that DksA-R125 is a major contributor to binding energy of this interface. It is interesting to note that while the

Figure 5

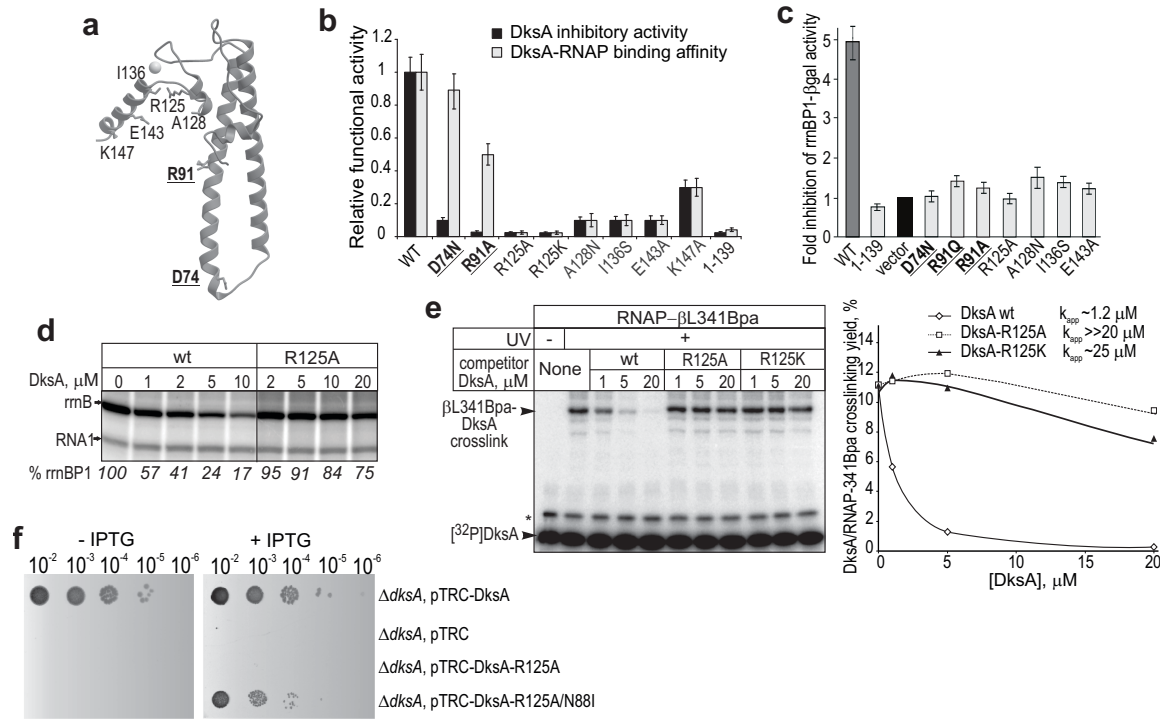


Figure 5. Phenotypes of selected single-point DksA mutants with significant functional impairment.

(A) Ribbon structure of *E. coli* DksA showing the position of critical residues (sticks). **(B)** Effect of mutations of critical residues in DksA on its binding affinity and ability to inhibit transcription from *rrnB-P1* *in vitro*. Data is plotted relative to activity of wt DksA; error bars represent standard deviation ($n=3$). In panels B and C, mutations resulting in significant reduction of DksA activity, but not binding affinity, are shown in bold typeface and underlined **(C)** *In vivo* transcriptional inhibitory activity of these same mutants measured as fold-inhibition of an *rrnB* P1-lacZ fusion reporter during stationary phase in *E. coli* $\Delta dksA$ cells expressing either plasmid-born wt or mutant DksA (upon induction with 1 mM IPTG). Data is plotted relative to that of $\Delta dksA$ cells (strain RLG7241) carrying empty vector. **(D)** Multiround run-off transcription assays (as in Figure 4A) comparing the concentration dependence of wt and R125 DksA for inhibition of *rrnB-P1* transcription. **(E)** Analysis of the binding affinity of DksA-R125 to RNAP with a competition-crosslinking assay. Autoradiogram of 6%-12% SDS PAGE of RNAP- $\beta\text{L341Bpa}$ photo-crosslinked to radioactive wt DksA in the presence of various amounts of competitor DksA (wt or mutant) as indicated (left panel). Radiolabeled protein kinase A present in the reaction mix is indicated by asterisk. Right Panel: quantification of the effect of mutant DksA concentration on the yield of RNAP-DksA crosslinking from which k_{app} is calculated **(F)** Growth complementation assay showing that upon IPTG induction, plasmid-expressed DksA-R125A/N88I, but not DksA-R125A, rescues the auxotrophy of *E. coli* $\Delta dksA$ cells (strain CF9240) during 24h growth on M9 minimal agar plates at 30° C. Serial dilution factor is indicated above.

The coiled-coil tip of DksA interacts with residues in the substrate binding region of the active site.

Identifying the position of the coiled-coil tip of DksA within the active-site region of RNAP is critical for understanding the mode of action of DksA. In our model, tip residue D74, one of the first to be identified as essential for DksA activity [3], is positioned to contact two residues of the substrate-binding site in β subunit, β -R678 and β -R1106 (**Fig. 2E, Fig. 3C**). This assignment is supported by crosslinking between DksA-V73 and the overlapping region (β 653-681), as well as functional analysis of mutants in D74, β -R678, and β -R1106.

We found that DksA-D74 substitutions D74N, D74S, and D74E all altered DksA activity without affecting binding, consistent with previous studies [3,12,20] (**Fig. 5B, Fig. S5B**). D74N was most defective of the substitutions (**Fig. 5C, Fig. S7, and Table S1**). This suggested that proper positioning and electrostatic charge of the aspartic acid carboxyl group is critical for D74 function.

The two residues in β (R678 and R1106) proposed to interact with DksA-D74 each play important roles in catalytic function during elongation. β -R678 binds to the nascent RNA 3'-end and orients it for nucleotide addition and β -R1106 stabilizes the incoming NTP [21, 22]. RNAP complexes with alanine-substitutions at either residue retained DksA affinity (**Fig. S9B**), but were refractory to DksA inhibition in *in vitro* transcription assays, even at the concentrations 10-fold higher than that required for wt RNAP (**Fig. 6A**). A complementary assay based on destabilization of RPo by DksA at the model promoter lacUV5 DNA [23] also indicated that these mutants were refractory to DksA action: although RNAP- β R678A and RNAP- β R1106A

Figure 6

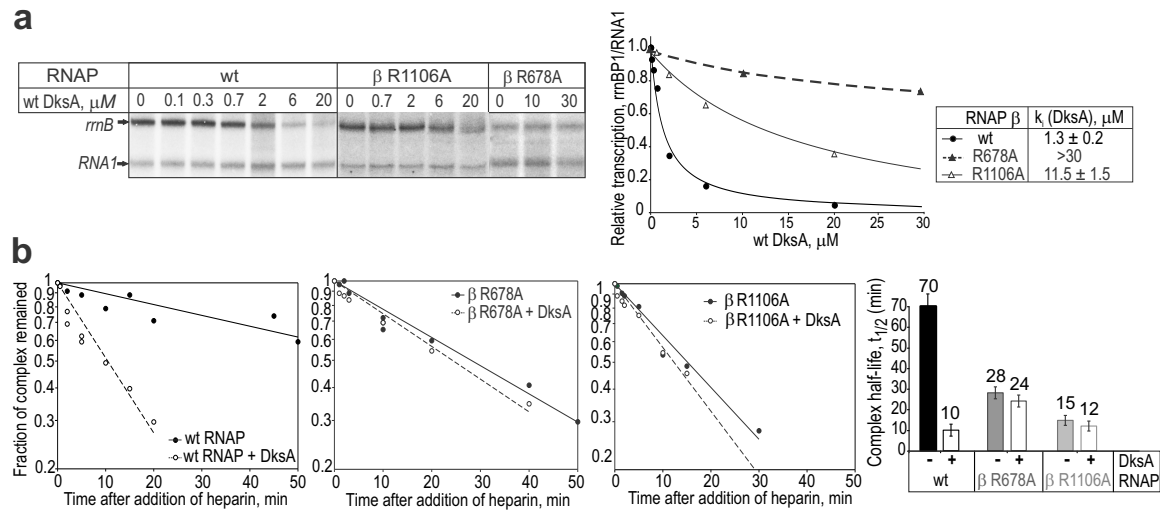


Figure 6. Susceptibility of the RNAP β active-site region mutants, β-R678A and β-R1106A, to DksA inhibition

(A) Multiround transcription assays comparing the concentration dependence of DksA inhibition of *rrnB*-P1 for wt (left), β-R678A (middle), or β-R1106A (right) RNAP, with quantification and the calculated k_i shown below. **(B)** Effect of 5 μM DksA on the lifetime of *lacUV5* open promoter complexes formed by wt, β-R678A and β-R1106A RNAPs, measured by DNA filter binding [30]. The decay curves show the fraction of complexes remaining at the indicated times after heparin addition. Bottom right indicates the $t_{1/2}$ calculated from these data.

exhibited shorter half-lives than wt they were insensitive to DksA-mediated destabilization (**Fig. 6B**). Substitution of the neighboring residues, β -N677A and β -S1105A, did not affect RNAP sensitivity to DksA (**Fig. S9A**) indicating that the effects observed with β -R678A and β -R1106A were specific.

The observations that DksA-D74 exhibits charge complementarity with β -R678 and β -R1106, that mutation of these residues abrogates DksA function, and that all three residues are highly conserved among different bacterial phyla (**Table S5**), together suggests that DksA-D74 forms a salt bridge with β -R678 and β -R1106 that is essential for DksA activity. We note that the proposed interaction of DksA-D74 with the substrate binding region of the active site places DksA-A76 tightly against β 'G782/L783 from the bridge helix. This provides an alternative explanation for the functional defects discovered for DksA-A76T, in that a steric clash from the bulky substitution would prevent DksA from inserting into the substrate binding region of the active site [20].

A novel DksA coiled-coil/ β ' rim helix functional interaction

Interestingly, we found that substitutions in DksA-R91 eliminate the activity of DksA and reduce, but do not eliminate, DksA binding (**Fig. 5B,C, Fig. S4B, Fig. S4C, Fig. S5B, Fig. S7 and Table S2**). This indicated that DksA-R91 is essential for DksA activity independent of binding, similar to the phenotype of the tip residue D74. The model positions DksA-R91 near β '-D684 (**Fig. 3D**) and substitution of β '-D684 also reduced the sensitivity of mutant RNAP to DksA *in vitro* (**Table S1**). Compared to other proposed interaction interfaces, both DksA-R91 and the residues centered at β '-D684 are less conserved between phyla (**Table S5**). We propose that an interaction between DksA-R91 with the β ' rim helix stabilizes the orientation of the DksA coiled-coil that allows an interaction between DksA-D74 and the substrate binding region of the

active site.

Discussion

We present a new evidence-based model of the DksA-RNAP complex that highlights a dispersed network of mutually dependent interactions required for both binding and activity of DksA. High-affinity binding requires an interaction between β -SI1 and the C-terminal α -helix of DksA as well as between the tip of the β' rim helices and the Zn^{2+} -binding region of DksA. Eliminating either interaction alone abolished binding, showing that both the β' rim helices and β -SI1 are necessary binding determinants of DksA.

DksA and β -SI1 are too distant to physically interact in our model, which is based on DksA and RNAP crystallized independently. The DksA C-terminal α -helix and β -SI1 both display conformational flexibility (by 7-15Å) based on the reported crystal structures of DksA (PDB: 1TJL; 4IJJ) and RNAP (PDB: 4LK1, 4YLN, 4JKR). The movement of the two domains towards each other by 5-10Å and 10-15Å, respectively, could easily bring β -SI1 close enough to interact with DksA. DksA binding could thus capture an alternative conformation to that found in the crystal structure of *E. coli* RNAP [25–27] and compete with any function of β -SI1 associated with this original conformation. Although we have clearly demonstrated that β -SI1 recruits DksA to RNAP, further efforts both to dissect this novel binding interface and to characterize the DksA-independent functions of β -SI1 will be critical for completing the picture of how the interaction between β -SI1 and DksA alters transcription.

Our work has revealed that the residues in the β substrate binding region of the active site, are required for sensitivity to DksA during initiation. We propose that DksA-D74 functions during initiation by neutralizing the positive charges of β -R678/R1106 and altering the dense network of polar/electrostatic interactions in the immediate vicinity of the active center [25,27–29]. This

could alter the conformation of two neighboring mobile elements of β , fork loop-1 and fork loop-2, destabilizing the intermediate on the pathway to open complex formation. Alternatively, The β' trigger loop (β' TL) has been previously demonstrated to be essential for sensitivity to DksA [7,19]. Our model predicts a steric clash between a folded β' TL and the coiled-coil of DksA, and an alternative mechanistic role of both DksA-D74 and DksA-91 could be to lock the coiled-coil in the appropriate orientation to mediate this interaction. Regardless of exact conformational changes that destabilize RPi, we have provided strong evidence that an interaction between the substrate binding region of the active site and DksA-D74 is a critical feature of DksA regulation during initiation.

DksA is known to alter the elongation properties of RNAP [3,19,37], and we note that DksA statically bound to RNAP as found in our model would preclude elongation by preventing folding of the β' TL. Our experimental efforts focused on the effects of DksA during initiation, but the position of the DksA coiled-coil in the channel may be dynamic and vary with RNAP conformation, the stage of transcription cycle, and the presence of additional factors such as ppGpp. Indeed, Fe^{2+} -mediated cleavage of DksA is reduced in the paused complex compared to free RNAP [19] and for mutants in the tip that inactivate DksA [20], which has been interpreted as representing a more distal position of the coiled-coil in these complexes [19]. One alternative model positions DksA so that binding would not clash with a folded β' TL and may represent a more relevant mode of binding during elongation [12].

For *E. coli* RNAP, DksA binding is modulated by two lineage specific insertions: β -SI1 and β' -SI3. While β' -SI3 antagonizes DksA binding and is hypothesized to contribute to the steric clash between DksA and a folded β' trigger loop [16], β -SI1 is essential for recruiting DksA to RNAP. This discovery has interesting implications for the conservation of DksA regulation among

diverse bacteria. Like β' -SI3 [16], β -SI1 co-occurs with DksA, present in 22/25 of the bacterial phyla with DksA homologues (**Table S3**). In most DksA-containing phyla, β -SI1 is present either as a full-length domain (containing all three proposed interacting loops), or as a short insertion containing only loop 1. In phyla with a truncated β -SI1, features of DksA may have evolved to compensate for this loss and maintain a high binding affinity. For example, 5 phyla that carry a truncated β -SI1 also have an extended C-terminal α -helix in DksA (**Table S3**). Comparing the regulatory capabilities of DksA in these bacteria to those of *E. coli*, would indicate the diversity of mechanisms that have evolved to allow for control of transcription by DksA.

Methods

Strains, oligos, and growth conditions

E. coli strains and plasmids are listed in the Supplemental Material (**Table S6**). Primers used in all PCR-based cloning were obtained from IDT; their sequences are available upon request. Deletions, single and multiple point mutations, and UAG-amber codon substitutions were introduced at various positions within the *dksA*, *rpoB* and *rpoC* genes using QuickChange site-directed mutagenesis kit (Agilent). Chromosomal mutants in *rpoB* and *dksA* were generated by oligo-mediated recombineering using the λ -red system and standard protocols [31]. Colony size estimations were made on arrayed colonies on agar plates using the same methodology as previously described for large-scale chemical-genomic screens [32].

Expression and purification of mutant DksA and RNAP proteins

Bpa substituted variants of DksA and RNAP were prepared using *E. coli* BL21(DE3) and CAG316 cells, respectively. Strains were co-transformed with a Bpa-specific evolved

tRNA/tRNA synthetase pEVOL-BpF vector [33] and the appropriate expression plasmid (**Table S6**). Transformants were grown to $OD_{600} \sim 0.5-0.6$ at 30°C in liquid LB media supplemented with ampicillin ($100 \mu\text{g/ml}$) and chloramphenicol ($30 \mu\text{g/ml}$). Protein expression was induced by addition of 1 mM Bpa, 1 mM IPTG and 0.02% arabinose to the growth media, and the induced cells were grown for ~ 20 hours at 30°C . DksA-Bpa and RNAP-Bpa proteins were purified under reduced light at 4°C by Ni^{2+} -chelating NTA-agarose (Qiagen) followed by size-exclusion chromatography on Superdex 75 and Superose 6 (GE Healthcare Life Sciences), respectively [34]. Other mutant DksA and RNAP proteins were expressed using same strains (without co-transformation with pEVOL-BpF) and purified as described above.

Protein crosslinking and mapping

Purified RNAP core enzyme carrying either N- or C-terminal PKA- and 6XHis-tag (NPH or CPH, respectively) on β' or β subunits were radiolabeled using $[\gamma\text{-}^{32}\text{P}]\text{-ATP}$ (3000Ci/mmol , MP Biomedicals) and protein kinase A (PKA, New England Biolabs) as described previously [34]. Crosslinking reactions were initiated by mixing $0.5 \mu\text{M}$ $[\alpha\text{-}^{32}\text{P}]\text{-RNAP}$ with $0.5\text{-}2 \mu\text{M}$ DksA-Bpa in $15 \mu\text{l}$ reaction buffer (40 mM Tris-HCl pH 7.9, 50 mM NaCl, 10 mM MgCl_2 , 0.2 mg/ml BSA) followed by irradiation by 365 nm UV-lamp for 20 min at 4°C . The reaction was terminated by addition of $3 \mu\text{l}$ of 5X SDS sample loading buffer containing β -mercaptoethanol. The crosslinked products were separated by 6% Tris-glycine SDS polyacrylamide gel electrophoresis (SDS-PAGE), visualized by autoradiography and quantified by Phosphorimager (GE Healthcare Life Sciences). The results of crosslinking experiments were essentially the same when RNAP $\sigma 70$ -holoenzyme was used instead of the core enzyme (data not shown). The free radiolabeled β and β' and their covalent adducts carrying DksA-Bpa were excised from the gel and eluted with three

volumes of 0.2% SDS at room temperature for one hour. The eluate was precipitated by acetone and re-dissolved in 20 μ l of 0.1% SDS, and then directly used in cleavage reactions.

Mapping of the crosslinked sites on β and β' was performed by limited chemical or enzymatic hydrolysis under single-hit conditions. Chemical hydrolysis was initiated by mixing the eluted radioactive material with 40 mM HCl and 40 mM BrCN in 10 μ l of 0.2% SDS followed by incubation at 30 °C for 5-30 min. The reaction was terminated by addition of 0.5 μ l of 1 M Tris-OH. Enzymatic cleavage was performed by mixing the eluted radioactive material with 1 μ g unlabeled RNAP and 1-10 ng trypsin (Thermo Fisher Scientific Inc) in 15 μ l of buffer (100 mM Na-phosphate pH 7.0, 0.05 % SDS) followed by incubation at 37 °C for 5-30 min. Reaction was terminated as described above, the products of cleavage reactions were resolved by 7% or 10% SDS-PAGE and visualized by PhosphoImager. Protein cleavages at Met and Arg/Lys residues was carried out as described [34,35] using BrCN and trypsin, respectively. Since the PKA sites are located at β and β' polypeptide termini, the single-hit hydrolysis generates a pattern of nested, easily identifiable fragments.

Modeling of the DksA-RNAP complex

Atomic-resolution representations of the structures of RNAP (PDB 4LK1) and DksA (PDB 1TJL-A) and the experimental crosslinking data were used as starting points for automated modeling. To account for ambiguous crosslinking data, our scoring function required that at least one possible crosslink criteria was satisfied ($C\alpha$ - $C\alpha$ distance < 20Å) for each Bpa-replaced residue of DksA (57, 69, 73, 79, 84, 119, 140, 144, and 148) that had a corresponding RNAP fragment in the structural model (**Fig. 2E**, **Fig. S3**). Because β' -SI3 domain is highly flexible as found in several RNAP crystal structures (PDB: 4LK1, 4LK0, 4JKR, 4IQZ, 4YLN), the crosslink from DksA-E146Bpa was excluded from this initial analysis. Sampling of models with

good shape complementarity using the PatchDock method, generated ~130,000 docking models. This set was then filtered using a crosslinking scoring function. Preliminary analysis revealed that none of the ~130,000 docking models satisfied all 10 crosslinks. However, exclusion of DksA-V119 and satisfaction of the remaining 9 crosslinks filtered the set to a single cluster of 2 models (model 1, yellow ribbons; and model 2, blue ribbons **Fig S3E**). The model that had the most favorable shape complementarity score and also satisfied the distance interaction criteria between DksA and the tip of the β' rim helices (model 2) was used for further refinement.

First, for the refined modeling, predicted positions of β' -SI3 in the RNAP structure (PDB 4JKR, PDB 4YLN, PDB 4LJZ) were used to put an additional constraint to possible positions of DksA in the secondary channel. At the same time, the potential steric clash that may occur between the N-terminal partially unstructured region of DksA (residues 1-13) and β' rim helices was allowed. Second, only the crosslinks from DksA-Bpa residues 57, 69, 73 and 84 to stationary β and β' structural elements [36] were used, because they allowed a more unambiguous placement of DksA. The crosslinking data from other DksA-Bpa residues were excluded from the analysis since the crosslinks were mapped to mobile structural elements (β' -trigger loop, β' -SI3, β -SI1 and β -lobe 1). Third, we used additional experimental data resulting from the functional analysis of ≥ 30 DksA mutants (**Fig. S4-S7**). Among these were the N- and C-terminal deletions (**Fig. S4A, S5A, S6**), and point mutations at or near the 6 residues for which Bpa- substitutions did not appreciably crosslink to RNAP (**Fig. 2C**). We reasoned that these surface exposed substitutions were unlikely to alter folding, and may identify critical binding interfaces that are unable to tolerate the bulky Bpa adduct. The latter group of mutants proved to be the most informative for the refined modeling, since substitutions of R91, R125, A128, I136, E143 and K147 were most detrimental for binding and/or activity (**Fig. 5, S4B, S4C, S5B**). In the final DksA model (**Fig.**

S3E; model 3, red ribbons) the coiled-coil and Zn^{2+} -binding domains are positioned closer to β' rim helices than that observed in model 2. As a result, the side chains of possible crosslinked residues (of DksA and RNAP) are located at interacting distances of $<4 \text{ \AA}$.

DNA filter binding assay

The lifetimes of a competitor-resistant RNAP-promoter complex were measured in a DNA filter-binding assay, as described [23]. The fraction of competitor-resistant RNAP-promoter complex remaining in either the absence or presence of DksA was measured by a DNA filter-binding assay using a 242 bp-long end-radiolabeled DNA fragment containing the *lacUV5* promoter (endpoints -60 to +40) prepared by filling in the ends of XhoI-digested pRLG4264 plasmid with [α - ^{32}P] TTP (MP Biomedicals) and Sequenase (USB). For the assay, 10-30 nM RNAP was mixed with 0.5 nM radiolabeled *lacUV5* DNA and 5 μM DksA in binding buffer (40 mM Tris-Cl pH 7.9, 100 mM NaCl, 10 mM MgCl_2 , 1 mM DTT and 0.1 mg/ml BSA), and incubated at 30 °C for 20 min. After addition of heparin (Sigma) to 10 $\mu\text{g/ml}$, 20 μl aliquots were removed from the mixture at indicated time intervals and filtered through nitrocellulose discs (Protran BA-85, Whatman). The discs were washed (2x200 μl) with 10 mM Tris-HCl buffer pH 8.0 containing 100 mM NaCl and 0.5 mM EDTA, air-dried, and quantified by scintillation counter (Beckman). RNAP-promoter complex half-lives were determined from semi-log linear regression plots of the fraction of filter-retained complex at each time point. Time zero was defined as 15 sec after heparin addition in the absence of DksA.

β -galactosidase activity assay

β -galactosidase activity was measured for WT and mutant *E.coli* strains containing chromosomal a *rrnB* P1 promoter-lacZ fusion reporter, as described [23], after growth to stationary phase in M9 rich defined media (M9-RDM) to OD₄₅₀ of 1.0-2.2 or in LB to OD₆₀₀ of ~5.5.

To measure the β -galactosidase activity of chromosomally-expressed mutant RNAPs, cells from fresh single colonies were grown in M9 rich defined media (M9-RDM) into stationary phase for 24 h at 30°C (to OD₄₅₀ of 1.0-2.2). Cultures were placed on ice for 30 min, and diluted 1:10 in ice-cold Z-buffer (60 mM sodium phosphate buffer pH 7.0, 13 mM NaCl, 1 mM Mg₂SO₄). Reaction mixtures were prepared by mixing 500 μ l of the culture dilution, 500 μ l lysis buffer (Z-buffer containing 0.006% (w/v) SDS, 38 mM β -mercaptoethanol), 50 μ l of chloroform, and vortexing for 10 s. Reactions were initiated by addition of 200 μ l of 4 mg/ml o-nitrophenyl- β -galactoside (ONPG), incubated for 7-30 min at 25°C and quenched with 500 μ l of 1M NaHCO₃.

To measure the β -galactosidase activity in cells expressing mutant DksA, *E. coli* $\Delta greA:\Delta dksA$ double mutant strain (RLG7241) carrying chromosomal *rrnB* P1 promoter-lacZ fusion was transformed with pTRC99A-derived vectors expressing the wt or mutant DksA. The double deletion strain was used to minimize the interference effect of competitor GreA on DksA activity [43]. Cells were grown in triplicates in LB media in the presence of 1mM IPTG and 100 mg/ml ampicillin for 24 h at 30 °C to an OD₆₀₀ of ~5.5 (stationary phase). 50 μ l of cell aliquots were centrifuged and placed on ice for ~20 min. Cell were resuspended in 100 μ l of lysis buffer (100 mM Na₂HPO₄, 20 mM KCl, 2 mM MgSO₄, 0.8 mg/ml CTAB, 0.4 mg/ml Na-deoxycholate, 80 mM β -mercaptoethanol and 100 μ g/ml chloramphenicol) and lysed by sonication. 300 μ l of substrate solution (60 mM Na₂HPO₄, 40 mM NaH₂PO₄, 1 mg/ml ONPG, 13 mM β -mercaptoethanol) was added to the lysate and incubated for 15-30 min at 37 °C. Reaction was

quenched as above and the OD₄₂₀ was measured. The β-galactosidase activity was calculated in Miller Units using the following equation: $(1000 \times OD_{420}) / (OD_{600} \times 0.1 \times t)$; where OD₄₂₀ - optical density of the supernatant at 420 nm; OD₆₀₀ - optical density of the cell suspension before lysis, at 600 nm; t - reaction time in min.

***In vitro* transcription assays**

To measure the inhibitory effect of DksA on RNAP transcription from ribosomal *rrnB* P1 promoter DNA, a multiround *in vitro* transcription assay was performed as described [2] using 40 ng of supercoiled plasmid pRLG862 (carrying *rrnB* P1 promoter with endpoints -88 to +50 relative to the transcription start site) mixed with 30 nM RNAP incubated in 10 μl of transcription buffer (40 mM Tris-HCl pH 7.9, 140 mM NaCl, 10 mM MgCl₂, 1 mM DTT, 0.1 mg/ml BSA) in the presence or absence of 0.2-35 μM of wild type (wt) or mutant DksA at 30°C for 5 min. Reactions were initiated by addition of NTPs (200 μM each of ATP, GTP, CTP; 10 μM UTP and 1 μCi [α -³²P]UTP) followed by incubation at 30°C for 10 min. Reactions were terminated with 15 μl of RNA gel loading buffer (95% formamide, 20 mM EDTA, 0.05% bromophenol blue, and 0.05% xylene cyanol), the RNA products were separated on denaturing 8% PAGE in the presence of 7M urea and quantified by Phosphorimager with ImageQuant.

DksA-RNAP binding assays

To assess the binding affinities of mutant RNAPs towards the wt DksA, a direct photocrosslinking (DksA-Bpa.RNAP) assay was used. A mixture of 10-30 nM of radiolabeled DksA-L84Bpa (or DksA-R87Bpa) and 30-900 nM RNAP in 15 μl of transcription buffer was UV-irradiated at 365 nm for 5 min at 4°C. Reaction was terminated by addition of 4 μl of 5X SDS sample loading buffer, the crosslinked products were separated by 12% Tris-glycine SDS-

PAGE, visualized by autoradiography and quantified by Phosphorimager (GE Healthcare Life Sciences). The apparent dissociation constant (K_d) was calculated from the graphs as the concentration of RNAP that yields half-maximum efficiency of crosslinking to DksA-Bpa. To determine the binding affinities of mutant DksA towards the wt RNAP, an indirect competition-crosslinking (DksA-Bpa/mutant DksA/RNAP) assay was used. An equimolar mixture of 50 nM radiolabeled DksA-L87Bpa and wt RNAP (or radiolabeled wt DksA and RNAP- β -L341Bpa) was incubated in the presence of 0-30 μ M of unlabeled wt or mutant DksA used as a competitor in 15 μ l of transcription buffer for 15 min at 4°C. Reactions were UV-irradiated, analyzed by SDS-PAGE and quantified as described above. The apparent relative dissociation constant (K_{app}) was calculated from the graphs as the concentration of competitor DksA that causes 50% decrease in the crosslinking efficiency between radiolabeled DksA and RNAP.

References

1. Braeken K, Moris M, Daniels R, Vanderleyden J, Michiels J. New horizons for (p)ppGpp in bacterial and plant physiology. *Trends Microbiol.* 2006;14: 45–54.
2. Paul BJ, Barker MM, Ross W, Schneider DA, Webb C, Foster JW, et al. DksA: A Critical Component of the Transcription Initiation Machinery that Potentiates the Regulation of rRNA Promoters by ppGpp and the Initiating NTP. *Cell.* 2004;118: 311–322.
3. Perederina A, Svetlov V, Vassylyeva MN, Tahirov TH, Yokoyama S, Artsimovitch I, et al. Regulation through the Secondary Channel—Structural Framework for ppGpp-DksA Synergism during Transcription. *Cell.* 2004;118: 297–309.
4. Dalebroux ZD, Svensson SL, Gaynor EC, Swanson MS. ppGpp Conjures Bacterial Virulence. *Microbiol Mol Biol Rev.* 2010;74: 171–199.

5. Haugen SP, Ross W, Gourse RL. Advances in bacterial promoter recognition and its control by factors that do not bind DNA. *Nat Rev Microbiol.* 2008;6: 507–519.
6. Vinella D, Potrykus K, Murphy H, Cashel M. Effects on Growth by Changes of the Balance between GreA, GreB, and DksA Suggest Mutual Competition and Functional Redundancy in *Escherichia coli*. *J Bacteriol.* 2012;194: 261–273.
7. Rutherford ST, Villers CL, Lee J-H, Ross W, Gourse RL. Allosteric control of *Escherichia coli* rRNA promoter complexes by DksA. *Genes Dev.* 2009;23: 236–248.
8. Bartlett MS, Gaal T, Ross W, Gourse RL. RNA polymerase mutants that destabilize RNA Polymerase-Promoter complexes alter NTP-sensing by *rrn* P1 promoters¹. *J Mol Biol.* 1998;279: 331–345.
9. Trautinger BW. Modulation of DNA repair by mutations flanking the DNA channel through RNA polymerase. *EMBO J.* 2002;21: 6944–6953.
10. Dorman G, Prestwich GD. Benzophenone Photophores in Biochemistry. *Biochemistry.* 1994;33: 5661–5673.
11. Forné I, Ludwigsen J, Imhof A, Becker PB, Mueller-Planitz F. Probing the Conformation of the ISWI ATPase Domain With Genetically Encoded Photoreactive Crosslinkers and Mass Spectrometry. *Mol Cell Proteomics.* 2012;11: M111.012088.
12. Lennon CW, Ross W, Martin-Tumasch S, Touloukhonov I, Vrentas CE, Rutherford ST, et al. Direct interactions between the coiled-coil tip of DksA and the trigger loop of RNA polymerase mediate transcriptional regulation. *Genes Dev.* 2012;26: 2634–2646.
13. Laptenko O, Borukhov S. Biochemical Assays of Gre Factors of *Thermus Thermophilus*.

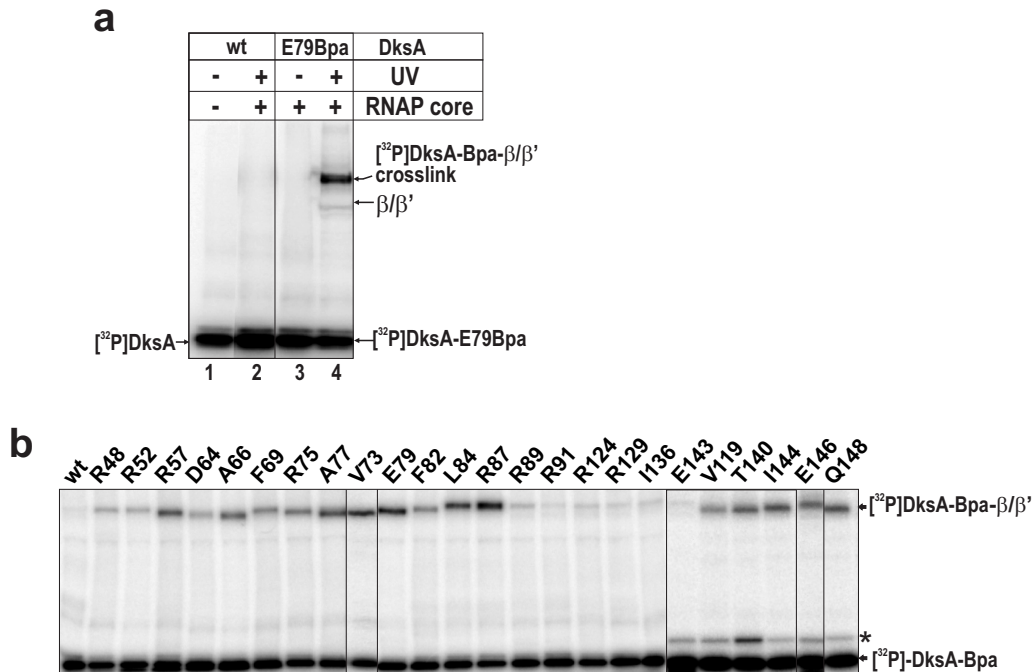
- Garges SLA and S, editor. *Methods Enzymol.* 2003;371: 219–232.
14. Mustaev A, Zaychikov E, Grachev M, Kozlov M, Severinov K, Epshtein V, et al. Strategies and Methods of Cross-Linking of RNA Polymerase Active Center. *Methods in Enzymology.* Academic Press; 2003. pp. 191–206.
 15. Schneidman-Duhovny D, Rossi A, Avila-Sakar A, Kim SJ, Velázquez-Muriel J, Strop P, et al. A method for integrative structure determination of protein-protein complexes. *Bioinformatics.* 2012;28: 3282–3289.
 16. Furman R, Tsodikov OV, Wolf YI, Artsimovitch I. An Insertion in the Catalytic Trigger Loop Gates the Secondary Channel of RNA Polymerase. *J Mol Biol.* 2013;425: 82–93.
 17. Satory D, Halliday JA, Sivaramakrishnan P, Lua RC, Herman C. Characterization of a Novel RNA Polymerase Mutant That Alters DksA Activity. *J Bacteriol.* 2013;195: 4187–4194.
 18. Rutherford ST, Lemke JJ, Vrentas CE, Gaal T, Ross W, Gourse RL. Effects of DksA, GreA, and GreB on Transcription Initiation: Insights into the Mechanisms of Factors that Bind in the Secondary Channel of RNA Polymerase. *J Mol Biol.* 2007;366: 1243–1257.
 19. Blankschien MD, Lee J-H, Grace ED, Lennon CW, Halliday JA, Ross W, Gourse RL, Herman C. Super DksAs: substitutions in DksA enhancing its effects on transcription initiation. *EMBO J.* 2009;28: 1720–1731.
 20. Furman R, Sevostyanova A, Artsimovitch I. Transcription initiation factor DksA has diverse effects on RNA chain elongation. *Nucleic Acids Res.* 2012;40 3392-3402
 21. Lee J-H, Lennon CW, Ross W, Gourse RL. Role of the Coiled-Coil Tip of Escherichia coli

- DksA in Promoter Control. *J Mol Biol.* 2012;416: 503–517.
22. Holmes SF, Santangelo TJ, Cunningham CK, Roberts JW, Erie DA. Kinetic Investigation of *Escherichia coli* RNA Polymerase Mutants That Influence Nucleotide Discrimination and Transcription Fidelity. *J Biol Chem.* 2006;281: 18677–18683.
 23. Vassylyev DG, Vassylyeva MN, Zhang J, Palangat M, Artsimovitch I, Landick R. Structural basis for substrate loading in bacterial RNA polymerase. *Nature.* 2007;448: 163–168.
 24. Barker MM, Gaal T, Josaitis CA, Gourse RL. Mechanism of regulation of transcription initiation by ppGpp. I. Effects of ppGpp on transcription initiation in vivo and in vitro. *J Mol Biol.* 2001;305: 673–688.
 25. Saecker RM, Record MT, deHaseth PL. Mechanism of Bacterial Transcription Initiation: RNA Polymerase - Promoter Binding, Isomerization to Initiation-Competent Open Complexes, and Initiation of RNA Synthesis. *J Mol Biol.* 2011;412: 754–771.
 26. Murakami KS. X-ray Crystal Structure of *Escherichia coli* RNA Polymerase σ 70 Holoenzyme. *J Biol Chem.* 2013;288: 9126–9134.
 27. Bae B, Davis E, Brown D, Campbell EA, Wigneshweraraj, SR, Darst SA Phage T7 Gp2 inhibition of *Escherichia coli* RNA polymerase involves misappropriation of sigma70 domain 1.1. *Proc Natl Acad Sci U S A.* 2013. 110:19772-19777.
 28. Zuo Y, Steitz TA. Crystal Structures of the *E. coli* Transcription Initiation Complexes with a Complete Bubble. *Mol Cell.* 2015;58: 534–540.
 29. Darst SA, Opalka N, Chacon P, Polyakov A, Richter C, Zhang G, et al. Conformational

- flexibility of bacterial RNA polymerase. *Proc Natl Acad Sci.* 2002;99: 4296–4301.
30. Zhang Y, Mooney RA, Grass JA, Sivaramakrishnan P, Herman C, Landick R, Wang JD. DksA guards elongating RNA polymerase against ribosome-stalling-induced arrest. *Mol Cell.* 2014;53: 766-778
 31. Sharan SK, Thomason LC, Kuznetsov SG, Court DL. Recombineering: a homologous recombination-based method of genetic engineering. *Nat Protoc.* 2009;4: 206–223.
 32. Nichols RJ, Sen S, Choo YJ, Beltrao P, Zietek M, Chaba R, et al. Phenotypic Landscape of a Bacterial Cell. *Cell.* 2011;144: 143–156.
 33. Young TS, Ahmad I, Yin JA, Schultz PG. An Enhanced System for Unnatural Amino Acid Mutagenesis in *E. coli*. *J Mol Biol.* 2010;395: 361–374.
 34. Laptenko O, Lee J, Lomakin I, Borukhov S. Transcript cleavage factors GreA and GreB act as transient catalytic components of RNA polymerase. *EMBO J.* 2003;22: 6322–6334.
 35. Mustaev A, Kozlov M, Markovtsov V, Zaychikov E, Denissova L, Goldfarb A. Modular organization of the catalytic center of RNA polymerase. *Proc Natl Acad Sci.* 1997;94: 6641–6645.
 36. Borukhov S, Nudler E. RNA polymerase: the vehicle of transcription. *Trends Microbiol.* 2008;16: 126–134.
 37. Borukhov S (2013) RNA polymerase structure, bacterial. *Encyclopedia of Biological Chemistry* (Academic, Waltham, MA), pp 173-184.

Supplementary Information

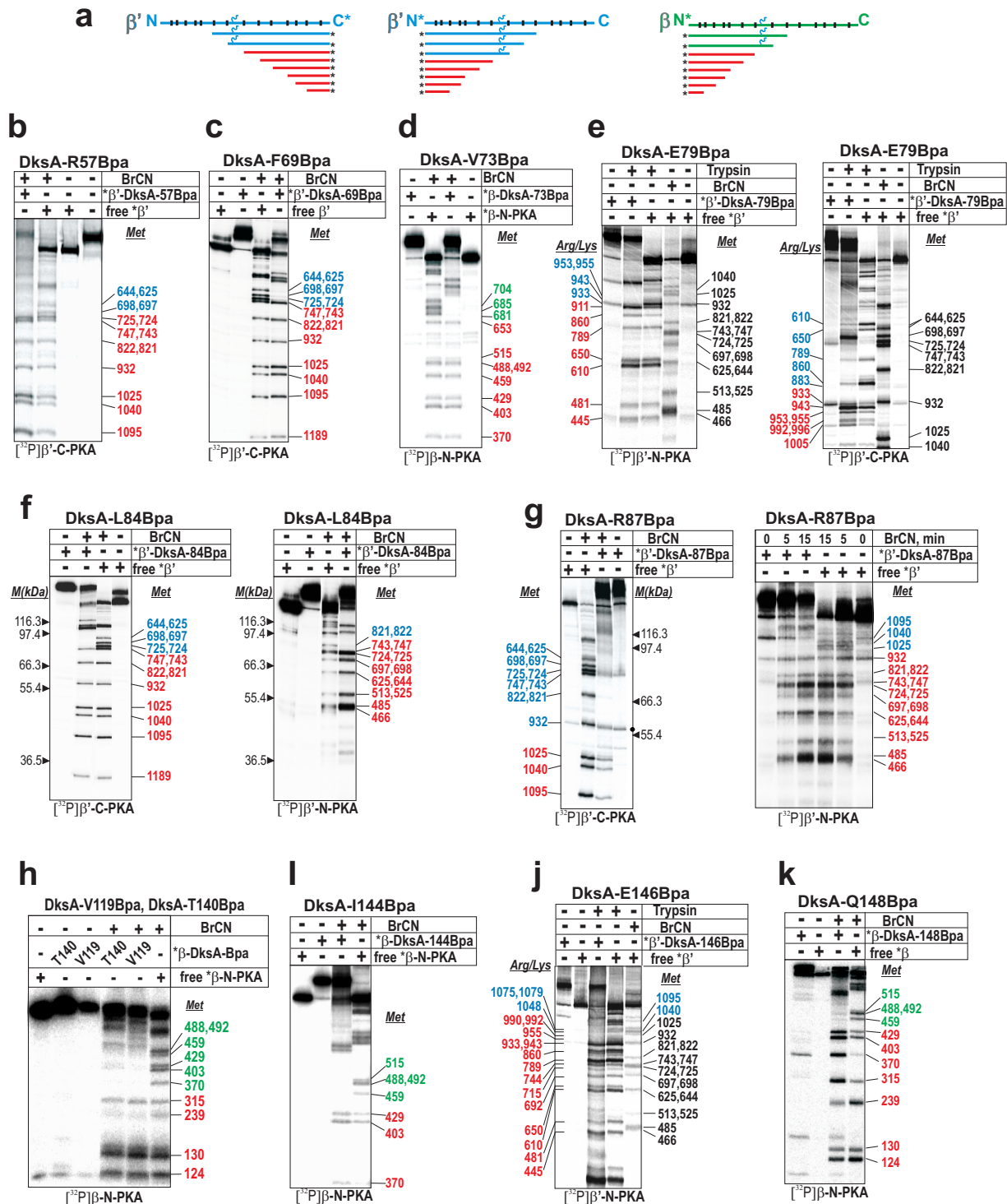
Supplementary Figure S1



Supplementary Figure S1. Site-specific DksA-Bpa crosslinking to RNAP β and β' subunits.

(A, B) Autoradiogram of a 6-15% SDS-gel electrophoresis of photo-crosslinking reactions. **(A)** Radiolabeled wt DksA (lanes 1, 2) or DksA-E79Bpa (lanes 3, 4) were incubated in the presence of unlabeled RNAP core with (lanes 2, 4) or without (lanes 1, 3) UV-irradiation. Specific photo-crosslinking to RNAP β/β' is observed only with DksA-E79Bpa after exposure to UV light (lane 4). **(B)** Screening of different radiolabeled DksA-Bpa variants for their ability to crosslink to RNAP core. Identity of each DksA-Bpa variant is indicated above the top panel. Positions of free DksA, β , β' and the crosslinked radiolabeled DksA-Bpa- β/β' species are indicated by arrows. Note that the electrophoretic mobility of the crosslink species varies depending on β/β' subunit identity and the position of a crosslink site within each protein.

Supplementary Figure S2

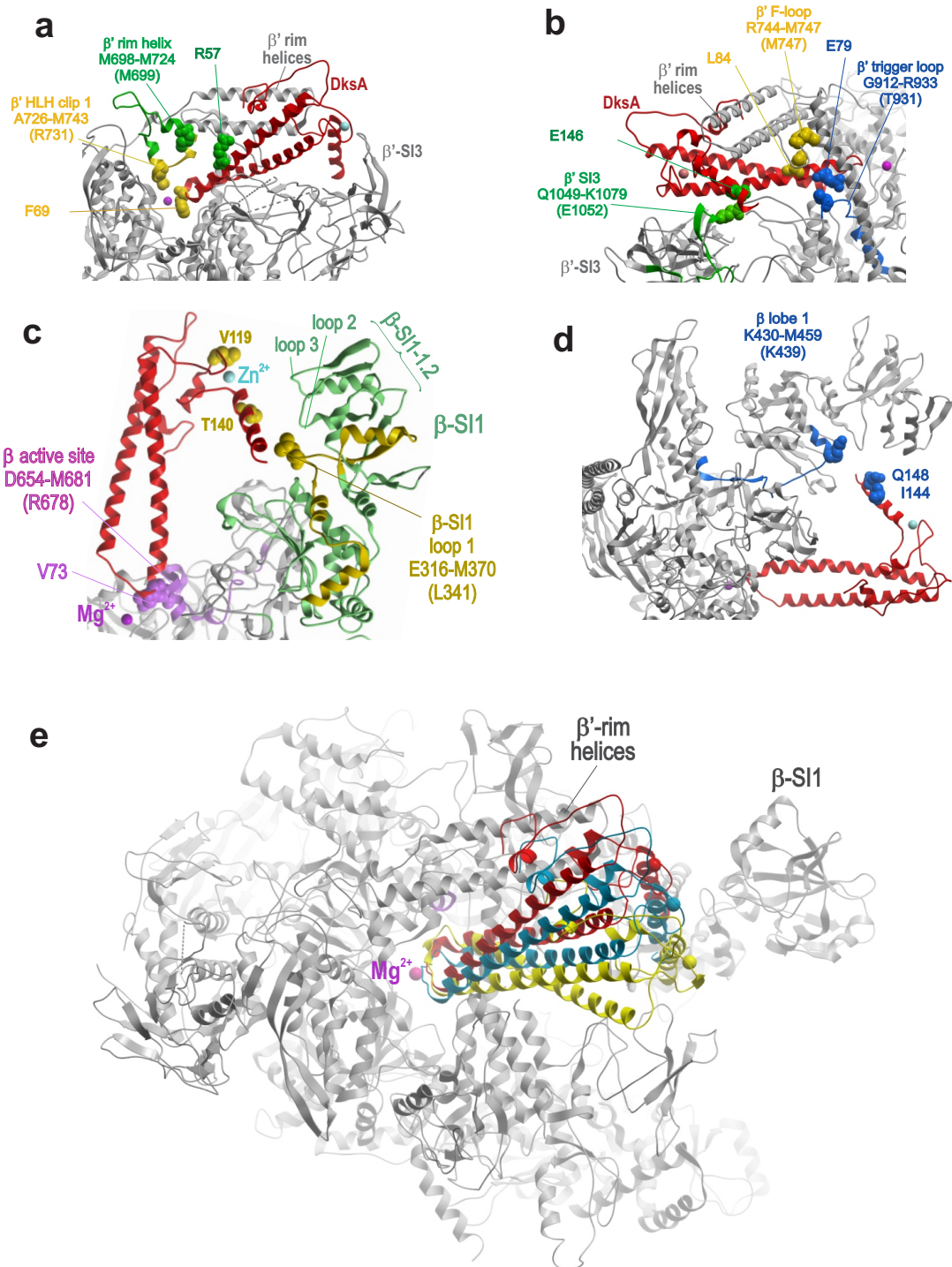
Supplementary Figure S2. Mapping of the crosslink sites on β and β' for DksA-Bpa variants.

(A) The single-hit mapping strategy. Schematic diagram depicting positions of the DksA crosslink site (small blue coil) and methionines (short black vertical bars) on N- or C-

terminally radiolabeled β' and β subunits (horizontal bars: β' , blue and β , green). Asterisk denotes position of radioactive phosphate. The N- and C-terminal Met-cleavage fragments that do not carry crosslinked DksA are colored in red.

(B-K) Autoradiograms of 7% **(B-G, I, J)** and 12% **(H, K)** SDS-gel electrophoresis of radiolabeled N- and C-terminal BrCN and trypsin cleavage products of β and β' crosslinked to DksA-Bpa variants and free β and β' . Positions of BrCN- and trypsin- cleavage sites in β and β' are indicated under Met and Arg/Lys, respectively. Fragments found in the crosslinked samples that had the same electrophoretic mobility as fragments in free β/β' (indicated by residue numbers shown in red) do not carry the crosslink. Fragments carrying the crosslink are indicated by residue numbers in blue (β') and green (β). DksA-Bpa variants used for crosslinking are indicated on top of each pane. The radiolabeled subunit used in crosslinking is indicated below each panel.

Supplementary Figure S3

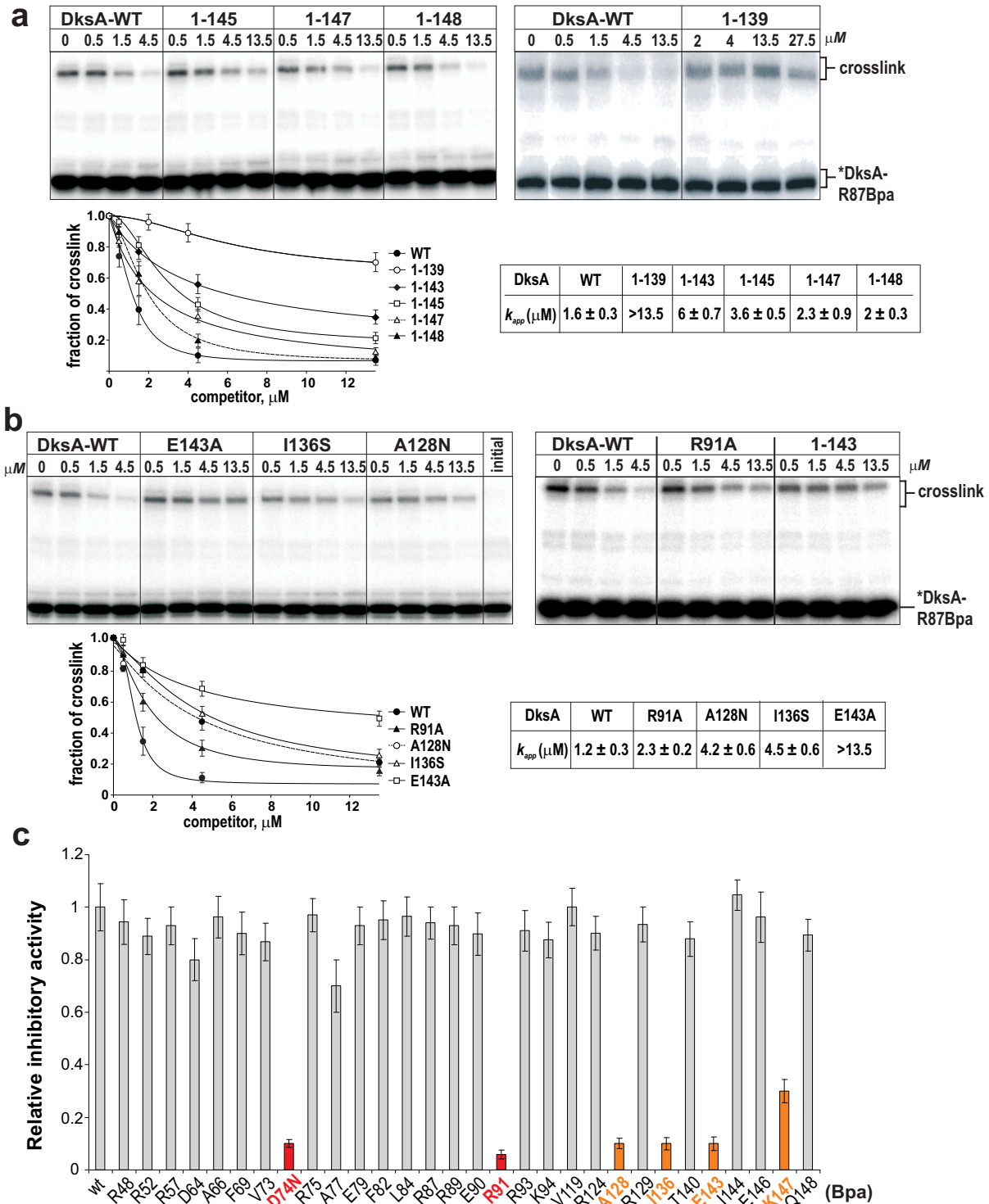


Supplementary Figure S3. Visualization of the DksA-Bpa crosslink sites in the 3D model of DksA-RNAP complex

(A-D) Zoomed-in views showing the location of the mapped crosslink sites in β and β' (colored ribbons) relative to the modeled position of DksA (PDB:1TJL, [9], red ribbon) in the crystal structure of *E. coli* RNAP (PDB: 4LK1, [26], grey ribbons). DksA-Bpa and their likely crosslinked

residues in β and β' are shown with the CPK spacefill balls of the same color and indicated by arrows. Shown are detailed views of DksA-Bpa/ β / β' proximity interfaces of: **(A)** R57Bpa/ β' rim helices and F69Bpa/ β' helix-loop-helix (HLH) element of Clip 1. **(B)** E79Bpa/ β' trigger loop, L84Bpa/F-loop and E146Bpa/ β -loop of β' -SI3. **(C)** V119Bpa/T140Bpa/ β -SI1 loop-1 and V73Bpa/ β active site,. **(D)** DksA-I144Bpa/Q148Bpa/ β lobe-1. **(E)** The secondary channel view of the three model structures of DksA-RNAP complex: generated by automated docking of DksA (model 1, yellow ribbons; and model 2, blue ribbons) and by refined modeling (model 3, red ribbons). Position of the catalytic Mg^{2+} (magenta sphere), β' rim helices and β -SI1 is indicated. β' -SI3 domain is omitted for clarity.

Supplementary Figure S4



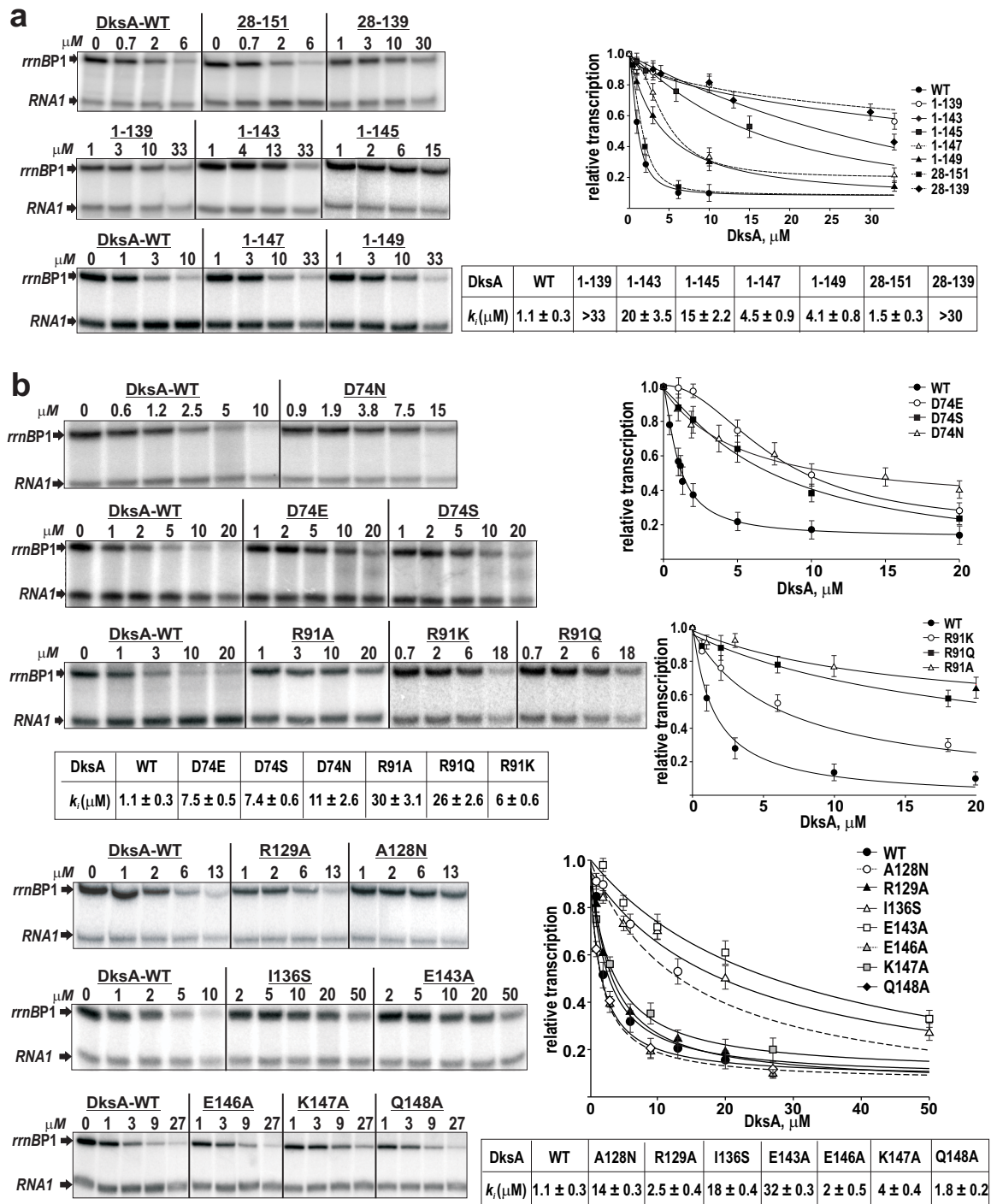
Supplementary Figure S4. RNAP-binding assay of mutant DksAs

(A, B) Competition (DksA-Bpa/mutant DksA/RNAP) crosslinking assay of DksA C-terminal truncation variants (A) and point mutations (B). Autoradiograms of a 6-15% SDS-gel electrophoresis show the effect of wt and mutant DksA proteins, used as competitors, on the efficiency of [32 P]DksA-R87Bpa crosslinking to RNAP. The identity and concentration of each

competitor is shown above the panels. Mobility of free DksA and DksA- β/β' crosslinks is indicated by arrows. Fraction of the crosslink as a function of competitor concentration plotted from multiple experiments is shown in graphs below the autoradiograms. The apparent binding affinity (k_{app}) values for wt and mutant DksA shown in tables on the right is determined as the ability of mutant protein to reduce the fraction of [32 P]DksA-R87Bpa crosslink to RNAP by two.

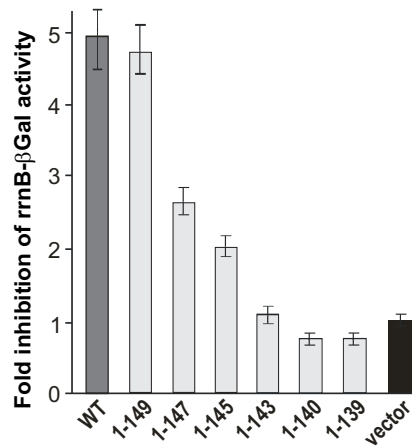
(C) Screening for functionally defective DksA-Bpa mutants. A bar graph shows relative inhibitory activity of each Bpa variant (except for D74N which is used as a reference) analyzed by in vitro transcription assay on *rrnB* P1 promoter. Residues that are critical for binding or inhibitory function are colored in orange or red, respectively.

Supplementary Figure S5



Supplementary Figure S5. Inhibitory activity of mutant DksAs.

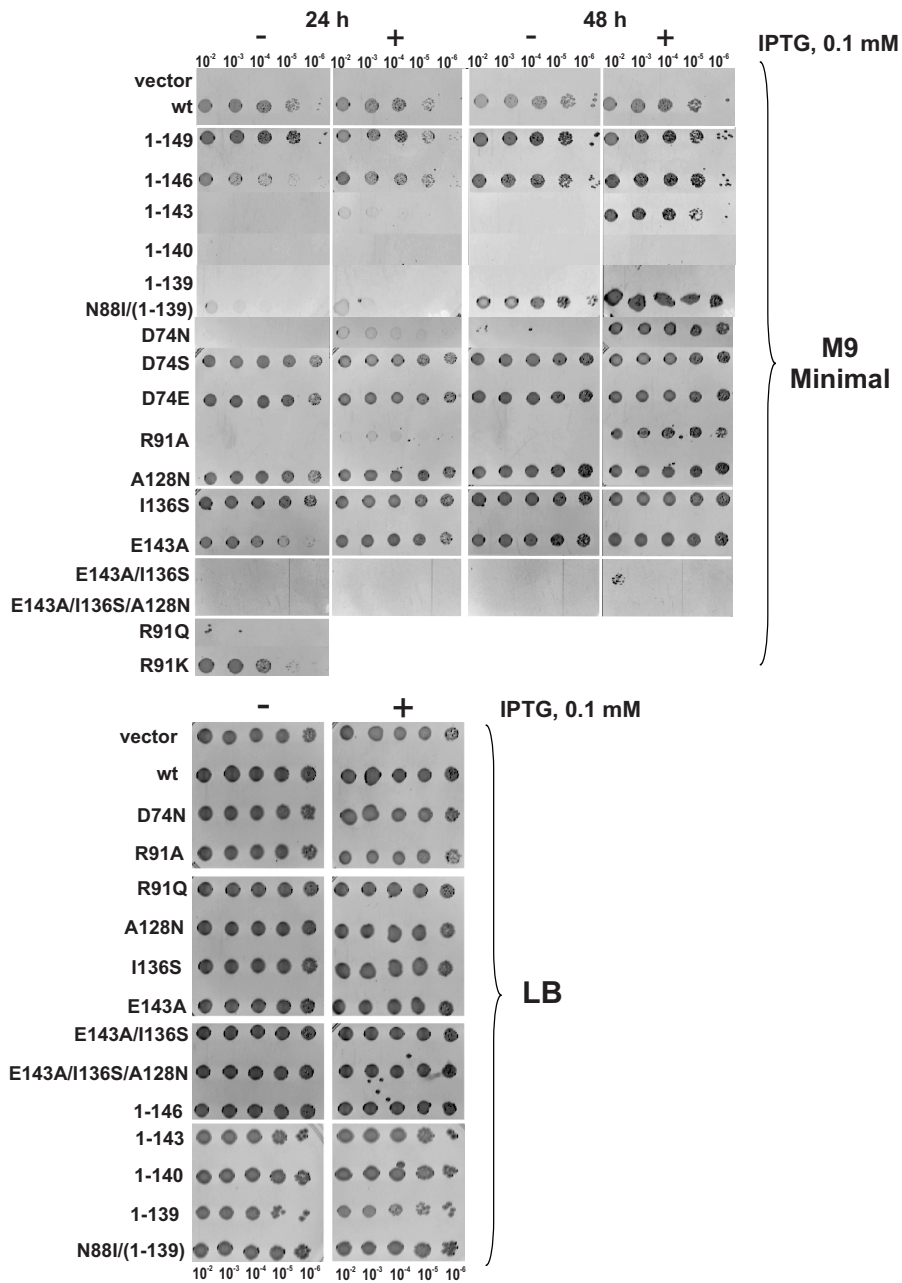
(A, B) Multiround transcription assays [8] comparing the ability of DksA C-terminal truncation variants **(A)** and point mutations **(B)** to inhibit *rrnBP1* transcription by wt RNAP. Left panels, autoradiograms of denaturing 10% urea-gel electrophoresis showing the terminated transcripts formed on plasmid DNA containing the *rrnB* P1 test-promoter and RNA1 control-promoter in the absence and presence of wt and mutant DksAs. Concentrations of DksA used in the assay are shown above each lane. DksA inhibitory activity (k_i) is quantified from plots on the right showing the dependence of relative *rrnB* P1 transcription on concentration of mutant DksAs.

Supplementary Figure S6**Supplementary Figure S6. *In vivo* inhibitory activity of DksA C-terminal truncation mutants.**

Fold inhibition of β -gal activity from *rrnB* P1-lacZ fusion reporter assayed in $\Delta dksA$ strain expressing plasmid-born mutant DksAs relative to that carrying empty vector. Activity (in Miller units) was measured after growing cells for 24 hrs to stationary phase.

Supplementary Figure S7. Growth phenotypes of $\Delta dksA$ cells expressing mutant DksAs during amino acid limitation. *E. coli* $\Delta dksA$ cells (CF9240) carrying an empty vector or a plasmid expressing wt or mutant DksA were grown in LB broth to a mid-log phase. Cells, washed once with M9 salts containing 10 mM MgSO₄, were then serially diluted in M9 medium and plated on M9 agar or LB agar supplemented with antibiotics and/or IPTG, and grown for 24 and 38 hours at 30°C.

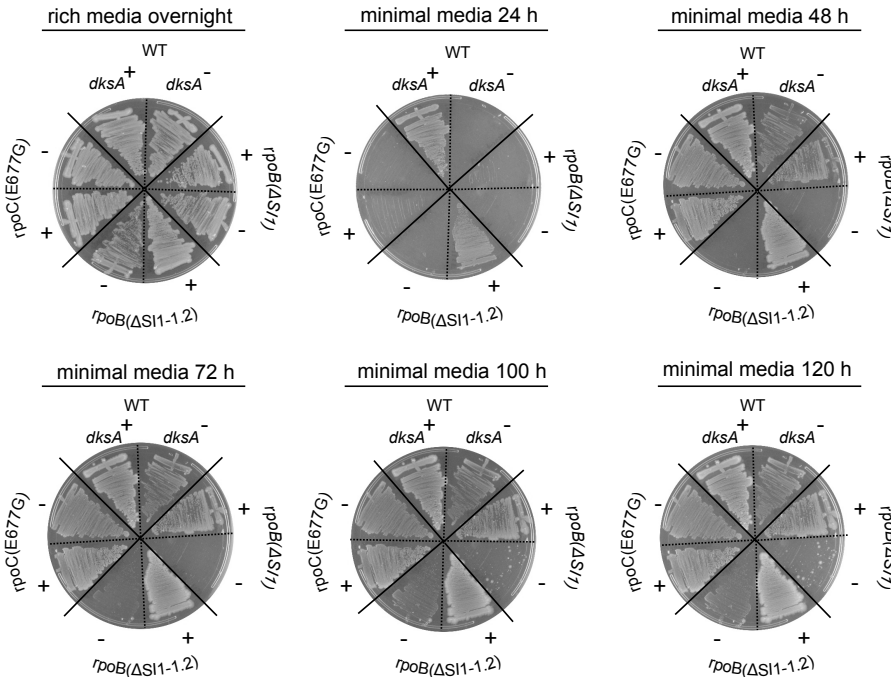
Supplementary Figure S7



Supplementary Figure S7. Growth phenotypes of $\Delta dksA$ cells expressing mutant DksAs during amino acid limitation.

E. coli $\Delta dksA$ cells (CF9240) carrying an empty vector or a plasmid expressing wt or mutant DksA were grown in LB broth to a mid-log phase. Cells, washed once with M9 salts containing 10 mM $MgSO_4$, were then serially diluted in M9 medium and plated on M9 agar or LB agar supplemented with antibiotics and/or IPTG, and grown for 24 and 38 hours at 30°C.

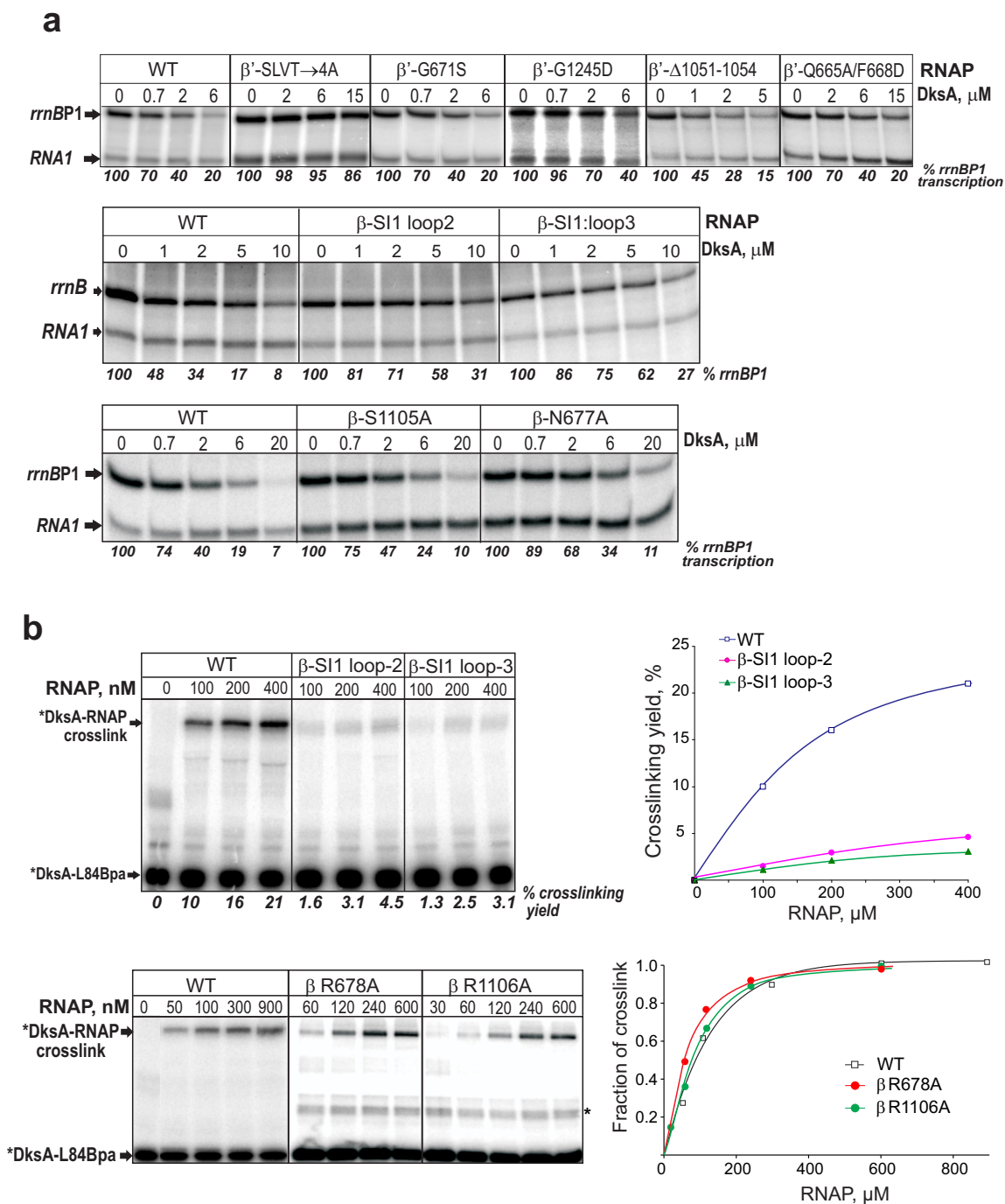
Supplementary Figure S8



Supplementary Figure S8. Mutations in β -SI1 display synthetic genetic interaction with $\Delta dksA$.

RNAP mutations with either *dksA*^{WT} (+) or $\Delta dksA$ (-) genetic backgrounds are grown on minimal media plates over the course of 120 hours. The phenotype of $\Delta dksA$, *rpoB(ΔSI1)*, and *rpoC(E677G)* is colony formation after a delay; 48 h of growth on minimal media. The double mutant *rpoC(E677G)ΔdksA* has the same delay in growth as either single mutation, indicating an epistatic genetic interaction. Conversely, combination of either *rpoB(ΔSI1)* or *rpoB(ΔSI1-1.2)* with $\Delta dksA$ leads to significant delays in growth of up to 100 hours; indicating a synthetic genetic interaction for either double mutant. These growth delays are specific to conditions of amino acid deprivation, as growth on rich media is not impaired any of the strains.

Supplementary Figure S9



Supplementary Figure S9. Effect of mutations in RNAP β and β' on the inhibitory activity and binding affinity of DksA.

(A) Multiround transcription assays (same as in Supplementary Figure 5) comparing the ability

of wt DksA used at indicated concentrations to inhibit *rrnBP1* transcription by wt and mutant RNAPs. The percentage of *rrnBP1* transcripts made with DksA relative to that without DksA is indicated below each lane on the autoradiograms of 10% denaturing urea-gel electrophoresis. **(B)** Direct DksA-Bpa/RNAP binding assay comparing the ability of wt and mutant RNAPs used at indicated concentrations to crosslink to radiolabeled photoactive probe [³²P]DksA-L84Bpa. Autoradiograms of 6-12% SDS gel-electrophoresis show the products of crosslinking reactions with wt, β -S11 loop-2 and loop-3 mutant RNAPs (top panel), or with wt and β -active site mutants R678R and R1106A (bottom panel), with crosslinking yield indicated below each lane. The crosslinking yield (top right) or the fraction of crosslink (bottom right) were plotted as a function of RNAP concentration shown on the graphs.

Supplementary Table S1: RNA polymerase mutants with altered DksA function

Structural element of the secondary channel ¹	RNAP β' or β mutants	Relative DksA binding affinity ²	Relative DksA inhibitory activity ³
β' rim helices	WT	1	1
	I664D	1	1
	Q667A	1	1
	Q665A/F668D	0.3	0.3
	D684A	nd	0.25
	Y679A	0.75	0.75
	G671S	1	1
	SLVT \rightarrow 4A ⁴	<0.1	<0.05
β' clip 1	G732V	1	1
β' clip 2	G1245D	0.3	0.3
β' F-loop	Δ F-loop ⁵	1	1
β' trigger loop	S942A	1	1
	R943A	1	1
β' SI3	Δ 1051-1054	3	3
	G1055V	1	1
β SI1	Δ SI1 ⁶	<0.1	<0.05
	Δ SI1-1.2 ⁷	<0.1	<0.05
	β SI1-loop 2 ⁸	0.3	0.2
	β SI1-loop 3 ⁹	0.2	0.15
β active site (-1/-3 RNA-binding helix)	R678A	1	<0.05
	N677A	1	0.5
β active site (NTP-binding loop)	R1106A	1	0.1
	S1105A	1	0.8

¹The secondary channel elements are described in (Borukhov, 2013). ²Measured by localized Fe²⁺-mediated protein cleavage assay, or by photo-crosslinking, and expressed relative to the binding affinity of DksA towards wt RNAP (K_d~250 nM). ³Measured by runoff transcription assay at ribosomal *rrnB* *P1* promoter. 100% of inhibitory activity is the concentration of DksA (1.5-2 μ M) that decreases the amount of runoff transcript by 2-fold. ⁴SLVT \rightarrow 4A, four-Ala substitutions of β' residues: S670A, L672A, V673A, T674A. ⁵ Δ F-loop, deletion of β' residues L746-P758 replaced by a Gly. ⁶ Δ SI1, deletion of β residues E226-L350 replaced by five Ala. ⁷ Δ SI1-1.2, deletion of β residues E240-L284 replaced by three Ala. ⁸SI1-loop 2, four-Ala substitution of β residues E244, R245, L246 and R247. ⁹SI1-loop 3, substitution of five β residues: R268A, T270A, A271T, R272 and R275A

Supplementary Table S2: Growth effects of $\Delta dksA$ mutants

	<i>dksA</i> mutant	no IPTG, 24h / 48h	0.1 mM IPTG, 24h / 48h
	empty vector	-/-	-/-
	WT	+/+/+	+/+/+
C-terminal deletions	1-149	+/+/+	+/+/+
	1-146	+/+	+/+/+
	1-143	-/-	-/+/+
	1-140	-/-	-/-
	1-139	-/-	-/-
	1-139/N88I	-/+/+	-/+/+
point mutations	R125A	-/-	-/-
	R125A/Q88I	-/-	-/+/+
	A128N	+/+/+	+/+/+
	I136S	+/+/+	+/+/+
	E143A	+/+/+	++++
	E143A/I136S	-/-	-/+
	E143A/I136S/A128N	-/-	-/-
	D74E	+/+/+	+/+/+
	D74S	+/+/+	+/+/+
	D74N	-/-	-/+/+
	R91A	-/-	-/+/+
	R91Q	-/nd	nd
	R91K	+/nd	nd

Supplementary Table S3: Evolutionary conservation of SI1

Phylum	DksA (M1-G151)	β -SI1 (E226-P345)	β' -SI3 (R943-T1131)
Proteobacteria	DksA	SI1	SI3
Chrysiogenetes	DksA	SI1	SI3
Deferribacteres	DksA	SI1	SI3
Elusimicrobia	DksA (Δ 5-C-term)	SI1	SI3
Acidobacteria	DksA	SI1	SI3
Nitrospirae	DksA	SI1	SI3
Nitrospinae	DksA	SI1	SI3
Thermodesulfobacteria	DksA	SI1	SI3
Planctomycetes	DksA (Ω 10-17 aa C-ter)	Small SI1 (Δ loop-2, -3)	SI3
Fibrobacteres	DksA (Ω 20 aa C-ter)	Small SI1 (Δ loop-3)	SI3
Verrucomicrobia	DksA (Ω 22-25 aa C-ter)	Small SI1 (Δ loop-2, -3)	SI3
Lentisphaerae	DksA (Ω 9 aa C-ter)	Small SI1 (Δ loop-2, -3)	SI3
Firmicutes	DksA (Ω 36-108 aa C-ter)	No SI1 (Δ 117 aa); Ω 70-100 aa at 414	No SI3
Gemmatimonadetes	DksA (Δ 14-C-ter)	SI1; Ω 35 aa at 292	SI3
Aquificae	DksA	Small SI1 (Δ loop-3); Ω 30 aa at 414	SI3
Unclassified bacteria	DksA (Δ 5 aa C-ter)	Small SI1 (Δ loop-2, -3)	SI3
Spirochaetes	DksA	Small SI1 (Δ loop-2, -3)	SI3
Synergistetes	DksA (Δ 4-C-ter)	Small SI1 (Δ loop-2, -3)	No SI3
Chlamydia	DksA	Small SI1 (Δ loop-2, -3)	SI3
Chloroflexi	DksA	No SI1 (Δ 110 aa)/Small SI1 (Δ loop-2,-3)	No SI3
Chlorobi	DksA (Δ 6 aa C-ter)	Small SI1 (Δ loop-2, -3)	SI3
Ignavibacteriae	DksA	Small SI1 (Δ loop-2, -3)	SI3
Bacteroidetes	DksA	Small SI1 (Δ loop-2, -3)	SI3
Marinimicrobia	DksA	Small SI1 (Δ loop-2, -3)	SI3
Actinobacteria	DksA (Δ 5-8 aa C-ter)	No SI1 (Δ 117 aa)	No SI3
Caldiserica	-	Small SI1 (Δ loop-2, -3)	No SI3
Dictyoglomi	-	No SI1 (Δ 117 aa)	SI3
Fusobacteria	-	Small SI1 (Δ loop-2, -3)	SI3
Thermotogae	-	Small SI1 (Δ loop-2, -3)	Small SI3 (20 aa)
Armatimonadetes	-	SI1 (Ω 55 aa 214-215)	Small SI3 (51 aa)
Deinococcus-Thermus	-	No SI1 (Δ 117 aa)	No SI3
Cyanobacteria	-	No SI1 (Δ 117 aa)	SI3 (Ω 70-100 aa)
Tenericutes	-	Small SI1 (Δ loop-2, -3)	No SI3

Supplementary Table S4: Conservation of the DksA interface

Phylum	Main contacts										Auxiliary contacts	
	DksA-Zn ²⁺ -binding domain - β ' rim helices					DksA-C-terminal α -helix - β SI1					DksA-coiled-coil - β ' F-loop	
	DksA R125	β ' E677	DksA A128; I136	β ' L672; V673	DksA E143	β ' T674	DksA I144-M149	β SI1 I229-P345	DksA N88	β ' I683	L746; I754	
Proteobacteria	R	E	A; I, V	L; V	E	T	DksA	SI1	N, S, T, L, I, A	I, V	L; I	
Chrysiogenetes	R	E	Y; R	I; S	E	T	DksA	SI1	M	I	L; I	
Deferribacteres	R	E	Y; T	A; L	E	T	DksA	SI1	R	I	L; I	
Elusimicrobia	R	E	A; V	I; I	E	T	DksA (Δ 5)	SI1	Q	I	L; I	
Acidobacteria	R	E	A; I	A; I	E	T	DksA	SI1	Q	I	L; I	
Nitrospirae	R	E	A; I	L; I	E	T	DksA	SI1	L	I	L; I	
Nitrospirae	R	E	V; V	L; I	E	T	DksA	SI1	L	I	L; I	
Thermodesulfobacteria	R	E	A; I	L; I	E	T	DksA	SI1	I	V	L; I	
Planctomycetes	R	E	A; I, V	L; M	E	T	DksA (Ω 10-17)	SI1-(Δ loop-2,-3)	M, L	L	L; I	
Fibrobacteres	R	E	A; V	V; I	K	T	DksA (Ω 20)	SI1-(Δ loop-3)	L	I	L; V	
Verrucomicrobia	R	E	A; A, V	V; I	E	T	DksA (Ω 22-25)	SI1-(Δ loop-2,-3)	M, L	I	L; I	
Lentisphaerae	R	E	A; V	V; I	E	T	DksA (Ω 9)	SI1-(Δ loop-2,-3)	V	I	L; I	
Firmicutes	R	E	A, F; V, L, I, K	L, F; I	E, D, S	T, S	DksA (Ω 36-108)	No SI1; (Ω 70-100)	L, V	I, S	L; I	
Gemmatimonadetes	R	E	I; V	N; I	-	T	DksA (Δ 14)	SI1; (Ω 35)	I	I	L; I	
Aquificae	R	E	A; I	L; I	E	T	DksA	SI1-(Δ loop-3); (Ω 30)	I	I	L; F	
Unclassified bacteria	R	E	A; F	I; I	S	T	DksA (Δ 5)	SI1-(Δ loop-2,-3)	F	I	L; I	
Spirochaetes	R	E	A; I	H; I	E	T	DksA	SI1-(Δ loop-2,-3)	L	V	L; I	
Synergistetes	R	E	A, V; I, L	I; L	E, D	T	DksA (Δ 4)	SI1-(Δ loop-2,-3)	K/E	E	L; I, V	
Chlamydia	R	E	A; V	I; I	E	T	DksA	SI1-(Δ loop-2,-3)	V	I	L; I	
Chloroflexi	R	E	A; I, M, V	L; I	E, D, A	T	DksA	No SI1 (SI1/ Δ loop-2,-3)	V, M, I	V, I, T	L; I	
Chlorobi	R	E	A; I	T; L	K	T	DksA (Δ 6)	SI1-(Δ loop-2,-3)	F	V	L; I	
Ignavibacteriae	R	E	A; L	V; I	E	T	DksA	SI1-(Δ loop-2,-3)	Y	I	L; I	
Bacteroidetes	R	E	A; V	F; I	E	T	DksA	SI1-(Δ loop-2,-3)	V	I	L; I	
Marinimicrobia	R	E	E; V	V; L	K	T	DksA	SI1-(Δ loop-2,-3)	F	I	L; I	
Actinobacteria	R	E	A, V; V, I, M	L; I	E, P, I, Q, S, R	T	DksA (Δ 5-8)	No SI1	L, I, V, Q, T	V, I	L; T, M, I, F	

Supplementary Table S5: Conservation within the DksA coiled-coil

Phylum	Main contacts				Auxiliary contacts	
	DksA coiled-coil tip	β substrate binding site	DksA coiled coil tip	β' F-bridge	DksA coiled-coil helix	β' rim helix
	D74	R678; R1106	A76	G782	R91	D684
Proteobacteria	D	R; R	A, T	G	R, H	D
Chrysiogenetes	D	R; R	A	G	R	G
Deferribacteres	D	R; R	A	G	T	D
Elusimicrobia	D	R; R	A	G	N	D
Acidobacteria	D	R; R	A	G	N	S
Nitrospirae	D	R; R	A	G	R	D
Nitrospinae	D	R; R	A	G	K	D
Thermodesulfobacteria	D	R; R	A	G	R	D
Planctomycetes	D, E	R; R	A	G	V, I, L	D
Fibrobacteres	D	R; R	A	G	R	D
Verrucomicrobia	D	R; R	G	G	A, S	D
Lentisphaerae	D	R; R	G	G	D	D
Firmicutes	D	R; R	G	G	N, H, T, M, I	S, Q, D, E
Gemmatimonadetes	D	R; R	G	G	R	D
Aquificae	D	R; R	A	G	R	D
Unclassified bacteria	D	R; R	G	G	R	D
Spirochaetes	D	R; R	A	G	K	E
Synergistetes	D, E	R; R	A	G	S	T, L
Chlamydia	D	R; R	G	G	K	S
Chloroflexi	D, E	R; R	A	G	R, K, N	E, T, R, N
Chlorobi	D	R; R	G	G	R	D
Ignavibacteriae	E	R; R	G	G	R	D
Bacteroidetes	D	R; R	G	G	K	D
Marinimicrobia	D	R; R	G	G	R	D
Actinobacteria	D, E	R; R	G, A, S	G	R, S, Q, N	E, K, T, A

Supplementary Table S6. Bacterial strains and plasmids

NAME	DESCRIPTION	SOURCE
Bacterial strains		
RLG7241	<i>dksA::tet, greA::tet</i> VH1000 λ system 1 <i>rrnB</i> P1(-61+1)- <i>lacZ</i>	Paul et al., 2005; Rutherford et al., 2007
APR14	BL21DE3 <i>dksA::tet</i>	This work
CF9240	MG1655 <i>dksA::tet Tn10</i>	a gift from M. Cashel (Brown et al., 2002)
CF15369	ppGpp ⁰ <i>rrnB</i> P1- <i>lacZ</i> Kn ^R (MG1655: Δ <i>relA</i> Δ <i>spoT</i> Δ <i>lacZ</i> <i>rrnB</i> P1- <i>lacZ</i> Kn ^R)	a gift from M. Cashel
APR2	CF15369 <i>dksA::tet Tn10</i>	This work
RLG5950	VH1000 λ system-1 <i>rrnB</i> P1(-61+1)- <i>lacZ</i>	Paul et al. 2005
RLG4764	VH1000 λ system-1 polylinker- <i>lacZ</i>	Paul et al. 2005
RLG5022	VH1000 λ system-1 <i>lacUV5</i> -46+1	Rutherford et al. 2007
CAG67766	RLG5950 <i>rpoBC::cat</i>	this work
CAG67745	RLG4764 <i>rpoBC::cat</i>	this work
CAG67767	RLG5022 <i>rpoBC::cat</i>	this work
CAG67768	RLG5950 <i>rpoBC::cat rpoB</i> (Δ <i>SI1</i>)	this work
CAG67749	RLG4764 <i>rpoBC::cat rpoB</i> (Δ <i>SI1</i>)	this work
CAG67769	RLG5022 <i>rpoBC::cat rpoB</i> (Δ <i>SI1</i>)	this work
CAG67770	RLG5950 <i>rpoBC::cat rpoB</i> (Δ <i>SI1</i> -1.2)	this work
CAG67753	RLG4764 <i>rpoBC::cat rpoB</i> (Δ <i>SI1</i> -1.2)	this work
CAG67771	RLG5022 <i>rpoBC::cat rpoB</i> (Δ <i>SI1</i> -1.2)	this work
CAG67772	RLG5950 Δ <i>dksA::aph</i>	this work
CAG67741	RLG4764 Δ <i>dksA::aph</i>	this work
CAG67773	RLG5950 <i>rpoC</i> (E677G) Δ <i>yjaZ::aph</i>	this work
CAG67756	RLG4764 <i>rpoC</i> (E677G) Δ <i>yjaZ::aph</i>	this work
CAG67202	BW25113 <i>rpoBC::cat</i>	this work
CAG68251	BW25113 <i>rpoBC::cat rpoB</i> (Δ <i>SI1</i>)	this work
CAG68369	BW25113 <i>rpoBC::cat rpoB</i> (Δ <i>SI1</i> -1.2)	this work
CAG68368	BW25113 <i>rpoC</i> (E677G) Δ <i>yjaZ::aph</i>	this work
CAG67649	BW25113 <i>rpoBC::cat</i> Δ <i>dksA::aph</i>	this work
CAG68510	BW25113 <i>rpoBC::cat rpoB</i> (Δ <i>SI1</i>); <i>rpoC</i> (Δ 215-220)	this work
CAG68502	BW25113 <i>rpoBC::cat rpoB</i> (Δ <i>SI1</i> ;P153L)	this work
CAG67645	BW25113 <i>rpoBC::cat dksA</i> (N88I) <i>yadL::tetAR</i>	this work
CAG67646	BW25113 <i>rpoBC::cat rpoB</i> (Δ <i>SI1</i>) <i>dksA</i> (N88I) <i>yadL::tetAR</i>	this work
CAG67647	BW25113 <i>rpoBC::cat rpoB</i> (Δ <i>SI1</i> -1.2) <i>dksA</i> (N88I) <i>yadL::tetAR</i>	this work
CAG67648	BW25113 <i>rpoC</i> (E677G) Δ <i>yjaZ::aph dksA</i> (N88I) <i>yadL::tetAR</i>	this work
CAG67650	BW25113 <i>rpoBC::cat rpoB</i> (Δ <i>SI1</i>) Δ <i>dksA::aph</i>	this work
CAG67651	BW25113 <i>rpoBC::cat rpoB</i> (Δ <i>SI1</i> -1.2) Δ <i>dksA::aph</i>	this work
CAG67652	BW25113 <i>rpoC</i> (E677G) Δ <i>yjaZ::aph</i> Δ <i>dksA::cat</i>	this work
Plasmids		
pRLG862	pRLG770 containing <i>rrnB</i> P1 (-88+1)	Barker et al., 2001
pRLG4264	pSL6 containing <i>lacUV5</i> (-59+38)	a gift from R. Gourse
pEVOL-pBpF	pBR322-derivative (<i>M. jannaschii</i> Bpa-tRNA synthetase/tRNA, Cm, araBAD/araC)	Provided by P. Schultz (Chin et al., 2002; Young et al, 2010)
pET-AP01	pET33b+ carrying <i>dksA</i> with N-terminal 6 \times His and PKA tags	This work
pET-AP02	pET-AP01 carrying <i>dksA</i> -R48TAG	This work
pET-AP03	pET-AP01 carrying <i>dksA</i> -R52TAG	This work

Supplementary Table S6. Bacterial strains and plasmids (continuation)

pET-AP04	pET-AP01 carrying <i>dksA</i> -R57TAG	This work
pET-AP05	pET-AP01 carrying <i>dksA</i> -D64TAG	This work
pET-AP06	pET-AP01 carrying <i>dksA</i> -A66TAG	This work
pET-AP07	pET-AP01 carrying <i>dksA</i> -F69TAG	This work
pET-AP08	pET-AP01 carrying <i>dksA</i> -V73TAG	This work
pET-AP09	pET-AP01 carrying <i>dksA</i> -R75TAG	This work
pET-AP10	pET-AP01 carrying <i>dksA</i> -A77TAG	This work
pET-AP11	pET-AP01 carrying <i>dksA</i> -E79TAG	This work
pET-AP12	pET-AP01 carrying <i>dksA</i> -F82TAG	This work
pET-AP13	pET-AP01 carrying <i>dksA</i> -L84TAG	This work
pET-AP14	pET-AP01 carrying <i>dksA</i> -R87TAG	This work
pET-AP15	pET-AP01 carrying <i>dksA</i> -R89TAG	This work
pET-AP16	pET-AP01 carrying <i>dksA</i> -R91TAG	This work
pET-AP17	pET-AP01 carrying <i>dksA</i> -V119TAG	This work
pET-AP18	pET-AP01 carrying <i>dksA</i> -R124TAG	This work
pET-AP19	pET-AP01 carrying <i>dksA</i> -R129TAG	This work
pET-AP20	pET-AP01 carrying <i>dksA</i> -I136TAG	This work
pET-AP21	pET-AP01 carrying <i>dksA</i> -T140TAG	This work
pET-AP22	pET-AP01 carrying <i>dksA</i> -E143TAG	This work
pET-AP23	pET-AP01 carrying <i>dksA</i> -I144TAG	This work
pET-AP24	pET-AP01 carrying <i>dksA</i> -E146TAG	This work
pET-AP25	pET-AP01 carrying <i>dksA</i> -Q148TAG	This work
pET-AP26	pET-AP01 carrying <i>dksA</i> -D74N	This work
pET-AP27	pET-AP01 carrying <i>dksA</i> -D74E	This work
pET-AP28	pET-AP01 carrying <i>dksA</i> -D74S	This work
pET-AP29	pET-AP01 carrying <i>dksA</i> -N88I	This work
pET-AP30	pET-AP01 carrying <i>dksA</i> -R91A	This work
pET-AP31	pET-AP01 carrying <i>dksA</i> -R91K	This work
pET-AP32	pET-AP01 carrying <i>dksA</i> -R91Q	This work
pET-AP33	pET-AP01 carrying <i>dksA</i> -R125A	This work
pET-AP34	pET-AP01 carrying <i>dksA</i> -A128N	This work
pET-AP35	pET-AP01 carrying <i>dksA</i> -R129A	This work
pET-AP36	pET-AP01 carrying <i>dksA</i> -I136S	This work
pET-AP37	pET-AP01 carrying <i>dksA</i> -E143A	This work
pET-AP38	pET-AP01 carrying <i>dksA</i> -E146A	This work
pET-AP39	pET-AP01 carrying <i>dksA</i> -K147A	This work
pET-AP40	pET-AP01 carrying <i>dksA</i> -Q148A	This work
pET-AP41	pET-AP01 carrying <i>dksA</i> 28-139	This work
pET-AP42	pET-AP01 carrying <i>dksA</i> 28-151	This work
pET-AP43	pET-AP01 carrying <i>dksA</i> 1-139	This work
pET-AP44	pET-AP01 carrying <i>dksA</i> 1-143	This work
pET-AP45	pET-AP01 carrying <i>dksA</i> 1-145	This work
pET-AP46	pET-AP01 carrying <i>dksA</i> 1-147	This work
pET-AP47	pET-AP01 carrying <i>dksA</i> 1-149	This work
pTRC-DksA-NPH	pTrc99A carrying <i>dksA</i> with N-terminal 6×His and PKA tags	This work
pTRC-AP49	pTRC-DksA-NPH with <i>dksA</i> -D74N	This work
pTRC-AP50	pTRC-DksA-NPH with <i>dksA</i> -D74E	This work
pTRC-AP51	pTRC-DksA-NPH with <i>dksA</i> -D74S	This work

Supplementary Table S6. Bacterial strains and plasmids (continuation)

pTRC-AP52	pTRC-DksA-NPH with <i>dksA</i> -N88I	This work
pTRC-AP53	pTRC-DksA-NPH with <i>dksA</i> -R91A	This work
pTRC-AP54	pTRC-DksA-NPH with <i>dksA</i> -R91K	This work
pTRC-AP55	pTRC-DksA-NPH with <i>dksA</i> -R91Q	This work
pTRC-DksA-R125A	pTRC-DksA-NPH with <i>dksA</i> -R125A	This work
pTRC-DksA-R125A/N88I	pTRC-AP48 with <i>dksA</i> -(R125A;N88I)	This work
pTRC-AP58	pTRC-AP48 with <i>dksA</i> -A128N	This work
pTRC-AP59	pTRC-AP48 with <i>dksA</i> -I136S	This work
pTRC-AP60	pTRC-AP48 with <i>dksA</i> -E143A	This work
pTRC-AP61	pTRC-AP48 with <i>dksA</i> -(E143A;I136S)	This work
pTRC-AP62	pTRC-AP48 with <i>dksA</i> -(E143A;I136S;A128N)	This work
pTRC-AP63	pTRC-AP48 with <i>dksA</i> 1-139	This work
pTRC-AP64	pTRC-AP48 with <i>dksA</i> (1-139;N88I)	This work
pTRC-AP65	pTRC-AP48 with <i>dksA</i> 1-140	This work
pTRC-AP66	pTRC-AP48 with <i>dksA</i> 1-141	This work
pTRC-AP67	pTRC-AP48 with <i>dksA</i> 1-142	This work
pTRC-AP68	pTRC-AP48 with <i>dksA</i> 1-143	This work
pTRC-AP69	pTRC-AP48 with <i>dksA</i> 1-144	This work
pTRC-AP70	pTRC-AP48 with <i>dksA</i> 1-145	This work
pTRC-AP71	pTRC-AP48 with <i>dksA</i> 1-146	This work
pTRC-AP72	pTRC-AP48 with <i>dksA</i> 1-147	This work
pTRC-AP73	pTRC-AP48 with <i>dksA</i> 1-148	This work
pTRC-AP74	pTRC-AP48 with <i>dksA</i> 1-149	This work
pTRC-AP82	pTRC-AP48 with <i>dksA</i> -R125K	This work
pBAD-JL-rpoC-CPH	derivative of pBADspc ^R III carrying <i>rpoC</i> with C-terminal 6×His and PKA tags (inserted between NdeI-XhoI)	This work
pBAD-AP02	pBAD-JL-rpoC-CPH with <i>rpoC</i> -I664D	This work
pBAD-AP03	pBAD-JL-rpoC-CPH with <i>rpoC</i> -Q667A	This work
pBAD-AP04	pBAD-JL-rpoC-CPH with <i>rpoC</i> -(Q667A;F668D)	This work
pBAD-AP05	pBAD-JL-rpoC-CPH with <i>rpoC</i> -G671S	This work
pBAD-AP06	pBAD-JL-rpoC-CPH with <i>rpoC</i> -Y679A	This work
pBAD-AP07	pBAD-JL-rpoC-CPH with <i>rpoC</i> -D684A	This work
pBAD-AP08	pBAD-JL-rpoC-CPH with <i>rpoC</i> -G732V	This work
pBAD-AP09	pBAD-JL-rpoC-CPH with <i>rpoC</i> -G1055V	This work
pBAD-AP10	pBAD-JL-rpoC-CPH with <i>rpoC</i> -G1245D	This work
pBAD-AP11	pBAD-JL-rpoC-CPH with <i>rpoC</i> -SLTV/4A (S670A, L672A, V673A, T674A)	This work
pBAD-AP12	pBAD-JL-rpoC-CPH with <i>rpoC</i> Δ 1051-1054	This work
pBAD-AP13	pBAD-JL-rpoC-CPH with <i>rpoC</i> -S942A	This work
pBAD-AP14	pBAD-JL-rpoC-CPH with <i>rpoC</i> -R943A	This work
pBAD-AP15	pBAD-JL-rpoC-CPH with <i>rpoC</i> -[Δ (L746-P758); Ω Gly]	This work
pBAD-JL-NPH-rpoC	derivative of pBADspc ^R III carrying <i>rpoC</i> with N-terminal 6×His and PKA tags (inserted between NdeI-XhoI)	This work
pTRC-JL-NPH-rpoB	derivative of pTRC99A carrying <i>rpoB</i> with N-terminal 6×His and PKA tags and S531Y Rif ^R -mutation (pTrc99A β -S531Y-NPH)	Laptenko et al., 2003
p-JL-rpoB-	pJL-NPH-rpoB with <i>rpoB</i> -L341TAG	This work

Supplementary Table S6. Bacterial strains and plasmids (continuation)

L341Bpa		
pAP-rpoB-R678A	pJL-NPH-rpoB with <i>rpoB</i> -R678A	This work
pAP-rpoB-R1106A	pJL-NPH-rpoB with <i>rpoB</i> -R1106A	This work
pJL-rpoB-6	pJL-NPH-rpoB with <i>rpoB</i> -R1106D	This work
pJL-rpoB-2	pJL-NPH-rpoB with <i>rpoB</i> Δ SI1 [Δ (E226-L350); Ω (AAAAA)]	This work
pJL-rpoB-7	pJL-NPH-rpoB with <i>rpoB</i> Δ SI1-1.2 [[Δ (E240-L284); Ω (AAA)]]	This work
pJL-rpoB-8	pJL-NPH-rpoB with <i>rpoB</i> -S11-loop2 (E244A, R245A, L246A and R247A)	This work
pJL-rpoB-9	pJL-NPH-rpoB with <i>rpoB</i> -S11-loop3 (R268A, T270A, A271T, R272A and R275A)	This work

Publishing Agreement

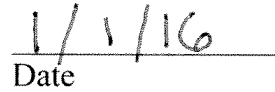
It is the policy of the University to encourage the distribution of all theses, dissertations, and manuscripts. Copies of all UCSF theses, dissertations, and manuscripts will be routed to the library via the Graduate Division. The library will make all theses, dissertations, and manuscripts accessible to the public and will preserve these to the best of their abilities, in perpetuity.

Please sign the following statement:

I hereby grant permission to the Graduate Division of the University of California, San Francisco to release copies of my thesis, dissertation, or manuscript to the Campus Library to provide access and preservation, in whole or in part, in perpetuity.

A handwritten signature in black ink, consisting of a large, stylized initial 'A' followed by a cursive name, written over a horizontal line.

Author Signature

A handwritten date '1/1/16' in black ink, written over a horizontal line.

Date